To the Graduate Council:

I am submitting herewith a dissertation written by Stacy Hutchens entitled "Characterization of a Biomimetic Calcium-Deficient Hydroxyapatite-Bacterial Cellulose Composite." I have examined the final electronic copy of this dissertation for form and content and recommend that it be accepted in partial fulfillment of the requirements for the degree of Doctor of Philosophy, with a major in Biomedical Engineering.

Roberto Benson

Dr. Roberto Benson, Major Professor

We have read this dissertation and recommend its acceptance:

Dr. David Gerard

Dr. Anthony English

Dr. Barbara Evans

Dr. Hugh O'Neill

Accepted for the Council:

Carolyn R. Hodges

Vice Provost and Dean of Graduate Studies

(Original signatures are on file with official student records)

CHARACTERIZATION OF A CALCIUM-DEFICIENT HYDROXYAPATITE BACTERIAL CELLULOSE COMPOSITE

A Dissertation Presented for the Doctor of Philosophy Degree in
Biomedical Engineering
The University of Tennessee, Knoxville

Stacy Hutchens
December 2007

Dedication

This dissertation is dedicated to my parents: Larry and Monina Hutchens. Their encouragement and inspiration fuel the fulfillment of my goals. Thanks also to Paul, for being a great brother and friend.

In addition, this dissertation is dedicated to my loving boyfriend, Emil, whose support and understanding enabled this achievement.

Acknowledgments

I am very grateful to the generous grants which have supported my work: The National Science Foundation Graduate Research Fellowship, The University of Tennessee Office of Research Scholarly Activity and Research Incentive Funds Graduate Research Assistantship, The Oak Ridge National Laboratory* Technology Transfer and Economic Development Maturation Funding Program, The P.E.O. Scholar Award, The Southern Regional Education Board Dissertation Year Award, and the U.S.A. Funds Access to Education Scholarship.

I wish to thank everyone who made my doctoral education possible. Dr. Roberto Benson has been an outstanding graduate advisor and provided endless support, advice, and guidance. Dr. Barbara Evans and Dr. Hugh O'Neill have fought in my corner for so long and I cannot express how grateful I am for their constant help and encouragement. I would also like to thank Dr. Claudia Rawn and Dr. Andrew Payzant for instructing me on the x-ray diffraction machine at the High Temperature Materials Laboratory** at Oak Ridge National Laboratory*. Thanks also to Dr. Jonathan Woodward for accepting me as a research assistant at Oak Ridge National Laboratory* and introducing me to a project that has taken me so far. I would also like to express my gratitude to Dr. Elias Greenbaum for allowing me to work in his laboratory.

* Oak Ridge National Laboratory is managed by UT-Battelle, LLC, for the U.S. Department of Energy under contract number DE-AC05-00OR22725

** Research sponsored by the Assistant Secretary for Energy Efficiency and Renewable Energy, Office of FreedomCAR and Vehicle Technologies, as part of the High Temperature Materials Laboratory User Program, Oak Ridge National Laboratory, managed by UT-Battelle, LLC, for the U.S. Department of Energy under contract number DE-AC05-00OR22725.

Abstract

Bone is the second most implanted tissue next to blood causing approximately 2.2 million people to receive bone grafts each year. Developing safe synthetic bone grafts allows quick and safe restoration of bone function while avoiding the surgical risks associated with bone autografting (self donation), and risks of disease transmission and immunogenic response associated with allografts (bone donated from other humans) and xenografts (grafts derived from animal tissue). This dissertation entails the study and development of a novel potential synthetic bone graft consisting of a composite of calcium-deficient hydroxyapatite (CdHAP) biomimetically deposited in a bacterial cellulose (BC) hydrogel.

To determine which conditions provided optimum cellulose growth from *Gluconacetobacter hansenii* (ATCC 10821), a statistical analysis of the effects of different culture parameters was carried out. This utilized fractional factorial design which allowed a large number of factors to be tested using an abbreviated set of experiments. Statistical software was also used to process the data to determine which factors and factor interactions were significant to bacterial cellulose production.

Purified bacterial cellulose was mineralized by sequential incubations in solutions of calcium chloride followed by sodium phosphate dibasic. This material was characterized using X-Ray Diffractometry, Fourier Transform Infrared Spectroscopy, Scanning Electron Microscopy, Electron Dispersive Spectroscopy, and mechanical testing. Characterization revealed that the CdHAP formed biomimetically in the BC in a manner similar to natural bone. It was also determined that the CdHAP had comparable structure, size, and composition to that found in natural bone.

An ideal bone replacement material will degrade after stimulating new osseous tissue production. A chemical modification of the cellulose was carried out with periodate oxidation to render it degradable in-vivo. The BC structure was preserved as well as its ability to mineralize

CdHAP after periodate oxidation. This composite was characterized and its capacity to degrade was analyzed by subjecting the samples to a simulated aqueous physiological environment.

The last chapter discusses how the BC-CdHAP composite may have clinical use in the major bone grafting procedures currently being administered. Several surgeons were surveyed for this portion of the study to determine which grafts they used, the reasons for graft selection, and to obtain their opinion of the BC-CdHAP material. It was ultimately determined that the BC-CdHAP composite has ideal properties for dental bone grafting procedures including site extraction preservation and sinus lifts.

Table of Contents

List of Tables

List of Figures

Chapter 1

Introduction

1.1. Bone Biology

Bone is a specialized form of hard connective tissue that fulfills multiple functions including support, protection, blood production, and movement [1]. Bone is a composite material consisting of 25% water, 15% organic materials, and 60% mineral phases (by weight) [2]. The organic matrix consists of 95% Type I collagen with proteoglycans and noncollagenous proteins comprising the remaining 5% [3]. The main mineral component is calcium-deficient hydroxyapatite with traces of carbonate, fluoride, magnesium, chloride, and citrate ions [3].

Bone consists of four types of cells: osteoblasts, osteocytes, osteoclasts, and bone lining cells. Osteoblasts, osteoclasts, and bone lining cells exist on the bone surface while osteocytes are located within the bone tissue (Figure 1.1) [4].

Osteoblast cells produce bone by creating a protein matrix layer called osteoid which is primarily collagen. The osteoid is then mineralized by calcium and phosphorus salts precipitated from blood plasma as well as from direct apatite deposition from matrix vesicles [5]. As the

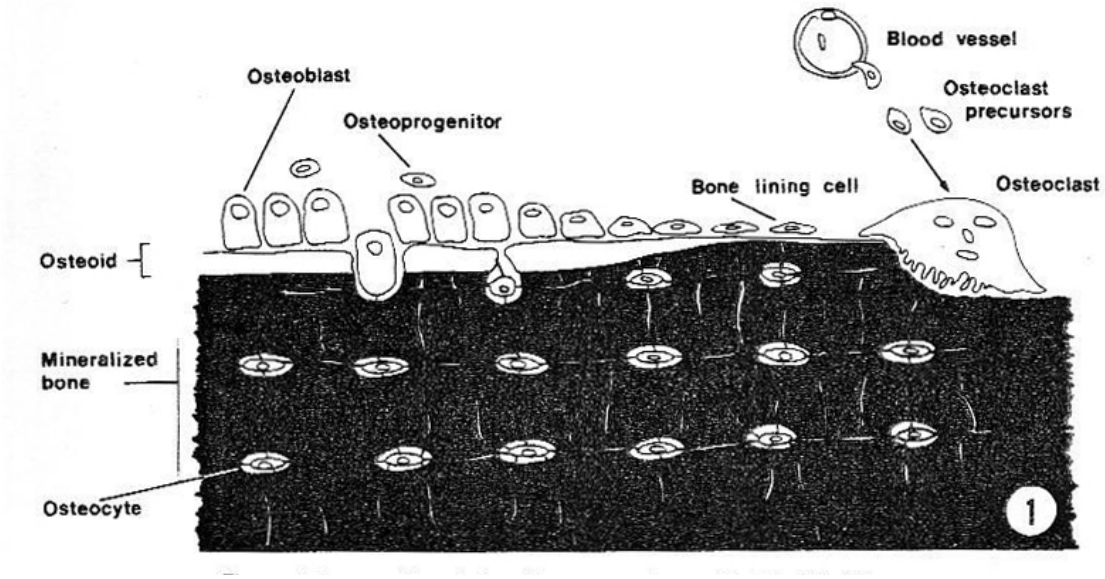

Figure 1.1: Topographic relationships among bone cells [4]

osteoblast becomes embedded within the mineralized osteoid, it matures into an osteocyte. The osteocytes are regularly spaced throughout the mineralized matrix and are responsible for bone maintenance. Osteocytes can also synthesize additional bone tissue and are capable of resorbing the bone matrix to a limited extent [3]. Bone lining cells are inactive flat osteoblasts that cover the surface of most bones. Bone lining cells are believed to serve as a selective barrier between bone and the extracellular fluid compartments. They may also regulate the movement of calcium and phosphate into and out of the bone [3].

Osteoblasts are derived from mesenchymal stem cells (MSCs). MSCs are most commonly found in the bone marrow and the periosteum [6]. They have the capacity to differentiate into a variety of other cells which can produce cartilage, muscle, fat, ligament, and tendon (Figure 1.2) [6,7]. During differentiation, certain genes are turned on while others are turned off to produce specific structures and perform certain functions. To differentiate into a mature osteoblast, MSCs must undergo several transitional steps via intricate pathways (Figure 1.3) which are regulated by a series of signaling factors [7]. Bone morphogenetic protein-2 (BMP-2) is a bone signaling factor which has been extensively studied [8,9]. Along with regulating bone development and osteogenesis, BMP-2 is also osteoinductive. This growth factor has the ability to convert undifferentiated mesenchymal cells into osteoblasts and chondrocytes [10]. A recent strategy of bone grafting is the incorporation of BMP-2 to induce mesenchymal cell proliferation, subsequent osteoblast differentiation, and new bone formation [10].

Other protein growth factors have been proven to affect bone growth including transforming growth factor β (TGF-β), platelet derived growth factor (PDGF), and insulin-like growth factor (IGF). Along with signaling factors, bone growth is also regulated by hormones such as calcitonin, vitamin D, and parathyroid hormone. Mechanical loading is also an important stimulus for bone growth as is dictated by Wolff's Law.

Osteoclasts are multinucleated cells that resorb old or worn bone to be subsequently replaced by new bone [3]. Unlike osteoblasts which are derived from MSCs, osteoclasts originate from the fusion of mononuclear precursors [4]. During bone remodeling, osteoclasts degrade the

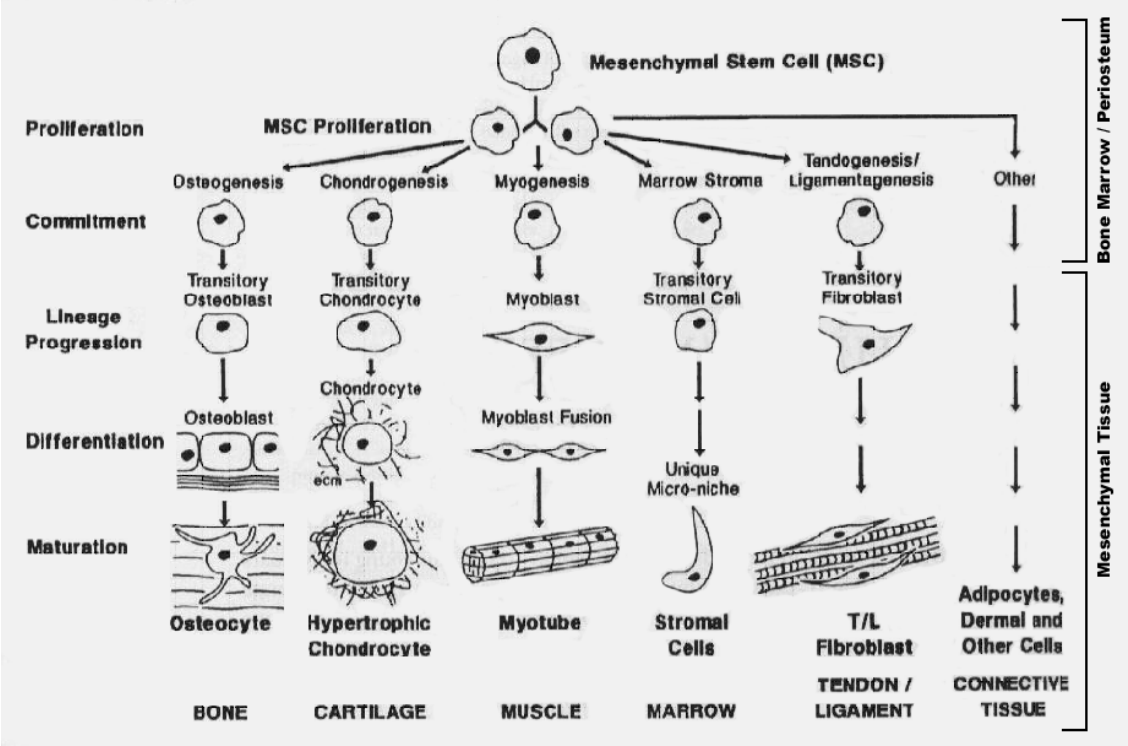

Figure 1.2: Mesenchymal stem cell lineages and resulting tissues [6]

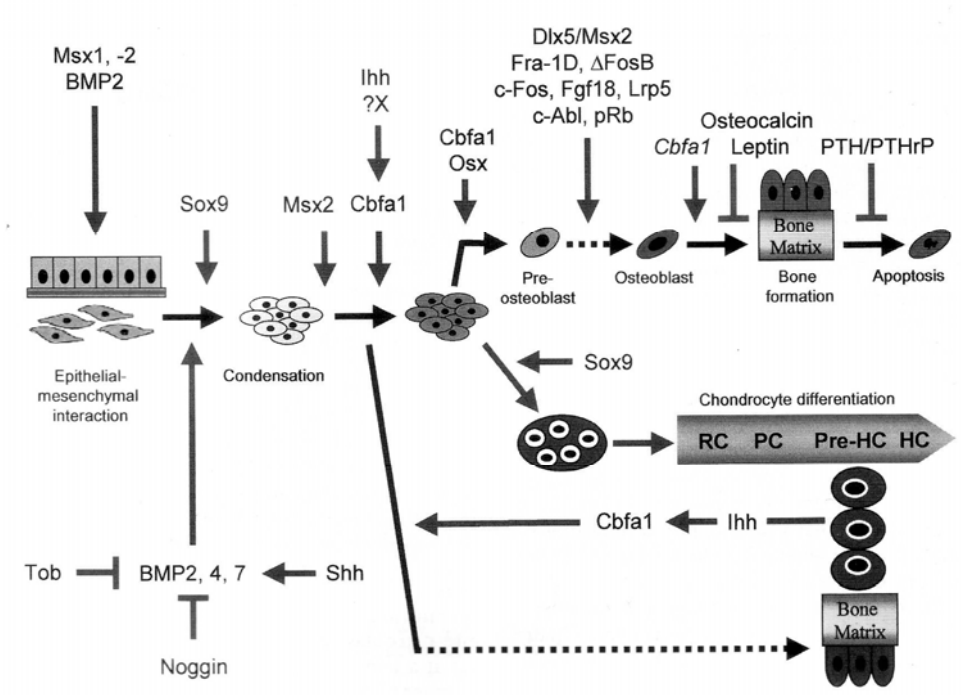

Figure 1.3: Schematic of signaling factor network that controls mesenchymal cell differentiation into osteoblasts and chondrocytes [7]

matrix which is replaced by new bone matrix produced by the osteoblasts [7].

Bone development is either classified as intramembranous or endochondral [3]. Intramembranous ossification entails the direct replacement of connective tissue with bony tissue. After connective tissue formation, osteoblasts migrate into the matrix and deposit osseous tissue. This occurs in the formation of the cranial vault, facial skeleton, parts of the mandible, and the clavicle. During endochondral bone formation, hyaline cartilage is replaced with bony tissue. The hyaline cartilage becomes infiltrated with blood vessels and osteoblasts to become the periosteum. The osteoblasts then deposit bone as the cartilage disintegrates. Weight bearing bones, bones that terminate in joints, most of the cranial base, and a portion of the mandible are formed via endocondral ossification [3].

Bone is classified as either cortical or cancellous. Cortical (or compact) bone is dense and primarily found in the shaft of long bones (the diaphysis). It also forms an outer shell at the ends of long bones (epiphysis) and also around vertebrae. The basic structure of cortical bone is called a Haversian System or osteon. In the osteon, the osteocytes are arranged in concentric circles (lamellae) around the central Haversian Canal which contain blood vessels and nerves (Figure 1.4). Volkmann's Canals are perpendicular tubular passages that link the blood vessels

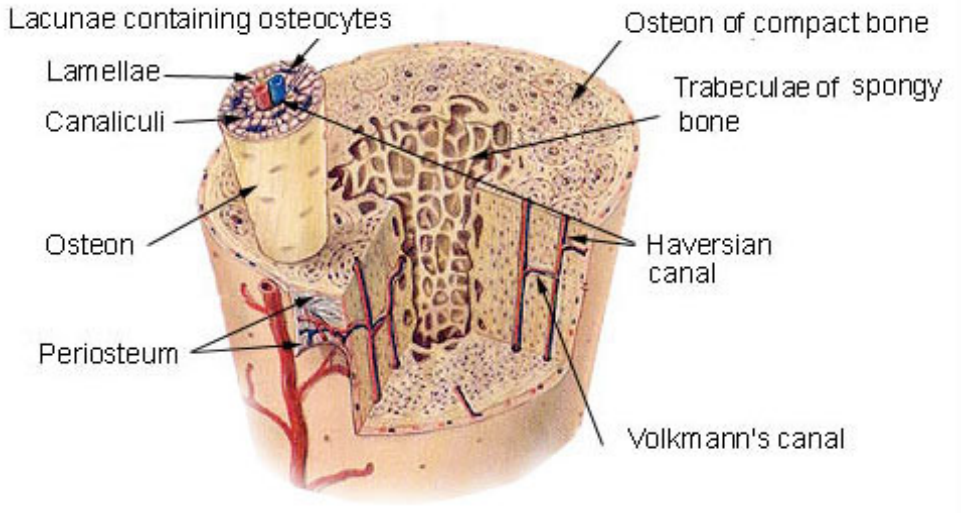

Figure 1.4: Structure of cortical and cancellous bone [Image taken from http://en.wikipedia.org]

of one Haversian System to another. Nutrients and metabolites from the Haversian Canal are unable to permeate the mineralized osteoid to the embedded osteocytes. To access these solutes and maintain communication with other cells, osteocytes rely on surrounding extracellular spaces (lacunae) and interconnecting cytoplasmic projections (canaliculi) [3].

Cancellous (or trabecular) bone is spongy and less dense than cortical bone. Cancellous bone is found at the ends of long bones (the epiphysis) as well as in vertebrae. It consists of trabeculae and bars of bone which are surrounded by the vascularized red marrow bed. In cancellous bone, the canaliculi connect to the osteocyte to the marrow bed to access the blood supply as opposed to a central Haversian Canal [3].

1.2. Bone Grafting

Bone is the second most implanted tissue next to blood. Bone grafts are used to repair defects caused by surgery, trauma, tumors, disease, congenital deformities, as well as implant revisions and infections [11]. Bone grafts are also used for spinal fusion and to strengthen the bone prior to orthopaedic and dental implantation [11,12]. Each year, approximately 450,000 bone graft procedures are performed in the U.S. with 2.2 million procedures conducted worldwide [13]. A market survey performed by Kalorama Information (Rockville, MD, U.S.A.) estimates that the global market for bone grafts in 2004 was approximately $1 billion and is projected to approach $4.5 billion by 2012 [14]. A similar survey conducted for the European market found that orthopaedic biomaterial sales were ~$1.1 billion in 2005 and should reach $5.0 billion in the year 2010 [15]. The primary drivers for this growth are increasing numbers of spinal fusion and revision joint replacement surgeries, as well as the aging population and inflationary price increases [14].

A bone graft stimulates new bone growth by three mechanisms: osteoconduction, osteoinduction, and osteogenesis [12,16,17]. In osteoconduction, the graft serves as a scaffold to support bone ingrowth and/or deposition [12,17]. Osteoconduction can only occur in bony sites since it relies on preexisting bone cells or mesenchymal cells [12,17]. Osteoinductive materials

can promote bone growth in soft tissues outside of the bony skeleton because they contain growth factors (e.g. BMP-2) that stimulate non-differentiated mesenchymal cells to become bone cells [12,16,17]. Osteogenic materials contain living cells (e.g. stem cells, osteoprogenitor cells) that are capable of differentiating and facilitating the bone formation process [16].

Bone grafts can be categorized into four main types: autografts (self-donated bone), allografts (donated from another human), xenografts (donated from another species), and alloplasts (synthetic bone grafts). The advantages and disadvantages of each technique will be discussed in the following sections.

1.2.1. Autografts

Termed the "gold standard" of bone grafts, autogenous bone exhibits all three mechanisms of bone healing: osteoconduction, osteoinduction, and osteogenesis. Currently, it is the only osteogenic material available. Autogenous bone grafts are histocompatible, do not transfer disease, and retain viable osteoblasts that produce new bone [18].

Autogenous grafts can be obtained in cancellous form, nonvascularized or vascularized cortical form, or a combination of the three [18]. Cancellous bone has a suitable hydroxyapatite/collagen framework for osteoconduction and possesses osteogenic cells [18]. Denser cortical bone is less suitable for osteoconduction, and does not possess osteogenic cells. However, cortical bone has superior compressive strength and a larger concentration of BMP that can stimulate osteogenesis from neighboring cells [12,17,18]. Cortical bone also provides a suitable barrier against soft tissue ingrowth [12,17]. Vascularized grafts prevent cell necrosis and improve viability [18]. However, vascularized grafts increase the chance of donor-site morbidity and prolong operation time [18]. While vascularized grafts are initially biomechanically superior to non-vascularized grafts, there is no significant difference between the two after six months [18].

Autogenous bone can be obtained from several areas. In selecting the donor site; the location of the recipient bed, the quality and quantity of bone required, and potential complications are considered [19]. For maxillofacial procedures, intraoral sources can be used

including the mandibular symphysis, maxillary tuberosity, ramus, and exostoses [12]. Ribs have also been used to reconstruct the mandible [17]. While a significant amount of cancellous bone can be obtained from the proximal tibia [20], the iliac crest offers the greatest amount of usable cortical and cancellous bone. The iliac crest is also easy to access making it the most common donor site for bone autografting [19].

The iliac can be accessed either anteriorly or posteriorly. In a typical anterior iliac bone graft harvesting procedure, a 3-6 cm incision is made parallel to the anterior iliac crest starting from at least 2 cm superolaterally from the anterior superior iliac spine (Figure 1.5) [21]. Posterior bone grafts require an almost vertical incision over and slightly lateral to the posterior iliac spine and parallel to route of the superior cluneal nerves [19]. After the skin is retracted, the dissection proceeds through the fascia to the superior border of the iliac [21]. The periosteum is dissected and the graft is cut with a bone saw (Figure 1.5) [21]. On average, 10-15 cm^3 of bone is harvested from the iliac during this procedure, though up to 55 cm^3 of bone can be obtained from this site [19].

While autografts are osteoconductive, osteoinductive, osteogenic, and do not elicit an immunogenic response; there are many shortcomings and potential complications associated

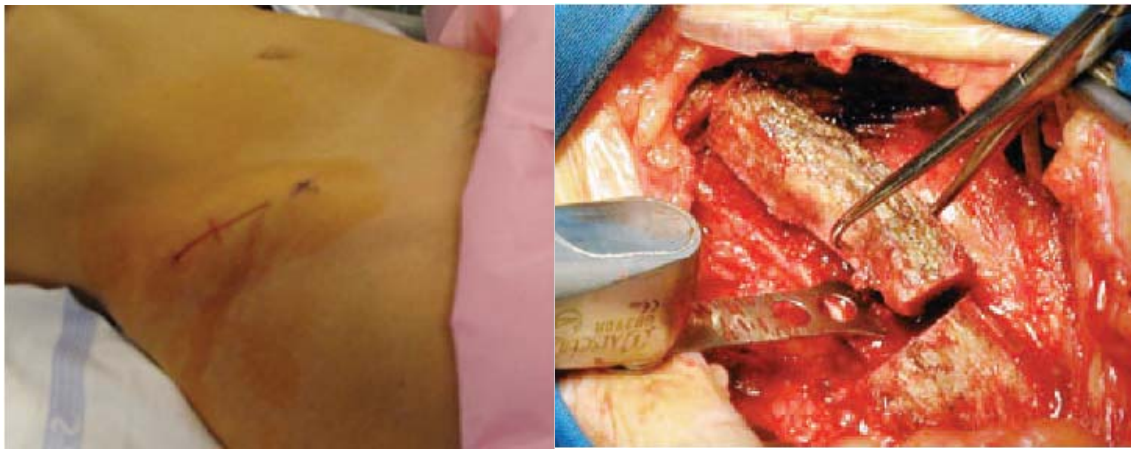

Figure 1.5: Photograph showing position and extent of incision required for anterior iliac crest (left). Operative photograph showing bone harvesting from ilium using a single-bladed oscillating bone saw (right) [21]

with this procedure. The most common drawbacks are associated with the second operation which can produce pain, infections, hematomas, donor site morbidity, prolonged anesthesia time, significantly increased operative blood loss, and a longer hospital stay [18-22]. A high rate of repeat operative interventions is associated with these postoperative problems [20]. Gazdag *et al.* report that the rate of donor site morbidity for the iliac crest is as high as 25% [18]. Patients have also reported having sensory disturbances associated with nerve damage, having complaints about cosmetic appearance, and experiencing functional disability [19]. Joshi and Kostakis performed a post-operative investigation of patients who underwent iliac crest graft harvesting and found that 14% of the patients surveyed experienced gait disturbance, and 22% required use of a walking stick or wheelchair from 0.5 to 26 weeks postoperatively [22]. While overall rates of patient complications vary between studies, reports range from 2.8% to as high as 49% [20,21]. Additionally, failure occurs in 15-25% of autogenous cortical transplants due to inadequate fixation and improper biological, physiological, and mechanical properties [23].

The amount of bone that can be obtained from autografting procedures is limited, especially in elderly patients [23]. Certain procedures, such as bone tumor surgery and joint implant revision, often require large quantities of bone which cannot be obtained in sufficient quantity and quality from the host without significant risk [23].

1.2.2. Allografts

Allograft bone is obtained from other individuals of the same species but with different genotypes. Bone allografts can be obtained from cadavers as well as living persons [11,12]. Allografts are processed into a variety of forms including fresh-frozen, irradiated, freeze-dried, and demineralized freeze-dried bone.

While fresh-frozen bone is osteoconductive, there is a significant risk of disease transmission and host-graft rejection associated with this graft. For this reason, it is not used in certain clinical applications including implant dentistry [11].

Irradiated bone is subjected to 6-8 million rads of radiation to decrease the risk of disease transmission [12]. It has been claimed that irradiated bone provides a response closest to that achieved with autogenous bone compared with other bone grafts [12]. However, it is not widely used due to continuing concerns about disease transmission [17].

Over 95% of bone allografts are freeze-dried [24]. This action causes osteoblasts to release BMPs and bestow osteoinductivity. However, freeze-dried bone is reported to have an unpredictable performance once implanted.

Demineralized freeze-dried bone (DFDB) is subjected to hydrochloric or nitric acid for 6-16 h which removes the calcium and phosphate salts from the bone matrix. This releases BMPs giving the graft osteoinductive potential, however it has been contested whether there are sufficient amounts of BMPs in DFDB to stimulate osteoinduction [17]. Other studies did not find a significant difference between the performance of DFDB and freeze-dried bone allograft [12].

Allografts are readily available and their use eliminates the complications associated with the second operation required with autografting [12]. Allogenic bone grafts are increasingly being used in orthopaedic reconstruction surgery [24]. Several commercialized bone graft products based on allograft bone or demineralized bone are currently on the market (Table 1.1).

Significant complications may occur with bone allografts. The chief disadvantage is the elicitation of an immunological response that can result in graft rejection [23]. Antigens present in the allograft can cause both humoral and cellular mediated rejection [14]. Graft rejection can cause disruption of blood vessels and an inflammatory reaction that includes lymphocyte infiltration, fibrous encapsulation, peripheral graft resorption, callus bridging, nonunions, and fractures [23]. Allograft remodeling requires a significant amount of time and could also result in a late rejection [23]. Bone allografts can also transmit a multitude of diseases and viruses including hepatitis B and C as well as human immunodeficiency virus [24].

While many of the aforementioned processes (freeze-drying, demineralization, irradiation) are employed to destroy antigens, these methods can mechanically weaken and chemically alter the graft. This can render the allograft unsuitable for successful bone

Table 1.1: FDA approved bone allograft products

Graft Name	Manufacturer	Material Description
Accell®	IsoTis OrthoBiologics: Laussanne, Switzerland	Putty consisting of demineralized bone matrix (DBM) in a polymer (pluronic) carrier
Dynagraft® II	IsoTis OrthoBiologics: Laussanne, Switzerland	DBM in a sodium hyaluronate carrier
Orthoblast®II	IsoTis OrthoBiologics: Laussanne, Switzerland	DBM in a polymer (pluronic) carrier
Allomatrix® Custom	Wright Medical: Arlington, TN, U.S.A.	Putty with DBM, allograft cancellous bone chips, and calcium sulfate
Allomatrix® Putty	Wright Medical: Arlington, TN, U.S.A.	DBM with a binding medium of calcium sulfate and carboxymethylcellulose
Osteoset® 2 DBM	Wright Medical: Arlington, TN, U.S.A.	DBM in calcium sulfate pellets
DBX® Demineralized Bone	Musculoskeletal Transplant Foundation: Edison, NJ, U.S.A.	DBM in a sodium hyaluronate carrier
Grafton®	Osteotech: Eatontown, NJ, U.S.A.	DBM in a starch carrier
Intergro™	Interpore Cross International: Irvine, CA, U.S.A.	DBM with coral-derived hydroxyapatite in a lecithin carrier
Opteform®, Optefil®	Exactech Inc: Gainesville, FL, U.S.A.	DBM, cortical and cancellous bone chips in a gelatin carrier
Optium DBM®	LifeNet: Virginia Beach, VA, U.S.A.	DBM combined with glycerol/glycerin

substitution, and none of these techniques can ensure complete removal of antigenicity [23].

In a study of patients who received allogenic bone, a 75-85% success rate was reported. However, only 50% of the patients had an entirely uncomplicated postoperative course. One quarter of the patients required further surgery such as autologous grafting, replating for stress fractions, or delayed union. Worst-case scenarios included graft excision due to infection, reimplantation, long term bracing, and amputation [24].

1.2.3. Xenografts

Bone xenografts are obtained from another species, most commonly bovine [17]. Several bone xenograft products either use entire bovine bone, hydroxyapatite isolated from bovine bone, or isolated bovine collagen in combination with other growth factors or ceramic particles. Another product called Bioset XC™ (Regeneration Technologies, Inc.: Alachua, FL,

U.S.A.) consists of bovine bone and human demineralized bone in a porcine gelatin carrier. Examples of other xenograft bone substitutes currently on the market are given in Table 1.2.

Many studies have reported the success of bone xenografts. For example, BioOss® (Osteohealth: Shirley, NY, U.S.A.) has had favorable results as a dental bone graft specifically in guided tissue regeneration around titanium implants [25,26]. While xenografts are extensively processed and sterilized to prevent immunogenic response, risks of disease transmission and adverse reactions can still occur. Additional investigations have shown poor performance of xenografts in other bone grafting procedures [27-30]. In a study of eleven patients who received bovine bone grafts for spinal fusion, Schutlheiss *et al.* found that only two patients had complete osseointegration and only three had partial osseointegration [27]. Xie *et al.* found that bovine bone incited fibrous tissue growth when used in spinal fusion which was attributed to low biocompatibility [28]. Charalambides *et al.* investigated the use of xenografts for hip revision

Table 1.2: FDA approved bone xenograft products

Graft Name	Manufacturer	Material Description
Sterling® Cancellous Chips and Cubes	Regeneration Technologies, Inc.: Alachua, FL, U.S.A.	Bovine bone
Bioset XC™	Regeneration Technologies, Inc.: Alachua, FL, U.S.A.	Bovine bone, human demineralized bone matrix, porcine gelatin
BioOss®	Osteohealth: Shirley, NY, U.S.A.	Bovine-derived hydroxyapatite
Osteograf®	Dentsply: Lakewood, CO, U.S.A.	Bovine-derived hydroxyapatite
PepGen P-15®	Dentsply: Lakewood, CO, U.S.A.	Bovine-derived hydroxyapatite enhanced with a synthetic peptide that mimics the cell-binding domain of Type-I collagen
Healos®	DePuy Spine: Raynham, MA, U.S.A.	Cross-linked bovine collagen fibers fully coated with hydroxyapatite
Collagraft®	Zimmer: Warsaw, IN, U.S.A.	Purified fibrillar bovine collagen with hydroxyapatite and tricalcium phosphate granules
CopiOs™	Zimmer: Warsaw, IN, U.S.A.	Calcium phosphate dibasic in bovine collagen
Vitoss®	Orthovita: Malvern, PA, U.S.A.	80% β-tricalcium phosphate, 20% bovine collagen
Infuse®	Medtronic: Minneapolis, MN, U.S.A.	Bovine collagen sponge with recombinant human bone morphogenetic protein-2

surgery and found a significant loss of bone incorporation and also reports of infection and rejection [29]. Another study used xenografts to repair tibial osteotomies and reported a significant number infections and absence of cell infiltration [30]. The extensive processing that animal bone must undergo to become safe grafts also causes xenografts to lose mechanical and structural integrity [31].

1.3. Alloplasts

Alloplasts are synthetic materials used for tissue substitution. Since they are readily available, they eliminate the complications associated with the second operation required of autografts. By utilizing biocompatible and hypoallergenic materials, alloplasts are devoid of the risks of disease transmission and immunogenic response related to allografts and xenografts. Alloplasts can also be economically produced in a variety of shapes of sizes and can be modified to host specific physical and chemical properties. Most alloplasts are composed of ceramics, polymers, or ceramic-polymer composites. These specific alloplasts will be discussed further in the following sections. Metals are also being investigated for bone substitution. A new metal bone graft called Trabecular Metal™ consisting of elemental tantalum is currently manufactured by Zimmer (Warsaw, IN, U.S.A.). Titanium is also widely used to repair severe fractures and reconstruct joints due to its unique ability to osseointegrate, or bond with bone [32].

1.3.1. Ceramic Bone Grafts

Most commercially available bone alloplasts are ceramic based (Table 1.3). Each of these materials exhibit osteoconduction by providing a scaffold for bone in-growth [12,33].

Calcium sulfate (Ca_2SO_4) was first reported to fill bony defects in 1892 by Dressmann [33]. Calcium sulfate is an inexpensive material often mixed with water to form a dense paste and used to fill the defect [17]. There are reports that antibiotic laden Ca_2SO_4 paste can successfully be used in the presence of infection [33].

A major complication of Ca_2SO_4 paste is the exothermic setting process which can

Table 1.3: FDA approved ceramic based bone alloplast products

Graft Name	Manufacturer	Material Description
Osteoset®	Wright Medical: Arlington, TN, U.S.A.	Calcium sulfate pellets
Stimulan®	Biocomposites Limited: Staffordshire, U.K.	Calcium sulfate pellets
NovaBone®, PerioGlas®	Novabone: Jacksonville, FL, U.S.A.	Bioactive glass comprised of silica and calcium
Allogran-R®	Biocomposites Limited: Staffordshire, U.K.	Porous β-tricalcium phosphate granules
GenerOs™	Berkeley Advanced Biomaterials Inc: Berkeley, CA, U.S.A.	Porous β-tricalcium phosphate granules
chronOS™	Synthes: West Chester, PA, U.S.A.	Porous β-tricalcium phosphate
Conduit™	DePuy Spine: Raynham, MA, U.S.A.	Porous β-tricalcium phosphate granules
Bioresorb®	Oraltronics: Bremen, DE	Micro and macroporous β-tricalcium phosphate
Cellplex®	Wright Medical: Arlington, TN, U.S.A.	β-tricalcium phosphate granules
TheriGraft™, TheriLok™, Theriwedge™, Therilink™	Therics: Akron, OH, U.S.A.	β-tricalcium phosphate in various forms (putty, granules, wedge, slab)
BoneSave™	Stryker: Kalamazoo, MI, U.S.A.	80% β-tricalcium phosphate, 20% hydroxyapatite granules
Genex®	Biocomposites Limited: Staffordshire, U.K.	Porous hydroxyapatite and β-tricalcium phosphate particles with a negative charge
Bi-Ostetic™	Berkeley Advanced Biomaterials Inc: Berkeley, CA, U.S.A.	60% hydroxyapatite, 40% β-tricalcium phosphate
MasterGraft™	Medtronic Sofamor Danek: Memphis, TN, U.S.A.	60% hydroxyapatite, 40% β-tricalcium phosphate
Cem-Ostetic™	Berkeley Advanced Biomaterials Inc: Berkeley, CA, U.S.A.	Nanocrystalline hydroxyapatite and β-tricalcium phosphate in a neutral pH bone putty that sets after application
Pro Osteon™	Interpore Cross International: Irvine, CA, U.S.A.	Porous hydroxyapatite derived from marine coral
Allogran-L®	Biocomposites Limited: Staffordshire, U.K.	Multiporous hydroxyapatite granules
Calcitite®	Zimmer Dental: Carlsbad, CA, U.S.A.	Sintered hydroxyapatite particles
Osteogen®	Impladent Ltd.: Holliswood, NY, U.S.A.	Resorbable synthetic hydroxyapatite
Norian SRS®	Synthes: West Chester, PA, U.S.A.	Carbonated apatite cement
α-BSM®	Johnson and Johnson: Piscataway, NJ, U.S.A.	Calcium phosphate paste that forms poorly crystalline hydroxyapatite after application
BoneSource®, HydroSet™	Stryker: Kalamazoo, MI, U.S.A.	Calcium phosphate cement that converts to hydroxyapatite after application

damage bone [17]. Utilizing calcium sulfate pellets like those in Osteoset® and Stimulan® (Table 1.3) alleviates problems associated with setting. However, Ca_2SO_4 dissolves quickly and the resorption profile has been reported as unpredictable [17]. Further concern has been raised regarding the release of sulfur into the body [17]. For these reasons, it is not widely used as a bone graft [17].

Bioactive glass is an amorphous material made from calcium, phosphate, sodium, and silicon salts [12]. This material is found in the commercial products NovaBone® and PerioGlas® (Table 1.3). Bioactive glasses permit a surface modification after implantation which allows bonding to soft and hard tissues [2]. However, certain studies have reported rapid dissolution of and breakdown of bioactive glass during oral implantation [12]. The production costs of bioactive glass are also significantly high [34].

As the mineral phase of bone is principally calcium phosphate, calcium phosphate ceramics are a common synthetic bone substitute, and have been used in medicine and dentistry for nearly 30 years [2]. The three most commonly used calcium phosphates in bone alloplasts consist of β- tricalcium phosphate (β-TCP), hydroxyapatite (HAP), and biphasic calcium phosphate (BCP) which is a mixture of β-TCP and HAP.

β-tricalcium phosphate (β-TCP) is biocompatible, is resorbable by osteoclasts, and can be replaced by new bone [17]. While it is chemically similar to hydroxyapatite, it is not a natural component of bone mineral [12]. β-TCP rapidly dissolves in approximately six weeks after implantation which makes it inappropriate for use in some applications [33]. It is also reported that its resorption rate is variable and dependent on the implant site as well as the material's structure, porosity, and chemistry. The chemical structure and properties of β-TCP may also be altered after heat sterilization [12].

β-TCP is not as widely used as hydroxyapatite (HAP), which is the preferred calcium phosphate alloplast [17]. Hydroxyapatite resembles the principal inorganic component of bone [2,12,17] and is found in several synthetic bone alloplasts (Table 1.3). Synthetic hydroxyapatite is biocompatible and readily bonds to hard and soft tissues [12].

Commercial production of HAP entails conversion from other calcium compounds or by aqueous precipitation (combination of a calcium salt and an alkaline phosphate or a reaction between calcium hydroxide or calcium carbonate and phosphoric acid) [2]. HAP can also be produced via solid-state processing, hydrolysis, and hydrothermal synthesis. The physical and chemical properties of HAP are dependent on its route of synthesis [2]. These properties directly affect its biological response, rate of resorption, and appropriate clinical application [12].

The stoichiometry of HAP is highly dependent on its processing conditions and greatly affects its biological properties. Stoichiometric hydroxyapatite (sHAP) is represented by the compound $Ca_{10}(PO_4)_6(OH)_2$. Fully calcium-deficient hydroxyapatite (CdHAP) takes on the form $Ca_9(HPO_4)(PO_4)_5(OH)$. Physiological HAP is almost always calcium deficient compared to stoichiometric hydroxyapatite due to contact with a constant flow of trace ions. Physiological apatite can take on the form $Ca_{10-x}(HPO_4)_x(PO_4)_{6-x}(OH)_{2-x}$ with $0< x \leq 1$ [35].

CdHAP is more favorable as a bone implant compared to sHAP because it dissolves faster in aqueous environments [36,37]. CdHAP quickly forms a biomimetic layer of apatite on its surface which enables rapid bonding with bone [38]. The stability and resistance to dissolution prevents sHAP from permitting this surface modification [39]. This is confirmed by an *in-vivo* study, conducted by Bourgeois *et al.*, which demonstrated that CdHAP induced rapid bone colonization with nearly complete degradation after two weeks while sHAP generated much less bone formation [37]. CdHAP also has a large specific surface area, which facilitates the loading of therapeutic agents that may further increase bone cell colonization [37]. As most synthetic HAP is processed and sintered at high temperatures, it assumes a stoichiometric form.

The hydroxyl groups of hydroxyapatite can undergo ionic substitution which affects its properties. Incorporation of carbonate ions has been shown to increase apatite dissolution and may increase the bone replacement process after implantation [40]. Apatites that contain fluoride ions are more likely to retard demineralization and dissolution [41].

Processing conditions also affect the physical form of HAP including particle size, porosity, and crystallinity [12]. Larger crystallites take a long time to resorb while small particles

dissolve more quickly. High crystallinity also imparts longer resorption time. Dense HAP blocks are brittle, but have high compressive strength. It is widely accepted that materials with 150-200 μm pores are necessary for optimal bone ingrowth and angiogenensis, but higher porosity decreases strength [12].

1.3.2. Ceramic-Polymer Composite Bone Grafts

While pure ceramic alloplasts possess strength, fatigue resistance, and bioactivity; they are much more brittle than natural bone. High stiffness causes ceramic alloplasts to weaken under tensile or shear loading, limiting their applications to either coatings or low weight bearing applications [42]. One method to improve the mechanical properties of ceramic bone grafts is to combine them with a polymer into a composite. By distributing a discontinuous phase of ceramic particles within a continuous polymer matrix, the polymer reduces the elastic modulus and becomes reinforced by the strength of the ceramic particles [42].

This mimics the composition of natural bone. Bone is a well-established natural composite whose structure enables the functional demands of locomotion, protection, support of an upright stance [43]. The composite structure of bone permits an effective transfer of stress between the matrix phase (collagen) and the reinforcing phase (CdHAP nanocrystallites) [43].

A few ceramic-polymer bone grafts are currently in clinical use (Table 1.4). Another ceramic-polymer bone graft called Cortoss® (Orthovita: Malvern, PA, U.S.A.) is in commercial use in Europe. Cortoss® consists of bioactive glass, barium boro-aluminosilicate glass, and amorphous silica particles suspended in a methacrylate matrix consisting of bisphenol-a-glycidyl dimethacrylate, bisphenol-a-ethoxy dimethacrylate, triethylene glycol dimethacrylate. It does not have FDA approval for use in the U.S.A., and is currently undergoing clinical trials.

A criticism to using methacrylate based polymers like those in Cortoss® and Bioplant® is that they are non-degradable [17]. Additionally, these polymers release a significant amount of heat during polymerization (e.g. setting). There are also concerns in using polylactic acid and

Table 1.4: FDA approved ceramic-polymer composite bone alloplast products

Graft Name	Manufacturer	Material Description
Bioplant®	Sybron Dental Specialties: Newport Beach, CA, U.S.A.	Copolymer of polymethylmethacrylate (PMMA) and polyhydroxyethylmethacrylate (PHEMA) with layers of barium sulfate and calcium hydroxide
Biogran®	3i: Palm Beach Gardens, FL, U.S.A.	Silica gel surrounded by a calcium phosphate shell
BIORCI™-HA	Smith and Nephew Endoscopy: Andover, MA, U.S.A.	Screw consisting of polylactic acid (PLA) and hydroxyapatite
COLLAXO™	Smith and Nephew Endoscopy: Andover, MA, U.S.A.	Screw consisting of poly(DL lactide-co-glycolide) and calcium carbonate

poly(DL lactide-co-glycolide) polyesters which are found in BIORCI™-HA and COLLAXO™. While these polymers are absorbable, they release a massive amount of acidic products (e.g. lactic and glycolic acid) as they degrade [44]. These products significantly accumulate beyond clearing rate when these polymers are used in orthopaedic applications, increasing the probability of a serious inflammatory response [44].

1.4. Bacterial Cellulose

Cellulose is a polysaccharide consisting of β-(1,4) glucan sugars connected by glycosidic linkages (Figure 1.6). As the primary component of plant cell walls, cellulose is the most abundant natural polymer in the world with an estimated 10^{10}-10^{11} tons produced each year [45]. Certain bacterial species, namely *Gluconacetobacter spp.,* possess the ability to secrete pure cellulose in the form of a hydrogel [46]. Though identical in chemical composition, the structure and physical properties of plant and bacterial cellulose differ greatly.

The main function of plant cellulose is to provide structure for the vegetable fibers. Plant cellulose is generally associated with other biopolymers such as hemicellulose and lignin to form a laminate. Extracting cellulose requires harsh chemical processes, such as treatment with sulfur dioxide, sodium hydroxide, and bleaching agents. This often causes the cellulose to lose strength.

Produced in a pure form, bacterial cellulose (BC) does not have to be isolated with extensive chemical treatment. The bacteria naturally synthesize the cellulose into a crystalline

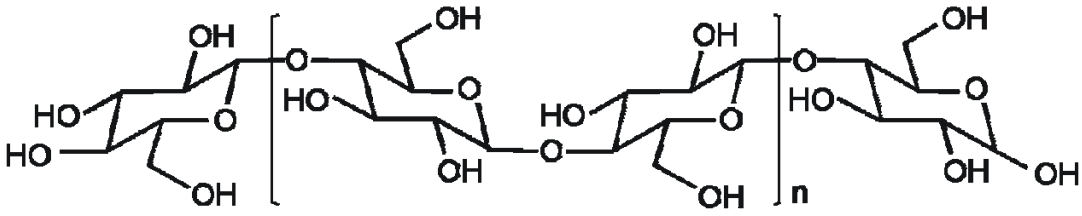

Figure 1.6: Chemical structure of cellulose chain

three-dimensional network. *Gluconacetobacter spp.* extrude cellulose subfibrils with a ~1.5 nm width which crystallize into nanofibrils that in turn bond together to form ribbons that are typically 3-4 nm thick, 70-80 nm wide, and 1-9 μm long. The ribbons twist and overlap to form parallel crystal lattice planes which stack on top of each other to form the thickness of the pellicle, a gel-like membrane [46]. Cellulose has an abundance of hydroxyl groups which permits extensive hydrogen bonding. As BC fibrils are up to 200 times finer than plant cellulose fibrils, it contains a higher density of inter- and intrafibrillar hydrogen bonds which gives the cellulose its network structure [47]. Nishiyama *et al.* performed a thorough structural analysis of cellulose I_α which is the main crystal component of bacterial cellulose [48]. Their results conclude that cellulose I_α has two alternative hydrogen bonding networks (Figure 1.7).

Hydrogen bonding enables the BC to hold water in its interstitial spaces allowing immense water retention [49]. Water makes up 99.8% of the total volume of the matrix with pure cellulose comprising the remaining 0.2% [50]. Hydrogen bonding also grants the cellulose high strength. Nishi *et al.* claimed that dried BC has the highest Young's Modulus (15-30 GPa) ever known in two-dimensional organic materials [49].

Though BC has been used as a food source ("nata-de-coco") in the Philippines for many years, additional uses for this biopolymer have emerged. Due to its high strength, dried BC is used in acoustic diaphragms for speakers and headphones (Sony Corporation: Tokyo, Japan). Modified bacterial cellulose and BC composites have been developed for fuel cell applications [51], while other composites are being investigated for electronic materials [52,53].

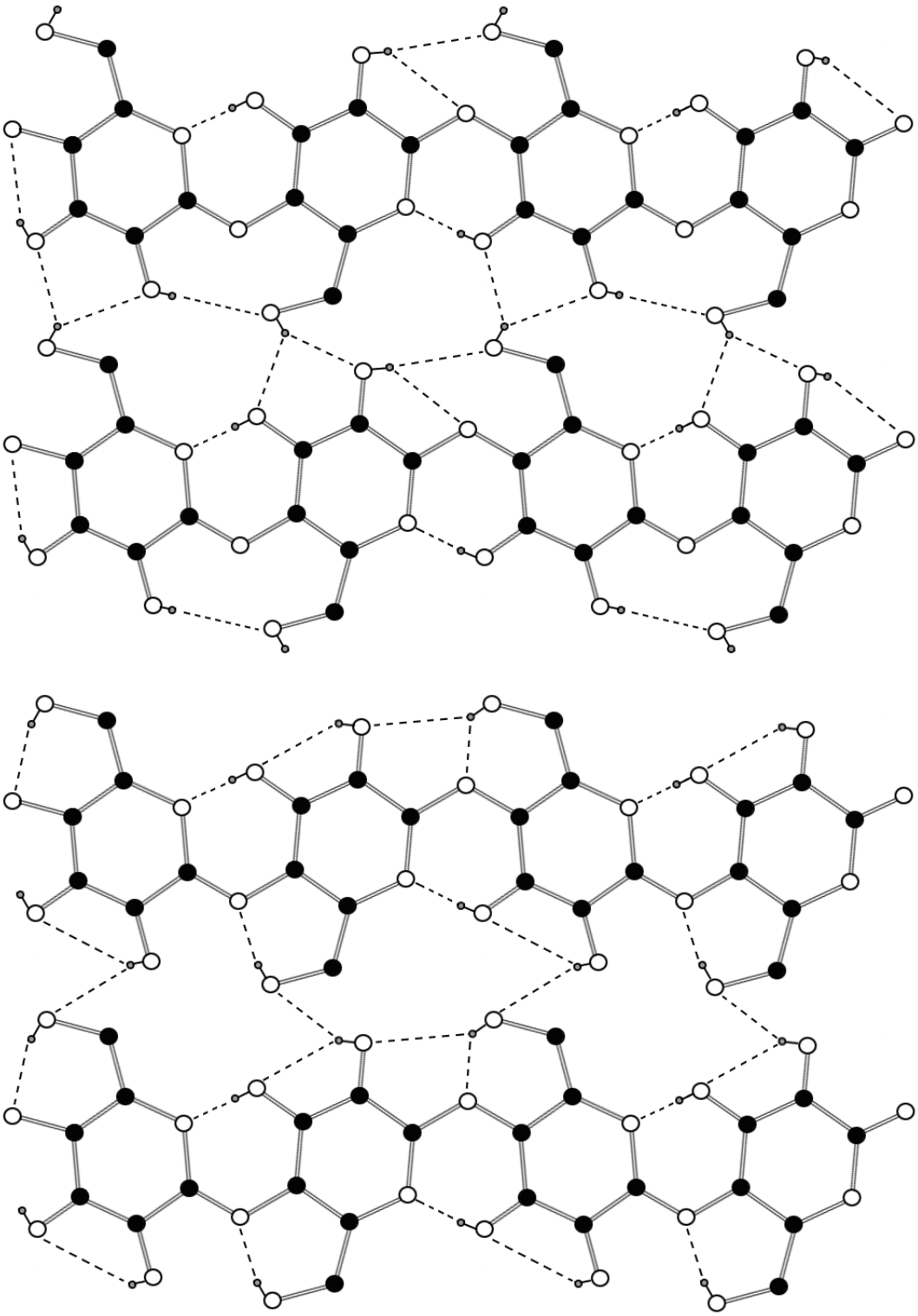

Figure 1.7: Two alternative hydrogen-bonding patterns of cellulose I_α as determined by Nishiyama *et al.* [adapted from reference 48]

1.4.1. Bacterial Cellulose in Medicine

Plant cellulose has been an established biomaterial for many years. It is a biocompatible polymer employed in the production of dialysis membranes, drug coatings, and blood coagulants, and many other products [54].

With the benchmark of plant cellulose, BC is currently being investigated for a variety of medical applications including tissue substitution. A tissue substitute should mimic the structure of natural extracellular matrices and be composed of biocompatible materials conducive to appropriate cell attachment and proliferation [55]. Collagen is the most ubiquitous extracellular matrix component and is found in almost every type of tissue including skin, ligament, muscle, cartilage, and bone. All of these tissues are composed of collagen fibrils which range in diameter from 50-500 nm [56]. The nanofibril matrix of bacterial cellulose mimics the structure and scale of collagen fibrils indicating its great potential for use as a biomaterial [57].

The BC hydrogel is also very hydrated and porous like living tissue. Hydrogels allow the permeation of water, metabolic products, and chemical signals in the aqueous physiological environment [58]. Because 99.8% of the cellulose mass is water, and the 0.2% cellulose that is present is an inert polysaccharide, bacterial cellulose is relatively pure.

Watanabe *et al.* found that modified bacterial cellulose was comparable to tissue culture dish as a substrate for mammalian cell adhesion [59]. Paul Gatenholm's group have studied the use of bacterial cellulose as a tissue engineering scaffold for cartilage and blood vessels [57,60]. It was found that chondrocytes grew better on unmodified bacterial cellulose compared to tissue culture dish and calcium alginate [60]. The mechanical properties of BC were determined to be similar to that of the carotid artery and smooth muscle cells were able to adhere, proliferate, and migrate into the BC scaffold [57]. Additionally, the candidate's master's thesis work showed that osteoblasts adhered and proliferated on bacterial cellulose indicating its potential for bone substitution [61].

The *in-vivo* biocompatibility of bacterial cellulose has been demonstrated as well [62-66]. When implanted subcutaneously in rats, Helenius *et al.* found that fibroblasts infiltrated BC and it

did not elicit inflammation, incur giant cells, or cause fibrotic capsulation [62]. Klemm *et al.* had positive *in-vivo* results with their product BASYC® which consists of hollow tubes of bacterial cellulose [63]. It was determined that BASYC® could successfully be used as blood vessel and nerve replacements [63]. Novaes *et al.* and Mello *et al.* found that BC could be used to substitute periodontal tissues [64] and the dura mater [65] in dogs. A recent rabbit *in-vivo* study concluded that a double network hydrogel consisting of bacterial cellulose and polyacrylamide gel had the appropriate properties to substitute cartilage [66].

One of the most promising medical applications of bacterial cellulose is in wound healing [67]. Bacterial cellulose dressings are an effective treatment for severe body burns, diabetic ulcers, abrasions, and lesions. A skin substitute based on BC called XCell® (Xylos Corporation: Langhorne, PA, U.S.A.) has been approved by the Food and Drug Administration and is currently on the market [47]. XCell® is a high performance dressing which maintains the moisture balance in the wound to speed up healing and epithelialization [47].

1.4.2. Oxidized Cellulose

A major limitation of using bacterial cellulose as a tissue substitute is the inability of cellulose to degrade in mammalian systems. Humans lack the enzyme necessary to cleave the β-1,4 glycosidic bonds between glucose residues in the cellulose polymer. An ideal tissue substitute should stimulate appropriate cell ingrowth, degrade as new tissue is produced, and then be safely resorbed by the body.

Various approaches have been employed to make cellulose susceptible to degradation in vivo [68]. These include treatment with nitrogen dioxide, periodic acid, chromic acid, hypochlorite, and alkaline hypobromite [68]. Chemical modification of cellulose fibrils using oxidizing agents has been shown to increase the biodegradability of this material. Some oxidants, such as chromic acid and alkaline hypobromite, tend to only react with amorphous regions and crystallite surfaces of cellulose and disrupt the physical structure of cellulose, often reducing it to powder [68]. In contrast, oxidizing reagents such as periodic acid and nitrogen dioxide are able to

penetrate and react with crystalline as well as amorphous regions of cellulose. They also have a significant advantage over other oxidizing agents in that minimize degradation and retain the mechanical and morphological properties of the starting material [68].

Surgicel™ is a commercially available hemostat used for a variety of surgical procedures (Ethicon, Inc.: Somerville, NJ, U.S.A.) [69]. It is produced by reacting regenerated plant cellulose with nitrogen tetroxide under controlled conditions which converts the primary hydroxyl group of cellulose into a carboxylic acid [68,70] (Figure 1.8). Several studies have explored the use of Surgicel™ for other medical applications including treatment of skin graft donor sites [71] and to supplement cartilage grafts [72]. Interceed® (Ethicon, Inc.: Somerville, NJ, U.S.A.) is another commercial FDA-approved product consisting of nitrogen tetroxide-oxidized regenerated cellulose which is used during gynecological pelvic surgery to reduce the incidence of postoperative pelvic adhesions [73]. Microdispersed cellulose oxidized with nitrogen tetroxide is found in the over-the-counter first-aid product, Seal-On™ (Alltracel Pharma Ltd: Dublin, Ireland), which is a hemostatic dusting powder used to treat cuts, abrasions, lacerations, or burns [74]. In a study by Dias and Peplow, it was reported that plant cellulose oxidized with nitrogen dioxide had the capacity to heal bone defects with complete replacement by lamellar bone at 6-8 weeks [75].

Aside from the highly corrosive and poisonous properties of nitrogen tetroxide, it also initiates many side reactions which produce additional reaction products, functional groups, and/or side chains [70]. These side reactions are difficult to control and can profoundly affect the properties of the product [68]. Conversely periodic acid (HIO_4) specifically reacts with molecules that have adjacent hydroxyl groups [76]. When applied to cellulose, the C2-C3 bond in the glucose residue is cleaved and the adjacent hydroxyl groups are converted to aldehydes producing dialdehyde cellulose (DAC) (Figure 1.9) [76]. There is evidence that DAC hydrolyzes at pH 7.4 into glycolic acid and 2,4-dihydroxybutyric acid [77]. These are natural metabolic products found in mammalian systems and can be safely excreted from the body [77].

Periodate oxidation has been performed on several types of cellulose including cotton linters [78], microcrystalline cellulose [79], cellulose powder derived from cotton [80], cellulose

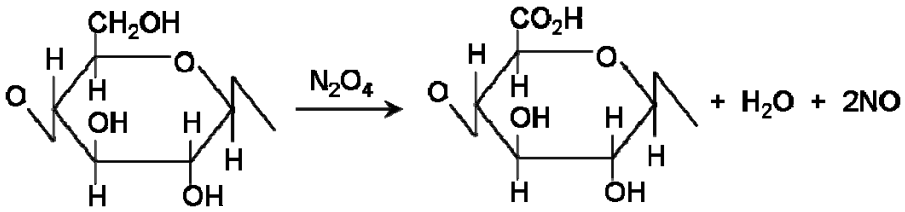

Figure 1.8: Oxidation of cellulose by nitrogen tetroxide [adapted from reference 68]

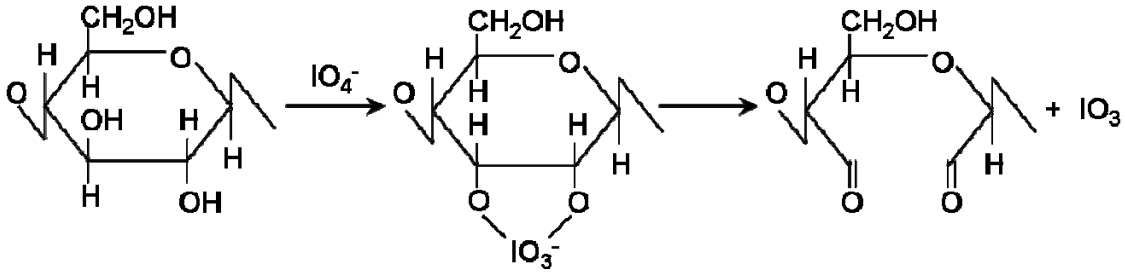

Figure 1.9: Periodate oxidation of cellulose [adapted from reference 68]

powder from beech wood pulp [80], and crystalline cellulose isolated from *Cladophora* sp. algae [76]. Regenerated plant cellulose has also been oxidized using periodate [77, 81]. Laurence *et al.* studied the effectiveness of periodate oxidized cellulose regenerated by the viscose process (CRVox) as a hemostat for osseous environments [77]. It was found that CRVox was a superior hemostat over Surgicel™ in bony sites, however bone only formed on the outlying areas of both implants with granulation tissue filling the central zones after one month [77].

1.4.3. Mineralized Bacterial Cellulose for Bone Substitution

Many synthetic and natural hydrogels undergo calcification after physiological implantation. While calcification can result in dystrophic failure of medical devices such as heart valves or vascular grafts, the deposition of calcium phosphate minerals is desirable for osseous or dental biomaterials [82]. In this dissertation, a composite consisting of calcium-deficient hydroxyapatite deposited in bacterial cellulose is proposed for use as a bone graft alloplast. Another embodiment consisting of oxidized bacterial cellulose with calcium-deficient

hydroxyapatite is presented whose degradation properties may be more suitable for bone replacement.

It was reported that bacterial cellulose had the capacity to initiate the formation of calcium-deficient hydroxyapatite in the candidate's master's thesis [61] and U.S. Patent Application [83]. In both of these documents, it was reported that apatite could be precipitated in bacterial cellulose by several techniques including: (i) incubation of BC in aqueous $CaCl_2$ followed by incubation aqueous Na_2HPO_4, (ii) incubation of BC in aqueous $CaCl_2$ followed by incubation in aqueous K_2HPO_4, (iii) incubation of BC in aqueous $CaCl_2$ followed by incubation in aqueous $Na_5P_3O_{10}$, (iv) incubation of BC in aqueous $Ca(OH)_2$ followed by incubation in aqueous Na_2HPO_4, (v) incubation of BC in simulated body fluid, (vi) incubation of phosphorylated BC in aqueous $CaCl_2$, (vii) incubation of phosphorylated BC in aqueous $CaCl_2$, (viii) incubation of phosphorylated BC in aqueous $CaCl_2$, (ix) incubation of phosphorylated BC in aqueous $Ca(OH)_2$, (x) incubation of phosphorylated BC in simulated body fluid, and (xi) incubation of phosphorylated BC in aqueous $Ca(OH)_2$ followed incubation in simulated body fluid. One of these mineralization techniques, incubation of BC in aqueous $CaCl_2$ and then in aqueous Na_2HPO_4, was thoroughly characterized and studied for this dissertation [84]. Another variation is reported entailing the mineralization of periodate oxidized bacterial cellulose by incubation in aqueous $CaCl_2$ and aqueous Na_2HPO_4.

Since the publication of the candidate's master's thesis and patent application, four related articles have been published regarding the formation of hydroxyapatite-bacterial cellulose composites. Bodin *et al.* surface modified the BC by ozone-induced graft polymerization of acrylic acid, pre-soaked the modified BC in $Ca(OH)_2$, then incubated it in simulated body fluid [85]. SEM showed the formation of crystals around the BC fibrils which had a calcium to phosphate ratio of 1.5, but the identification of the mineral was never confirmed [85]. Hong *et al.* mineralized BC by presoaking it in 0.1 M $CaCl_2$ followed by incubation in simulated body fluid. SEM showed the formation of spherical particles which had penetrated into the BC matrix. X-ray diffraction (XRD) identified the particles as 20 nm crystallites of calcium-deficient hydroxyapatite. FTIR showed that the hydroxyapatite was carbonate substituted [86]. A similar study by the

same group first phosphorylated the BC then incubated it in 0.1 M $CaCl_2$ and simulated body fluid [87]. This modification caused the calcium to deposit as a fiber coating as opposed to discrete spherical particles. The crystal phase was identified as hydroxyapatite by XRD and FTIR confirmed carbonate substitution [87]. A last study by Nge and Sugiyama added carboxylate groups to BC by either culturing the bacteria in the presence of carboxymethyl cellulose salt (BC-CMC) or by oxidizing the cellulose with TEMPO (2,2,6,6-tetramethylpyperidine-1-oxyl) (BC-TEMPO) [88]. The native BC, BC-CMC, and BC-TEMPO were incubated in 0.1 M $CaCl_2$ followed by immersion in simulated body fluid. Globules formed in all of the samples, though the size depended on the modification. TEM showed that the globules were composed of thin filmed flakes which ranged in size from 60-140 nm [88]. FTIR showed the presence of an HPO_4^{2-} and carbonate groups indicating the mineral was carbonated calcium-deficient hydroxyapatite. FTIR also showed that there was a precursor octacalcium phosphate phase [88].

This dissertation study explores the use of a mineralization technique not previously reported (use of aqueous calcium chloride and sodium phosphate dibasic), as well as the use of a degradable bacterial cellulose matrix which underwent periodate oxidation. The physical, chemical, and degradation properties of these composites are presented. Another chapter reports a statistical optimization of bacterial cellulose production using fractional factorial design. The last chapter offers a discussion of the possible clinical applications of BC-CdHAP in bone substitution.

Chapter 2

Materials and Methods

This chapter describes the techniques used to produce and analyze the materials. Sample synthesis entails the culturing of bacterial cellulose, either chemically modifying the bacterial cellulose (via periodate oxidation) or leaving it in its native form, and finally mineralizing the cellulose to produce calcium-deficient hydroxyapatite. The instruments and techniques used to characterize the samples described. Procedures used to determine the degradation properties of the chemically modified cellulose are also given.

2.1. Sample Preparation

2.1.1. Cultivation of Bacterial Cellulose

The bacterial strain *Gluconacetobacter hansenii (G. hansenii)* was obtained from the American Type Culture Collection (Manassas, VA, U.S.A.) (ATCC 10821) to synthesize bacterial cellulose. The bacteria were cultivated on Schramm-Hestrin Media [89]. This nutritional broth is made by combining the reagents listed in Table 2.1. An optimized formulation that substitutes mannitol for glucose was used in this study [90]. The reagents were dissolved in distilled/deionized water, the volume was brought up to one liter, and the pH was adjusted to 6.0 with the addition of hydrochloric acid or sodium hydroxide. The media was then autoclaved at 121°C for 20 minutes.

The bacteria were maintained on Mannitol 1 Agar as recommended by ATCC. The

Table 2.1: Reagents used in Schramm-Hestrin 2% Mannitol Medium [89]

Reagent	Amount
Mannitol	20 g
Yeast Extract	5 g
Peptone	5 g
Sodium Phosphate Dibasic	2.7 g
Citric Acid	1.15 g
Distilled Water	1 L

reagents in Table 2.2 were dissolved in water, and brought to a 1 L volume. The mixture was then autoclaved at 121°C for 15 minutes and poured into culture dishes. A preculture was then streaked onto the agar plates with bacterial inoculation loops. Without further maintenance, colonies began to form on the agar within a few days. New precultures were made by removing a single colony from the agar plates, placing it in 10 ml of Schramm-Hestrin medium, and allowing it to culture under agitated conditions provided by an orbital shaker.

For synthesis of cellulose pellicles, larger precultures were made by adding to 50-200 ml of Schramm-Hestrin medium to the 10 ml preculture in a flask under agitated conditions. After 2-3 days of incubation, the preculture was diluted in a 1:10 ratio with the prepared Schramm-Hestrin medium and poured into appropriate culture dishes. The static cultures were kept at room temperature (~23°C) for a given amount of time. The cellulose was then harvested by lifting the pellicle off the liquid surface with forceps.

2.1.2. Purification of Bacterial Cellulose

After harvesting, the cellulose pellicles were placed in a beaker of distilled/deionized water, put into a water bath, and heated to 90°C for 1-2 h to kill the bacteria. The pellicles were then rinsed with distilled/deionized water, and treated with a sodium hydroxide to remove bacterial debris and growth media components. The pellicles were incubated in 1% NaOH under agitated conditions at room temperature (23°C). Every 24 h, the NaOH was decanted and fresh solution was added. This process was continued until the cellulose was purified.

Polypeptides and DNA left in the bacterial cellulose after cultivation absorb in the UV

Table 2.2: Reagents used in ATCC Mannitol 1 Agar [protocol from the American Type Culture Collection: Manassas, VA, U.S.A.]

Reagent	Amount
Yeast Extract	5 g
Peptone	3 g
Mannitol	15 g
Agar	15 g
Distilled Water	1 L

region. Their presence in the used sodium hydroxide solution indicated the purity of the bacterial cellulose. The absorbance at 280 nm was read on Carey50 Spectrophotometer (Varian: Palo Alto, CA, U.S.A.) (Figure 2.1). A high absorbance indicated that the NaOH had removed a great deal of impurities. As the absorbance decreased with daily NaOH changes, it was assumed that less proteins and nucleic acids remained in the cellulose (Figure 2.1). An absorbance reading of approximately 0.05 - 0.10 signified that enough debris had been removed to deem the cellulose pure.

After the sodium hydroxide treatment, the cellulose was soaked in several changes of distilled/deionized water to neutralize the NaOH in the cellulose. The washings continued until the pH was near neutrality (pH ~7). The cellulose was stored in distilled/deionized water under refrigeration (5-10°C).

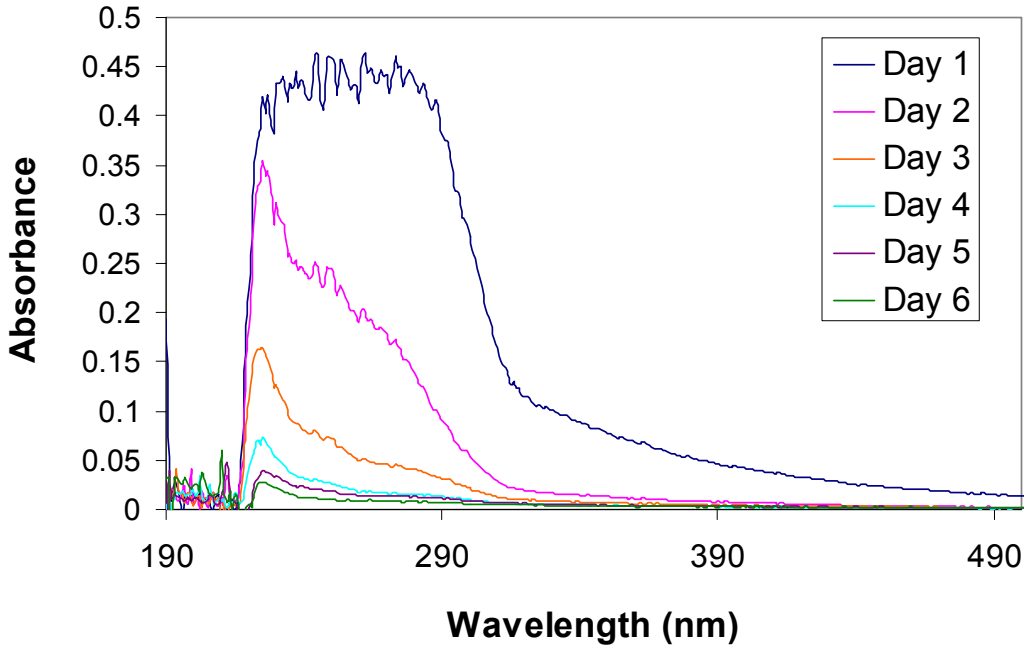

Figure 2.1: Absorbance scans of daily changes of 1% NaOH for bacterial cellulose purification

2.1.3. Oxidation of Bacterial Cellulose

To chemically modify the cellulose into a degradable hydrogel, periodate oxidation was performed. The method used was modified from a protocol given by Painter in 1988 [91]. In brief, cellulose pellicles were placed in a capped vessel containing 50 mM $NaIO_4$ in 5% n-propanol. The vessel was covered in aluminum foil and placed on an orbital shaker for 24 h at 23°C. The reaction was stopped by adding 0.5 ml of glycerol and placing the vessel in an ice bath. The cellulose was then purified with several changes of distilled/deionized water to remove the oxidation reagents.

2.1.4. Deposition of Calcium-Deficient Hydroxyapatite

Bacterial cellulose pellicles were deposited with calcium-deficient hydroxyapatite (CdHAP) by sequentially incubating the cellulose in aqueous calcium chloride followed by incubation in aqueous sodium phosphate dibasic [61,83]. Different amounts CdHAP can be deposited into the cellulose by varying the concentration of the $CaCl_2$ and Na_2HPO_4 solutions or varying the number alternating incubation cycles in the ion solutions. An incubation cycle is defined as suspending the BC for 24 h in 100 mM $CaCl_2$ (pH 4.83) under agitation followed by incubation in 60 mM of Na_2HPO_4 (pH 8.36) for 24 h under agitation at room temperature (23°C). After mineralizing the cellulose, it is rinsed in several changes of distilled/deionized water.

2.2. Material Characterization

2.2.1. X-Ray Diffraction

X-ray diffraction can be used to identify a substance based on its crystal structure, to measure the size and dimensions of the crystal, as well as qualitatively compare the degree of crystallinity of polymers [92]. Crystals have a distinct arrangement of atoms with specific distances between them. When an x-ray beam is directed through a crystal, the different interatomic distances produce a series of reflections to form a diffraction pattern [92]. The position and intensity of the diffraction peaks are indicative of the unique crystal structure [92].

Hundreds of thousands of diffraction patterns have been collected in the Powder Diffraction File (PDF) (International Centre for Diffraction Data File: Newtown Square, PA, U.S.A.). By using indexes like the Hanawalt Index, or database software such as Jade 6.0 (Materials Data Incorporated: Livermore, CA, U.S.A.), it is possible to identify a material based on its x-ray diffraction pattern.

Crystallite size, crystallite strain, and instrumental factors contribute to the broadening of x-ray diffraction peaks [92]. The Scherrer Equation is used to calculate the thickness of crystallites from the peak breadth:

$$t = \frac{0.9\lambda}{\beta \cos\theta} \qquad \{2.1\}$$

where t is the diameter of the crystallites, λ is the wavelength of the x-ray beam, and β is the corrected breadth of the broadened diffraction peak at a specific 2θ value [92]. Assuming that the peaks are Gaussian, β is calculated by:

$$\beta^2 = B^2 - b^2 \qquad \{2.2\}$$

Where B is the measured full width at half maximum (FWHM) of the peak and b is instrumental broadening. Instrumental broadening can be measured by evaluating a sample with a relatively large grain size [92].

In order for these thicknesses to hold true, several assumptions must be made. First, all the broadening in the peaks must come from particle size. The broadening cannot be attributed to crystal strain or inhomogeneity of the composition. Second, the peaks must be Gaussian in shape. By measuring the thickness in different plane directions from different peaks, the geometry and size of the crystallites can be determined [92]. Jade® software utilizes Scherrer's Equation to calculate the crystallite size of the CdHAP in each plane direction. The program referred to an XRD pattern of a single crystal silicon standard to correct for instrumental broadening.

Hydrated samples of BC and bacterial cellulose-hydroxyapatite composites (BC-CdHAP) were placed on a gel-dryer (Drygel Jr., Model SE540, Hoefer Scientific Instruments: San

Francisco, CA, U.S.A.) for 30 minutes at 80°C with application of a 68 kPa vacuum. The samples were mounted on a silicon zero-background holder. Room Temperature X-Ray Diffraction data were obtained on a Scintag PADV instrument operated at 45 kV and 40 mA with CuKα radiation and a Si(Li) Peltier-cooled solid state detector. Data were collected between 10 and 70° *2θ* at a scan rate of 1° *2θ*/min. Jade software was used to identify the crystal structure of the cellulose and calcium-deficient hydroxyapatite (CdHAP) by comparing patterns to those present in the Powder Diffraction File (PDF). Jade® was also used to calculate the CdHAP crystallite size for each reflection. JMP software (SAS: Cary, NC, U.S.A.) was used to determine statistical significance of the CdHAP crystallite sizes by performing Tukey-Kramer tests at $\alpha=0.05$.

2.2.2. Scanning Electron Microscopy

Scanning Electron Microscopy (SEM) provides three-dimensional quality surface images with excellent resolution and depth of field. During SEM, a focused high energy electron beam is scanned across a sample which causes secondary electrons to be emitted. A detector is used to measure the intensity of the secondary electron emission which is dependent on the sample's composition and geometry [93]. Surface topography can be observed under magnifications of up to 100,000x [93].

To produce samples to be analyzed with SEM, the samples were first lyophilized. Briefly, the hydrated samples were placed in a -80°C freezer for 24 h. They were then placed on a freeze-dryer (Refrigeration for Science: Island Park, NY, U.S.A.) where the water was pulled off at 40 Pa under -50°C refrigeration for 24 h. The samples were then mounted on carbon tape and sputtered with gold on a Spi Module Sputter Coater (Spi Supplies: Westchester, PA, U.S.A.) at 20 mA for 10 s. They were then analyzed on a LEO 1525 Scanning Electron Microscope (Zeiss: Oberkochen, Germany) at various accelerating voltages as indicated in the micrographs. To obtain the 50,000x magnification on the BC-CdHAP sample, it was mounted on silver paint and sputtered with gold at 20 mA for 15 s. Energy Dispersive Spectra was also used to determine the calcium to phosphorus ratio of the hydroxyapatite particles.

2.2.3. Fourier Transform Infrared Spectroscopy

Infrared (IR) spectroscopy is an established method used in material characterization. When molecules interact with infrared light, vibrations occur at specific frequencies based on the arrangement of atoms and their interconnecting bonds [94]. In order to be infrared active, the absorbed radiation must induce a change of dipole in the molecule. The IR spectra shows the frequencies at which the various functional groups in the sample absorbs the radiation and the intensities of the absorptions. IR spectroscopy can be used to determine a material's chemistry and structure orientation. It can also provide information regarding bonding interaction. Identification of materials can be achieved by comparing the data to reference spectra. IR spectroscopy can be used to characterize the bulk specimen, the surface, or used perform depth profiling [93].

Hydrated samples of BC and BC-CdHAP were placed in a -80^{o}C freezer for 24 h and then granulated in a commercial blender for 1-2 minutes. The frozen powders were then lyophilized as indicated in the previous section and then further dried for 24 h in a vacuum oven (100°C at 68 kPa).

Approximately 1 mg of powdered sample was combined with 45 mg KBr powder and compressed into a pellet using a screw-type press. Fourier Transform Infrared Spectroscopy was performed on a BioRad FTS6000 Spectrometer (BioRad: Randolph, MA, U.S.A.). The spectra are the result of 256 scans collected with a resolution of 4 cm^{-1}.

Functional groups of the cellulose and hydroxyapatite were identified as absorption bands at specific wavenumber positions. Changes in the chemical environment of functional groups within a sample are reflected in its IR spectrum. If the characteristic bands of a specific functional group shift to lower wavenumbers, it can be concluded that there is a change in the molecular environment, such as the formation of a new inter or intramolecular chemical bond [95].

Deconvolution of the cellulose hydroxyl bands (3600-3100 cm^{-1}) was performed with the use of PeakFit® v.4.6 software (SeaSolve Software: Framingham, MA, U.S.A.). PeakFit® separated overlapping peaks by statistically fitting peak functions to the data set. The program

initially placed peaks by finding local maxima in a smoothed data stream. Hidden peaks were found by searching for local minima within the smoothed second derivative of the data set. The deconvolution procedure then used a Gaussian-Lorentzian response function with a Fourier deconvolution and fitting algorithm. This ensured that the sharpened peaks had the equivalent area of the overlapping peaks [96].

2.2.4. Mechanical Testing

The mechanical behavior of a biomaterial is of great importance. Mechanical testing provides information as to how the appliance will perform under load when it is placed in the physiological environment. Once implanted, the material will be exposed to various stresses and strains. Successful biomaterials often mimic the mechanical properties of the substituted tissue. During tensile testing, an applied stress causes a change in the original length of the specimen which can be measured to find the strain. These parameters can then be used to calculate the elastic modulus, ultimate tensile strength, and elongation. The elastic modulus, or Young's Modulus, is an inherent material property which characterizes stiffness or brittleness in a given direction.

During testing in tension mode, a specimen is subjected to a continually increasing uniaxial tensile force while simultaneous observations are made of the elongation of the specimen. The stress-strain curve is constructed from the load elongation measurements. A typical stress-strain curve is shown in Figure 2.2. The engineering stress (σ_e) is found by measuring the load (F) and dividing it by the original area of the cross-section of the specimen (A_o):

$$\sigma_e = F / A_o \qquad \{2.3\}$$

The engineering strain (ε_e) is determined by dividing the elongation of the sample ($L - L_o$) by the original gage length L_o where L is the gage length after elongation:

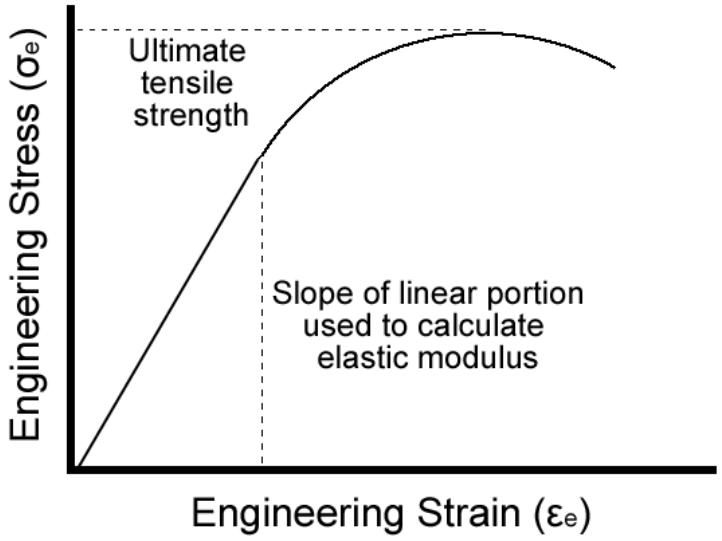

Figure 2.2: Stress-strain curve of a material showing how the elastic modulus and ultimate tensile strength can be extrapolated

$$\varepsilon_e = (L - L_o) / L_o \qquad \{2.4\}$$

The engineering stress is related to the engineering strain by the engineering modulus of elasticity (E_e) as is shown:

$$\sigma_e = E_e \varepsilon_e \qquad \{2.5\}$$

The engineering modulus of elasticity is typically determined from the stress strain curve by calculating the slope of the initial linear portion of curve (Figure 2.1). The ultimate tensile strength is the peak stress of the engineering stress-strain curve (Figure 2.1).

2.3. In-Vitro Degradation Study of Oxidized Cellulose Samples

The degradation behavior of the samples was analyzed by immersion in HEPES buffer. Originally, phosphate buffered saline (PBS) was used. However, it was determined that the salt

in PBS adsorbed onto the oxidized cellulose membranes and could not be easily removed by washing in water. Low-salt HEPES buffer consisting of 25 mM HEPES and 75 mM NH_4Cl was selected to reduce salt adsorption. The solution was titrated to pH 7.4 using hydrochloric acid or sodium hydroxide and then subsequently autoclaved at 121°C for 20 minutes.

Two separate studies were carried out on two identical batches of samples. The samples consisted of native bacterial cellulose (BC), oxidized bacterial cellulose (oxidized BC), native bacterial cellulose with calcium-deficient hydroxyapatite (native BC-CdHAP), and oxidized bacterial cellulose with calcium-deficient hydroxyapatite (oxidized BC-CdHAP). All of the samples were autoclaved in HEPES buffer. Each of the samples were then placed in a sterile 50 ml conical tube and added to 5 ml of sterile HEPES buffer. Half of the samples from each group were placed in a 37°C Forma Scientific Water Jacketed Incubator (Thermo Electron Corporation: Waltham, MA, U.S.A.) for static incubation. The remaining samples from each group were placed in a 37°C controlled environment incubator shaker (New Brunswick Scientific Co., Inc.: Edison, NJ, U.S.A.) for dynamic incubation.

In the first study, the buffer was removed from the samples and analyzed at specific time points. Every other day, the samples were separated from the HEPES buffer by centrifugation at 3500 x g for 15 min. The absorbance of the supernatant was measured on a Cary spectrophotometer (Varian: Palo Alto, CA, U.S.A.) from 190-350 nm. Five milliliters of fresh sterile HEPES buffer was then added to each sample of cellulose before being returned to the incubators. The samples were removed from the HEPES buffer after fourteen days of incubation, rinsed in several changes of distilled/deionized water, dried, and weighed.

The initial set-up of the second study was identical to the first. The only difference was that the samples remained in the original buffer throughout the 14 days. At the end of the 14 day period, the buffer was removed from the sample by centrifugation at 3500 x g for 15 min. The buffer was then analyzed for degradation products: free carbohydrate and glycolic acid.

2.3.1. Identification of Degradation Products

It has been reported that dialdehyde cellulose hydrolyzes at pH 7.4 to yield glycolic acid and 2,4 dihydroxybutyric acid [77,78,97]. A proposed mechanism is shown in Figure 2.3. It has also been theorized that dialdehyde cellulose also breaks down into smaller soluble molecules (free carbohydrate) [77]. To verify whether periodate oxidized bacterial cellulose produced these degradation products, the separated buffer obtained in the second in-vitro degradation study was spectrophotometrically analyzed. These assays had previously been used to analyzed the degradation products of periodate oxidized regenerated plant cellulose [77].

To determine the amount of free carbohydrate, 0.5 ml of the separated HEPES buffer was added to 2 ml of 0.16% anthrone (Fisher Scientific: Waltham, MA, U.S.A.) in concentrated sulfuric acid. Standard solutions (0.5 ml volume) with concentrations ranging from 5-100 µg/ml glucose in low salt HEPES buffer were also added to 2 ml of the anthrone solution. The mixtures were vortexed, incubated at 90°C for 20 min, then allowed to cool. The absorbances of the solutions were measured at 587 nm using HEPES buffer as a blank. The concentrations were determined from a standard curve.

To determine the amount of glycolic acid released, 0.2 ml of the HEPES supernatant was

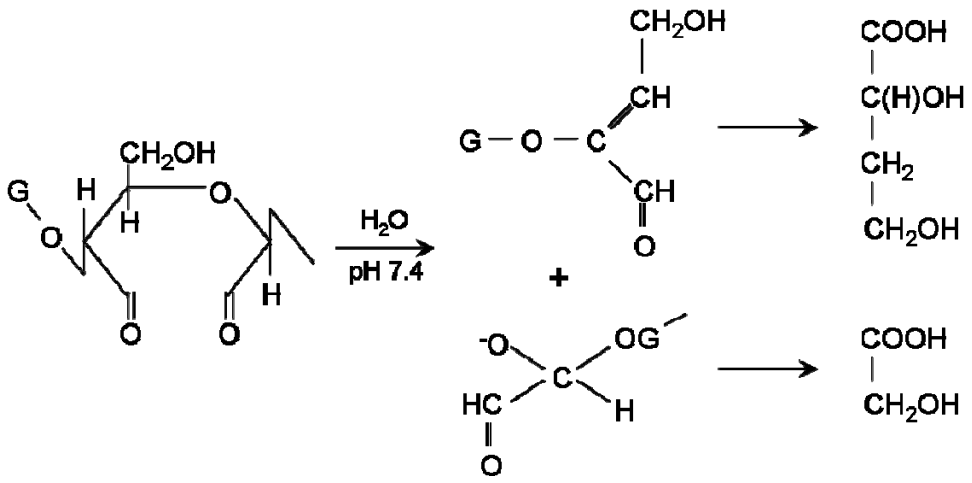

Figure 2.3: Proposed degradation mechanism of dialdehyde cellulose into 2,4-dihydroxybutyric acid and glycolic acid [adapted from reference 97]

added to 2 ml of 0.01% 2,7-dihydroxynaphthalene (Acros Organics: Geel, Belgium) in concentrated sulfuric acid. Standard solutions (0.2 ml volume) with concentrations ranging from 5-100 µg/ml glycolic acid (Fisher Scientific: Waltham, MA, U.S.A.) in HEPES buffer were also added to 2 ml of the 2,7-dihydroxynaphthalene solution. The mixtures were vortexed, incubated at 90°C for 20 min, then allowed to cool. Four ml of 4 N H_2SO_4 was then added to each sample, vortexed, and allowed to cool. The absorbances of the solutions were measured at 530 nm using HEPES buffer as a blank. The concentrations were determined from a standard curve.

Chapter 3

Statistical Determination of Optimal Bacterial Cellulose Production from *Gluconacetobacter hansenii*

In order to produce a medical product based on bacterial cellulose, it is necessary to culture the bacteria on a large scale. Cultivation conditions must be optimized to produce the most cellulose in the shortest amount of time at the most economical cost. Many different nutritional media components and environmental conditions have been used in cellulose production. The aims of this study were to statistically design and execute an approach whereby several different parameters could simultaneously be tested to determine the best conditions for cellulose growth from *Gluconacetobacter hansenii* (ATCC 10821). In this work, it was of interest to determine the effect of five culture factors. The results of this study were published in the journal *Letters in Applied Microbiology* [90].

3.1. Selection of Factors to Test

Glucose is typically used as a carbon source in nutritional growth medium for the bacteria [89]. However, a sugar alcohol such as mannitol may stimulate increased cellulose production. The bacteria contain alcohol dehygrogenase enzymes capable of oxidizing alcohol to produce electrons which could provide an energy “boost” for the bacteria [98]. Presence of ethanol in the culture may likewise enhance cellulose synthesis. Previous studies have shown that the addition of ethanol removes non-cellulose producing bacterial cells which increases overall cellulose synthesis [99]. When the bacteria produce the cellulose, they also produce acidic byproducts such as gluconic acid and acetic acid. This decreases the pH and may eventually inhibit cellulose production. By using a more basic medium, this acidity may be decreased and more cellulose may be produced. Culturing at a higher temperature may also provide better production. It has been shown that at lower temperatures, the bacteria are not as mobile which may hinder the metabolic activity necessary for cellulose production [100]. Cellulose production may also be enhanced by increasing the ratio of bacterial inoculant to the nutritional growth

medium. By having larger populations of bacteria, a greater amount of cellulose could be produced. For these reasons, this study analyzed the effects of five culture factors: carbon source in the growth medium, ethanol addition to the growth medium, inoculation ratio of the bacteria, pH of the growth medium, and temperature on the amount of cellulose produced by *G. hansenii*.

3.2. Fractional Factorial Design

In experiments with two or more independent factors, factorial design can be used to plan experiments such that the effect of the factors and each factor interaction can be elucidated. In full factorial design, every value of every factor appears with each value setting of every other factor to test all possible combinations. For example, if there are n factors and each factor has two possible values, a full factorial analysis would have 2^n sample runs. Factorial design is especially suited for the investigation of the optimal growth conditions of microbial cultures since the interactions of several independent factors may all play a role. However, this technique can be unwieldy if the system contains several factors. Fractional factorial design is better suited for a system of five or more factors. It is a more efficient approach which uses only a portion of the combinations which are selected to ensure each two factor interaction is represented. Since five culture condition parameters were tested in this study, a five-factor, half-fraction resolution five design was used to construct the experiment. This design permits the estimation of each of the main effects and the two factor interactions if it is assumed that three factor interactions and higher are negligible.

JMP Software (SAS: Cary, NC, U.S.A.) was used to design this five-factor, resolution-five fractional factorial design. The five factors investigated were carbon source, ethanol addition, inoculation ratio, pH, and temperature. Table 3.1 shows the 16 specific culture conditions designed to assess all main effects and two-factor interactions. Three replicates of each culture condition were made for a total of 48 cultures.

Table 3.1: Culture conditions of each fractional factor combination and subsequent mass of cellulose produced [90]

Carbon Type	Ethanol Present	Inoculation Ratio	pH	Temperature (°C)	Mean Cellulose Mass (mg)
Glucose	No	1:10	5.5	30	3.2
Glucose	No	1:10	6.5	20	13.5
Glucose	No	1:5	5.5	20	12.8
Glucose	No	1:5	6.5	30	6.1
Glucose	Yes	1:10	5.5	20	5.3
Glucose	Yes	1:10	6.5	30	4.0
Glucose	Yes	1:5	5.5	30	3.0
Glucose	Yes	1:5	6.5	20	8.8
Mannitol	No	1:10	5.5	20	16.0
Mannitol	No	1:10	6.5	30	7.9
Mannitol	No	1:5	5.5	30	12.7
Mannitol	No	1:5	6.5	20	14.8
Mannitol	Yes	1:10	5.5	30	8.6
Mannitol	Yes	1:10	6.5	20	14.3
Mannitol	Yes	1:5	5.5	20	13.5
Mannitol	Yes	1:5	6.5	30	7.0

3.3. Bacterial Cellulose Synthesis

After the cultures were inoculated, visible clouds of cellulose began to form within one to two days. A thick “skin” of cellulose formed on the surface of the media within 5-7 days (Figure 3.1). After purifying the samples as described in section 2.2.1, the cellulose is a transparent and slippery gelatinous pad (Figure 3.1). To analyze the dry mass of the cellulose, the samples were dehydrated by using a gel-dryer (Drygel Jr., Model SE540, Hoefer Scientific Instruments) for 30 minutes at 80°C with application of a vacuum (20 inches Hg). The dry weight of each sample was then measured and recorded in milligrams (mg) on a Mettler AE200 electronic analytical balance (Mettler-Toledo: Toledo, OH, U.S.A). Box plots of the resulting cellulose yields are given in Figure 3.2.

3.4. Statistical Analysis of Results

JMP software was used to fit the data to a statistical model which included all the main factors and each two-factor interaction. Due to the efficient planning of the experiment, there were no degrees of freedom for error since it was a resolution five design. A normal plot of the

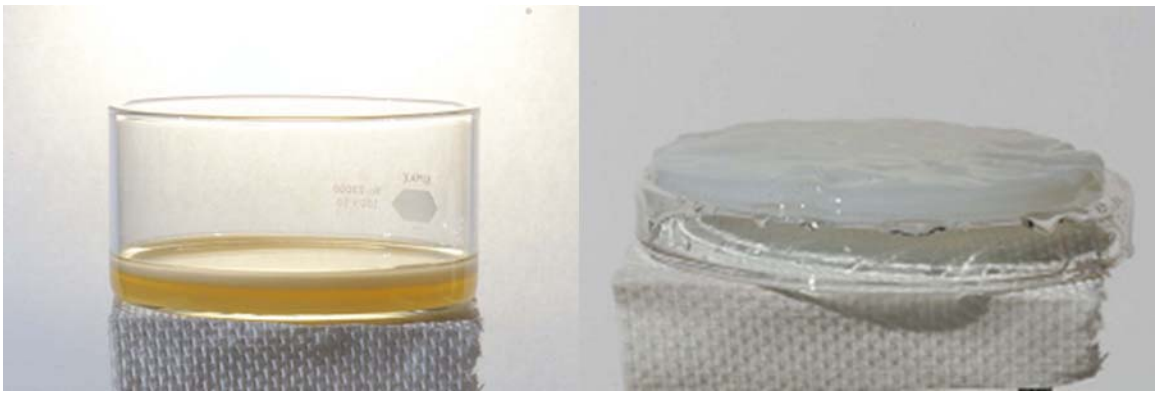

Figure 3.1: Bacterial cellulose culture consisting of Gluconacetobacter hansenii in Schramm-Hestrin Medium (left) with purified bacterial cellulose (right)

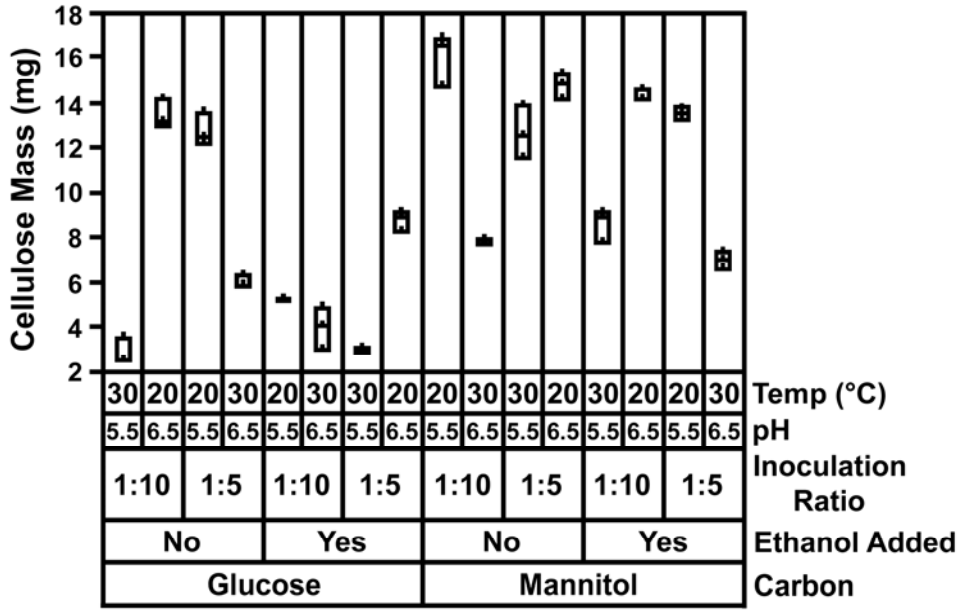

Figure 3.2: Mass of cellulose produced under different culture conditions [90]

parameter estimates of the model was used to screen the effective factors (Figure 3.3). If all the effects were random, the entire plot would follow a straight line with a slope equal to the standard error. Effects that deviate substantially from this line indicate significant factors and are shown in Figure 3.3. It was seen that temperature, ethanol addition, and carbon source were active factors in cellulose production since their factor values significantly deviated from the normal line. The plot also indicated that the carbon source – pH factor interaction may also have actively contributed to cellulose growth.

To investigate these phenomena further, a new model was constructed using these active factors and the active factor interaction: carbon source, ethanol addition, temperature, and the carbon source – pH factor interaction. Although pH itself is not an active factor, it was included in this model to ensure a hierarchical model since its interaction with carbon was significant. Removing the insignificant inoculation ratio factor and remaining two-factor interactions allowed estimation of error in the model and permitted the use of an analysis of variance test to assess the significance of the factors (Table 3.2). The null hypothesis of this test

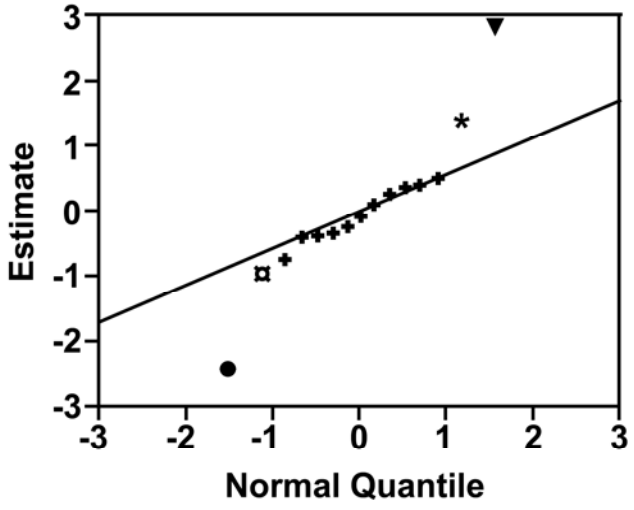

Figure 3.3: Normal plot of the parameter estimates obtained from the fitted model. The following factors and factor interaction deviate from the straight line and contribute significantly to the model: 20°C Temperature (▼), No Ethanol (*), Glucose and pH 5.5 Interaction (¤), Glucose (●) [90]

Table 3.2: Effects test for the reduced statistical model [90]

Source	Degrees of Freedom	Sum of Squares	F-Ratio	Prob > F
Carbon	1	92.00007	34.8132	0.0002
Ethanol Added	1	31.26674	11.8314	0.0063
Temp (°C)	1	133.98062	50.6988	<.0001
pH	1	0.09507	0.0360	0.8534
Carbon*pH	1	13.87563	5.2506	0.0449

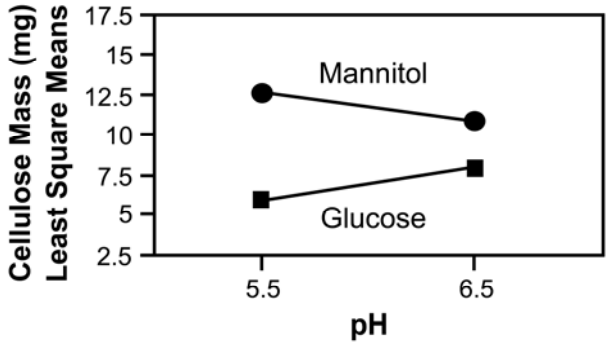

Figure 3.4: Least squares means plot of the carbon source and pH factor interaction [90]

was that the included factors and two-factor interactions do not contribute to the model. This was tested by calculating the F- ratio on JMP. Briefly, the F-ratio was obtained by dividing the mean square for the effect by the mean square for error. The mean square for the effect was calculated by dividing the sum of squares for each effect by its degrees of freedom. If the p-value (Prob > F) of the F-ratio was less than the alpha level (α = 0.05), the null hypothesis would have been rejected proving that the parameter contributed a significant effect. From Table 3.2, it can be concluded that carbon source, ethanol addition, and temperature were all very significant factors in the model. Though pH on its own was not significant, it was seen that the pH interaction with carbon was significant.

The specific dependence of carbon on pH was elucidated by constructing a least squares means plot of the carbon – pH interaction given in Figure 3.4. It is seen that the average cellulose produced for both carbon sources at pH 5.5 is relatively the same as that at pH 6.5. However, there is significant variation between cultures grown on glucose at pH 5.5 and 6.5 and

between cultures grown on mannitol at different pH values. Bacteria cultured on a glucose medium at pH 6.5 produced more cellulose than at pH 5.5. A medium containing mannitol shows the opposite behavior, causing the bacteria to produce more cellulose at the lower pH 5.5 as opposed to 6.5.

The model can be fitted with the following mathematical equation:

$$y = 9.47 - 2.40\, x_1 + 1.40\, x_2 + 2.89\, x_3 - 0.08\, x_4 - 0.93\, x_1 x_4 \qquad \{3.1\}$$

where y is the mass of cellulose produced in milligrams and x_1, x_2, x_3, and x_4 are dummy variables representing carbon source, ethanol addition, temperature, and pH factors respectively. The values of x_1, x_2, x_3, and x_4 are as follows:

Carbon source: $x_1 =$ { 1 for Glucose; -1 for Mannitol }

Ethanol added: $x_2 =$ { 1 for No; -1 for Yes }

Temperature: $x_3 =$ { 1 for 20°C; -1 for 30°C }

pH: $x_4 =$ { 1 for pH 5.5; -1 for pH 6.5 }

An illustrative example of how the model equation predicts cellulose growth for each of the factor values is given in Figure 3.5. It is seen that the most cellulose (17.02 ± 2.2 mg) would be produced using mannitol, with no ethanol, at a temperature of 20°C and a pH of 5.5. Though pH solely does not affect cellulose production, mannitol coupled with a pH of 5.5 produces significantly more cellulose than if it were at pH 6.5.

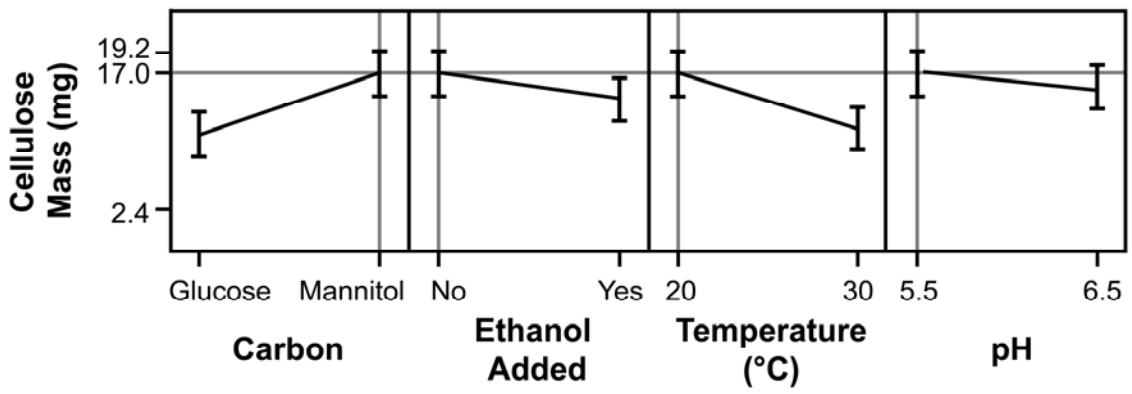

Figure 3.5: Predicted cellulose mass using the statistical model with a given a set of factor values [90]

3.5. Discussion and Conclusion

By planning the experiment using fractional factorial design, relevant data could be obtained using a smaller number of samples. Full factorial design for the five parameters would necessitate $2^5 = 32$ sample conditions. With three replicates, 96 samples would have to be made in all. While full factorial design would test every possible parameter combination, the experiment size would be large and not necessarily produce pertinent information. Fractional factorial design instead tests all two parameter combinations producing 16 sample conditions. With three replicates, only 48 cultures had to be made. Fractional factorial design reduced the number of samples by half while still obtaining statistically significant results.

By fitting the data to a statistical model, it was confirmed that carbon source, ethanol addition, and temperature are significant culture factors in the production of cellulose from this *Gluconacetobacter hansenii* strain. Though pH on average did not show an active effect, the carbon source – pH factor interaction did significantly affect cellulose production. When using mannitol, the optimal amount cellulose is produced at pH 5.5 while more cellulose is produced at pH 6.5 if glucose is used. The bacteria produced the most cellulose when cultured on mannitol, without ethanol, at 20°C, and at a pH of 5.5.

In *Gluconacetobacter spp.*, cellulose synthesis competes for glucose with glucose oxidation by the membrane-bound glucose dehydrogenase that supplies metabolic processes

with electrons. Repression of glucose oxidation by addition of ethanol or glycerol as an alternative electron source has been reported to increase cellulose yield [99]. These bacteria also contain membrane-bound alcohol and aldehyde dehydrogenases which can oxidize alcohol to acetic acid to obtain electrons [98]. Mannitol, a sugar alcohol, provided electrons for bacteria metabolism and stimulated a higher yield of cellulose compared to glucose which had been reported in a previous study [101]. It was predicted that presence of ethanol would likewise provide an energy source for the bacteria while they converted the carbon source to cellulose. Presence of ethanol increases cellulose production in shaken cultures by preventing the bacteria from forming a non-cellulose producing mutant [99,102]. Since static cultures do not normally produce the non-cellulose producing mutation, the ethanol did not show an appreciable effect in increasing cellulose production. This is verified by a previous study with another cellulose-producing strain, *Acetobacter xylinus,* which showed that ethanol had no significant effect on cellulose synthesis in static cultures [102].

The byproducts produced when glucose is oxidized by the bacterial enzymes also explain why each carbon source produced optimal cellulose yields at different pH values. As the membrane-bound glucose dehydrogenase oxidizes glucose, gluconic acid is produced and expelled into the medium. This can cause the pH to decrease to as low as 3 during cultivation [102] which may inhibit cellulose production. By having a more basic medium, the acidity is decreased which improves cellulose production. No acidification of the culture medium is observed during growth on mannitol. This is consistent with the metabolic pathway for mannitol assimilation reported for the closely related genus *Gluconobacter*, in which mannitol is oxidized to fructose [103], which is then assimilated by the bacteria following a second oxidation to 5-keto-D-fructose [104]. By precluding the formation of the sugar acid, the pH does not decrease drastically as with the glucose and cellulose growth is not inhibited.

It was suspected that a higher temperature may stimulate the bacteria to produce more cellulose. Hirai *et al.* showed that the bacteria are not as mobile at lower temperatures which may hinder the metabolic activity necessary for cellulose production [100]. However the converse

effect was proven to be true. The elevated 30°C temperature actually inhibited the cellulose production by *Gluconacetobacter hansenii* while the 20°C environment produced significantly more cellulose.

Inoculation ratio did not affect cellulose production as a factor or in a factor interaction. While it was expected that having a higher initial bacteria population in the culture would result in higher cellulose yields, there was no significant difference in the cellulose yields between the two inoculation ratios. It is possible that each of the bacteria populations either divided to a critical value once inoculated, or that the discrete amount of medium was a limiting factor causing the bacteria to decrease. In either case, it is likely the amount of bacteria in each culture equilibrated to approximately the same population number despite the initial inoculation ratio.

Fractional factorial design enabled an efficient study of the effect of five culture parameters on the production of cellulose from *Gluconacetobacter hansenii* (ATCC 10821). Using statistical analysis, it was proven that mannitol medium, without ethanol, cultured at 20°C and at a pH of 5.5 is more optimal for cellulose growth from this bacterial strain. While cellulose production was affected by the factors of carbon source, ethanol addition, and temperature; pH alone was not significant. However, the interaction between carbon source and pH did affect cellulose growth. This was attributed to the acidic byproducts produced by the bacteria when cultured on glucose media. Inoculation ratio was not a significant factor nor was it involved in any significant factor interactions. The statistical model was described by a mathematical equation which can predict cellulose yields given a set of factor values. These preliminary results have determined an advantageous factor coupling for optimized cellulose production by this microorganism.

Chapter 4

Analysis of Composites with Varying Amounts of BC-CdHAP

In this study, a series of bacterial cellulose-calcium-deficient hydroxyapatite composites were made with varying amounts of CdHAP. This was accomplished by increasing the number of sequential incubations of the BC in aqueous calcium chloride and sodium phosphate dibasic. The composites were characterized with X-Ray Diffraction (XRD), Fourier Transform Infrared Spectroscopy (FTIR), Scanning Electron Microscopy (SEM), and Electron Dispersive Spectroscopy (EDS). The results of this study were published in the journal *Biomaterials* [84].

4.1. Deposition of varying amounts of CdHAP in bacterial cellulose

Twenty-four bacterial cellulose pellicles were cultured as described in section 2.1.1. In brief, 24 six centimeter culture dishes were filled with 15 ml of inoculated Schramm-Hestrin medium and cultured for 31 days. The bacterial cellulose was then purified using the protocol in section 2.1.2.

Calcium-deficient hydroxyapatite (CdHAP) was formed in bacterial cellulose (BC) by performing alternating incubation cycles with calcium and phosphate solutions [61,83]. An incubation cycle is defined as suspending the cellulose pellicle in 100 mM $CaCl_2$ (pH 4.83) under agitation in an orbital shaker for 24 h (23°C), rinsing the BC briefly in distilled/deionized water, then transferring the pellicle to 60 mM Na_2HPO_4 (pH 8.36) under agitation for another 24 h (23°C). Six groups of four BC pellicles each were synthesized with zero, one, two, three, four, and five incubation cycles. The group with no incubation cycles (native cellulose) was used as a control.

Four replicates of each sample were made so that they could later be dried and weighed to determine the amount of CdHAP in each composite. It was assumed that approximately the same amount of cellulose existed in all the composites since they were synthesized under identical conditions. The mass of the CdHAP in the cellulose was determined by subtracting the

total composite weight from the average weight of the control cellulose group. CdHAP weight percentages were calculated by dividing the mass of the CdHAP by the total composite weight.

A homogenous white precipitate immediately formed throughout the bacterial cellulose matrix when it was placed the phosphate solution after incubation in aqueous calcium chloride. A picture of a cellulose pellicle that underwent three incubation cycles in 100 mM $CaCl_2$ and 60 mM Na_2HPO_4 compared to unaltered native bacterial cellulose is shown in Figure 4.1.

Three of each of the composites made according to the conditions in Table 2.4 were placed on a gel-dryer (Drygel Jr., Model SE540, Hoefer Scientific Instruments: San Francisco, CA, U.S.A.) for 30 minutes at 80°C with application of a 68 kPa vacuum. The dry weight of each sample was measured on a Mettler AE200 electronic analytical balance (Mettler-Toledo: Toledo, OH, U.S.A) and recorded in milligrams. It was assumed that approximately the same amount of cellulose existed in all the composites since they were synthesized under identical conditions. The mass of the CdHAP in the cellulose was determined by subtracting the total composite weight from the average weight of the control cellulose group.

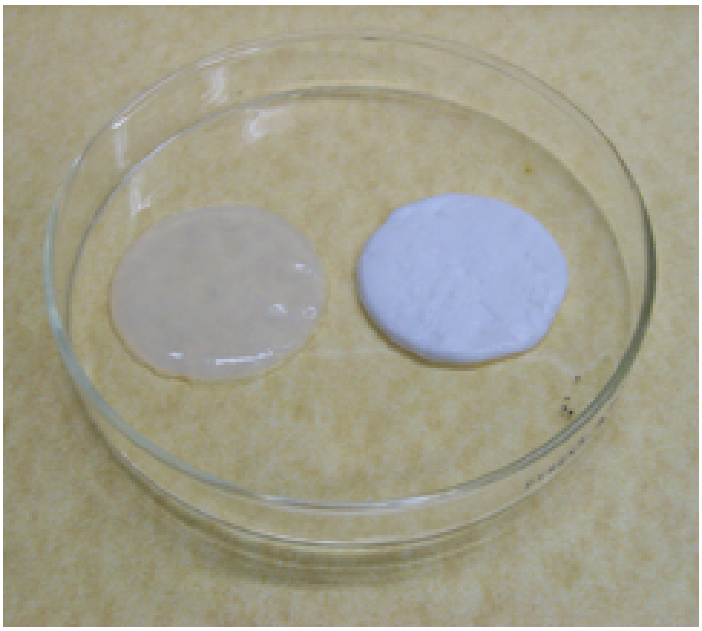

Figure 4.1: Comparison of unaltered bacterial cellulose (left) and cellulose after three incubation cycles in 100 mM $CaCl_2$ and 60 mM Na_2HPO_4 (right)

CdHAP weight percentages were calculated by dividing the mass of the CdHAP by the total composite weight. The dry weight of the composites and the mass of their respective hydroxyapatite components are shown in Figure 4.2. The composites appear to linearly increase in weight with the number of incubation cycles. The hydroxyapatite weight percentage of each composite is also shown in Figure 4.2. These weight percentages will be used to distinguish the composites.

4.2. X-Ray Diffraction

The X-Ray Diffraction patterns of the bacterial cellulose (BC) and cellulose composites (BC-HAP) are given in Figure 4.3. The control bacterial cellulose was identified as native cellulose (PDF#03-0289) and the characteristic peaks are indexed. The sharp peaks indicate that the cellulose is highly crystalline which has been previously reported [50,63].

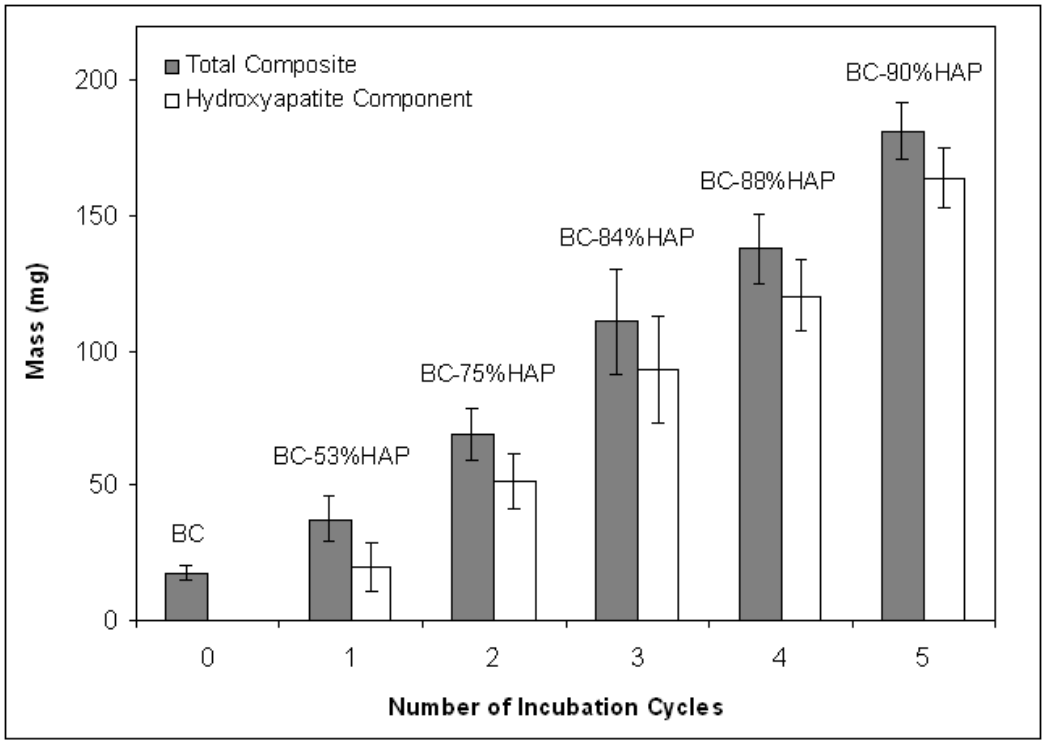

Figure 4.2: Mass of composites and hydroxyapatite components synthesized with increasing incubation cycles. Standard deviations were propagated to obtain error bars [84]

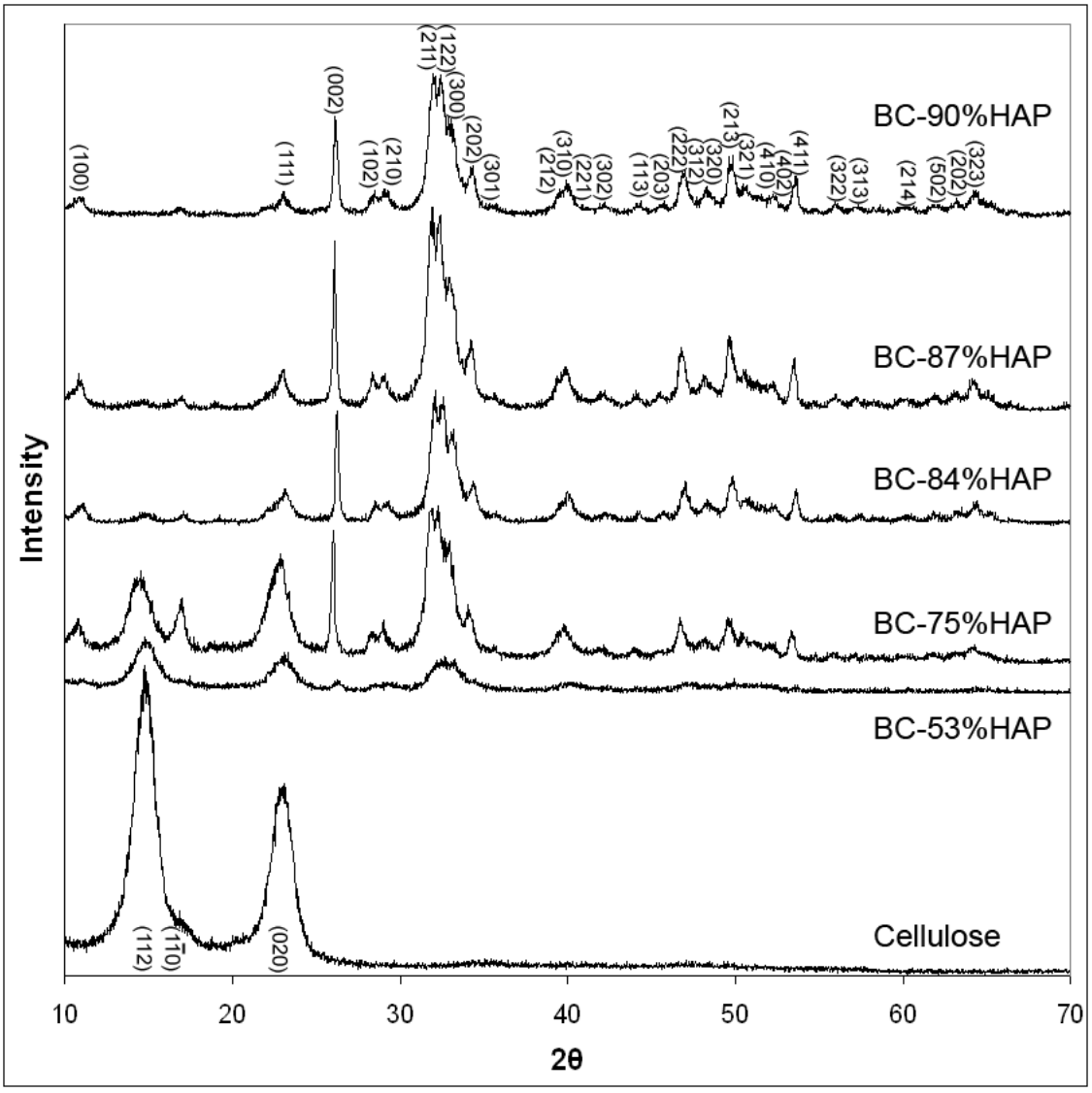

Figure 4.3: X-ray diffraction patterns of bacterial cellulose (BC) and bacterial cellulose-hydroxyapatite composites (BC-HAP). The characteristic HAP peaks are indexed at the top for BC-HAP 90% while the characteristic peaks of cellulose are indexed at the bottom [84]

The peaks for the BC-HAP composites are identified as calcium-deficient hydroxyapatite (CdHAP) (PDF#46-0905). The CdHAP crystallite peaks are indexed for BC-90%HAP (Figure 4.3). The low background of the composites indicates that the CdHAP is crystalline. The decrease in the intensity of the cellulose peaks in the patterns shows that CdHAP is the dominating component of the composite. The XRD pattern of the composite is very similar to the XRD pattern of bone apatite (Figure 4.4) [105].

Hydroxyapatite is the only thermodynamically stable calcium phosphate that exists in aqueous solution at a pH greater than 4.2 [35]. Since the cellulose was incubated in solutions with pH greater than 4.2 (100 mM $CaCl_2$ at pH 4.83 and 60 mM Na_2HPO_4 at pH 8.36), hydroxyapatite was the expected mineral to form. As was discussed in the introduction, physiological apatite is almost always calcium deficient compared to stoichiometric hydroxyapatite (sHAP) due to contact with a constant flow of trace ions. CdHAP is more favorable as a bone implant compared to sHAP due to quicker dissolution, surface modification, and bone bonding.

The CdHAP crystallite sizes of the composites for each reflection were measured for two samples of each group (Figure 4.5). The characteristic CdHAP peaks of BC-53%HAP were not substantial enough to obtain accurate crystallite dimensions and thus were omitted from Figure

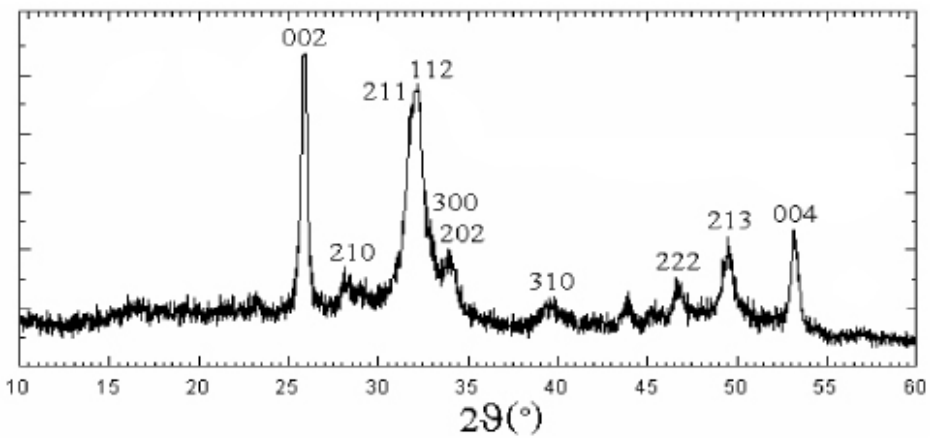

Figure 4.4: X-ray diffraction pattern of bovine cortical bone [adapted from reference 105]

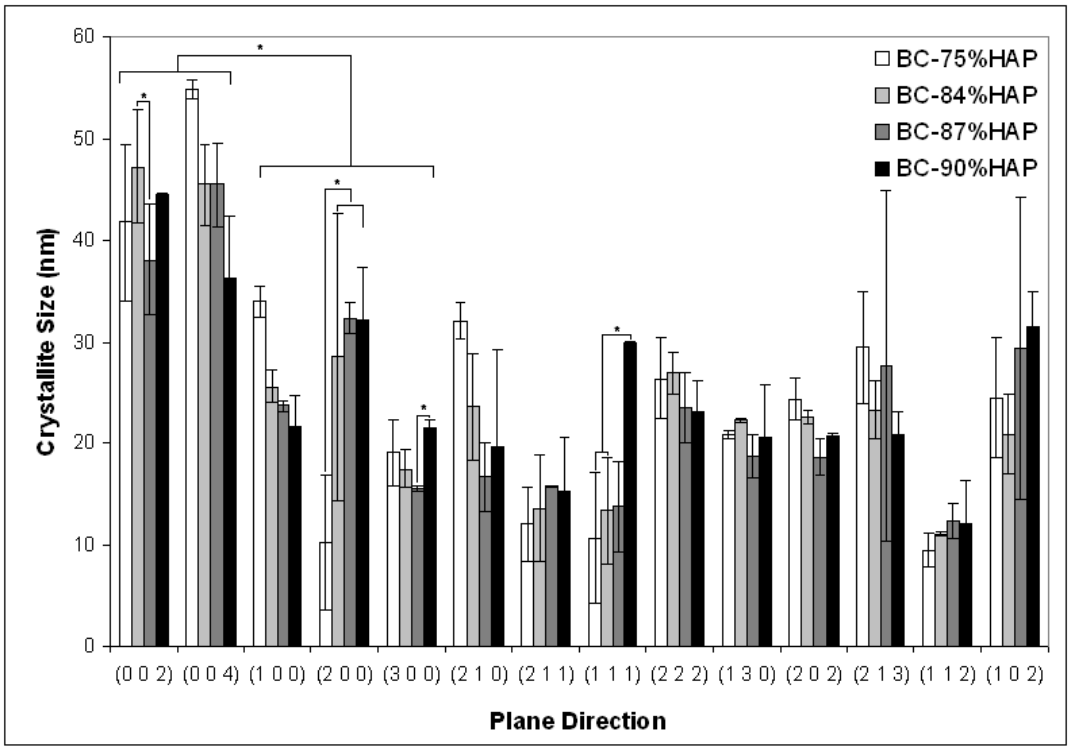

Figure 4.5: Hydroxyapatite crystallite sizes for various reflections. Standard deviations were propagated to obtain error bars. The crystallite sizes in the c-axis (002) and (004) are significantly larger than those in the a- and b-axes (100), (200), and (300) [84]

4.4. The crystallites were approximately 10-50 nm. The crystallite size of CdHAP in the composite was comparable to bone apatite crystallites which are 20-40 nm in length [106]. For the majority of the plane directions, the crystallite sizes of the composites did not vary significantly indicating that the CdHAP crystallites shared the same geometry regardless of the HAP volume percentage. Crystallite sizes amongst composites in the (002), (200), (300), and (111) plane directions showed some significant variation as shown in Figure 4.4.

It was determined that the average crystallite sizes of the (002) and (004) reflections (the c-direction) were significantly larger than the (100), (200), and (300) reflections (the a and b-directions). This indicates that the crystallites were elongated in the c-axis. The crystallites consistently shared these dimensions regardless of the mass of CdHAP in the composite. This geometry mimics actual bone apatite crystals which are anisotropic and elongated in the c-axis [105].

4.3. Scanning Electron Microscopy and Electron Dispersive Spectroscopy

Scanning Electron Micrographs of the BC and the BC-HAP composites at various magnifications are shown in Figures 4.6, 4.7, and 4.8. The crystalline lattice composed of fine cellulose fibrils is seen in Figures 4.7.a and 4.8.a. In BC-53%HAP, it is observed that regular 1 μm hydroxyapatite clusters had formed within the cellulose fibrils (Figure 4.6.b). These orderly clusters become rough and irregular in shape as more hydroxyapatite is formed in the matrix (Figures 4.6.c and 4.6.d). At 1000x, the hydroxyapatite particles in the BC-53%HAP composite appear as uniform solid spheres (Figure 4.6.b). At higher magnifications (Figure 4.7.b and 4.8.b), it is seen the spheres are not solid, but are instead composed of discrete crystallites. Figure 4.9 shows images of the BC-53%HAP sample at various magnifications. Higher magnifications reveal that the clusters are composed of six-sided plates characteristic of the hexagonal crystal structure of hydroxyapatite (Figures 4.9.c and 4.9.d).

It has been reported that round “calcospherites” like those seen in the BC-53% composite mimic that seen during physiological calcification process in the cartilage of human fetal growth

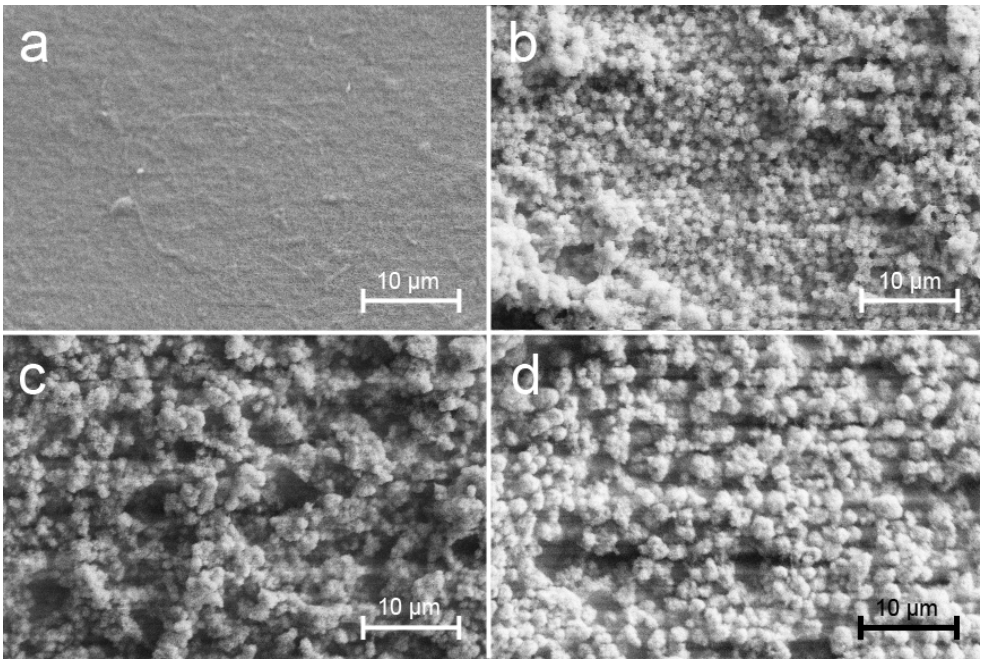

Figure 4.6: SEM images of (a) BC, (b) BC-53%HAP, (c) BC-75%HAP, (d) BC-90%HAP at 1000x. A 5 kV accelerating voltage was used for all of the samples

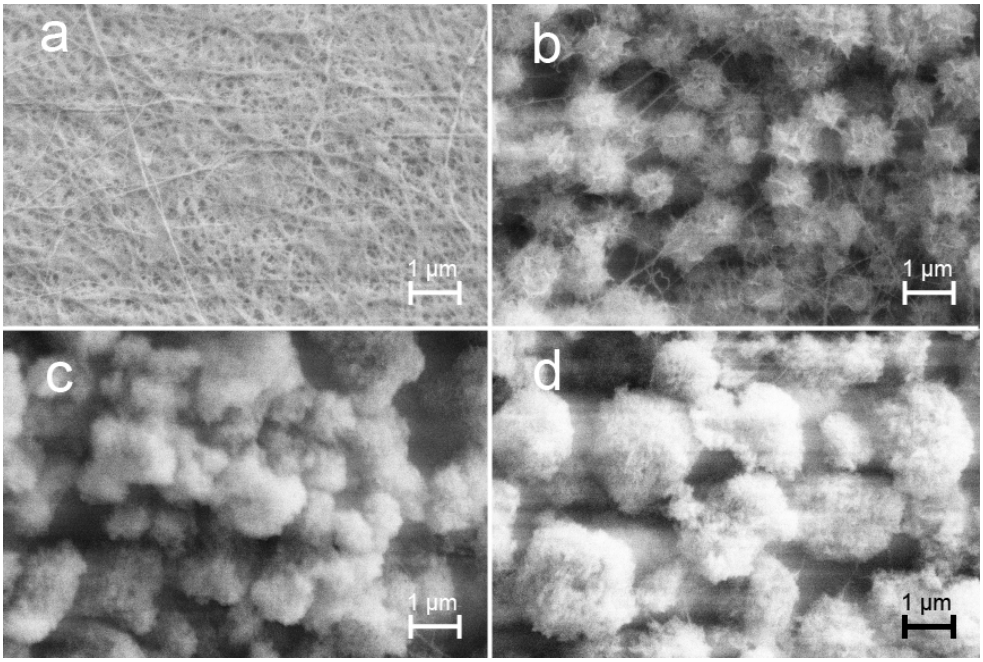

Figure 4.7: SEM images of (a) BC, (b) BC-53%HAP, (c) BC-75%HAP, (d) BC-90%HAP at 5000x. A 3 kV accelerating voltage was used for the BC sample and a 5 kV was used to image the BC-HAP composites [84]

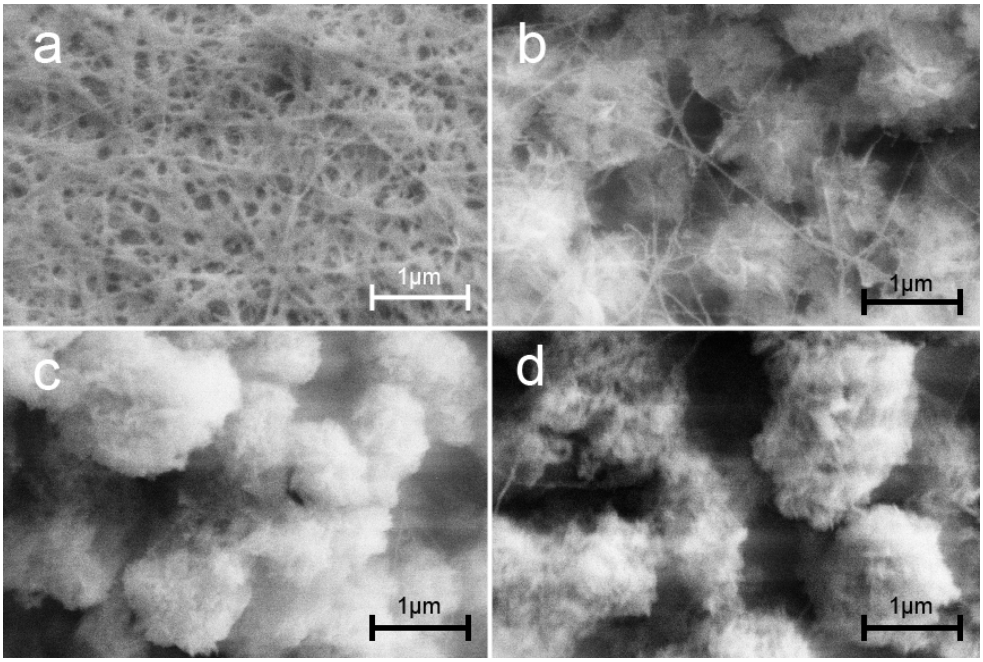

Figure 4.8: SEM images of (a) BC, (b) BC-53%HAP, (c) BC-75%HAP, (d) BC-90%HAP at 10000x. A 3 kV accelerating voltage was used for the BC sample and a 5 kV was used to image the BC-HAP composites

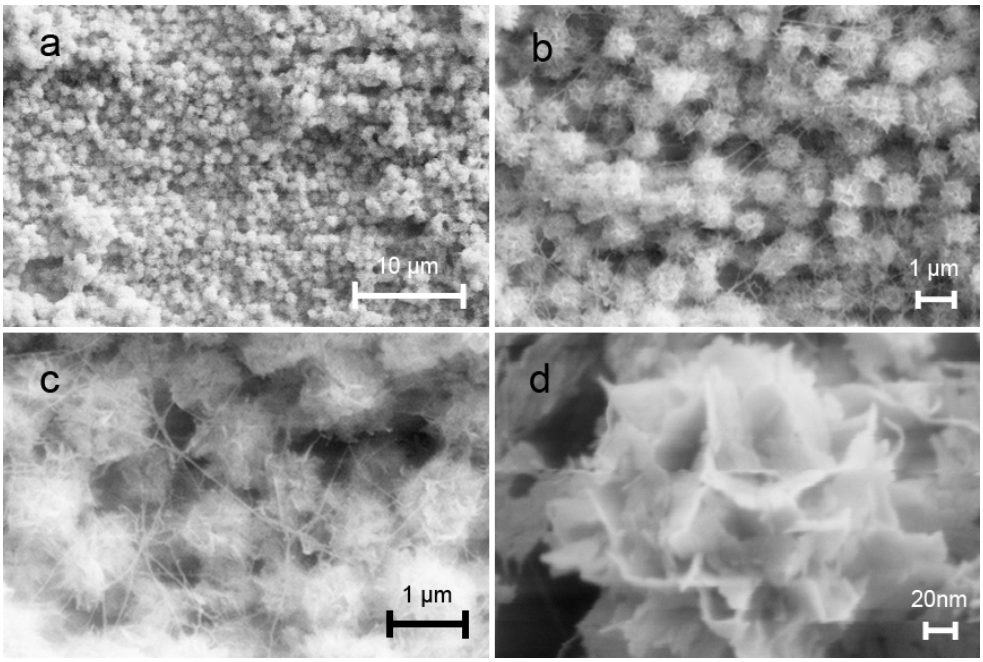

Figure 4.9: SEM images of bacterial cellulose-hydroxyapatite composite (BC-53%HAP) at (a) 1000x, (b) 5000x, (c) 10,000x, (d) 50,000x. A 5 kV accelerating voltage was used for the 1000x-10,000x images while 2 kV was used to for the 50,000x image [84]

plates and in woven bone [107]. It has also been claimed that the calcospherite morphology is favorable for adhesion and spreading of osteoblasts [107].

The Energy Dispersive Spectra of four of the samples are given in Figures 4.10. The calcium to phosphorus ratios varied between 1.46-1.54 demonstrating that the hydroxyapatite is calcium deficient. The ratios did not depend on the weight percentage of the calcium-deficient hydroxyapatite. Traces of sodium and carbon also appear in the spectra. The Na_2HPO_4 used during mineralizing may have left some sodium residue, while the carbon present is attributed to the cellulose.

4.4. Fourier Transform Infrared Spectroscopy

The chemical structure of the cellulose chain is shown in Figure 1.6 and the IR spectrum for native bacterial cellulose is given in Figure 4.11. Each of the IR peaks can be attributed to characteristic chemical groups in the cellulose structure. Cellulose is composed of sugar

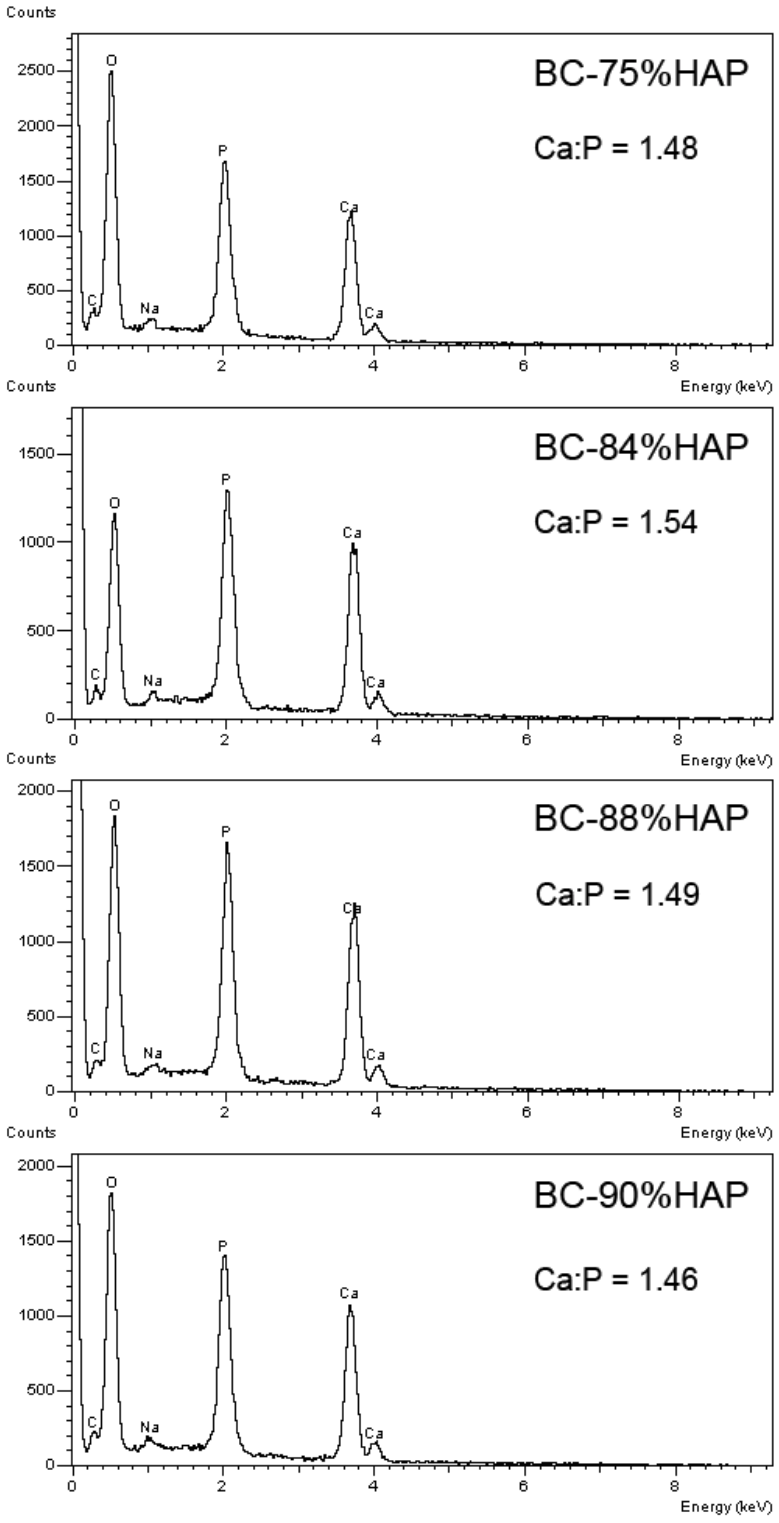

Figure 4.10: Energy Dispersive Spectra of the BC-HAP composites and the respective calculated calcium to phosphorus ratios

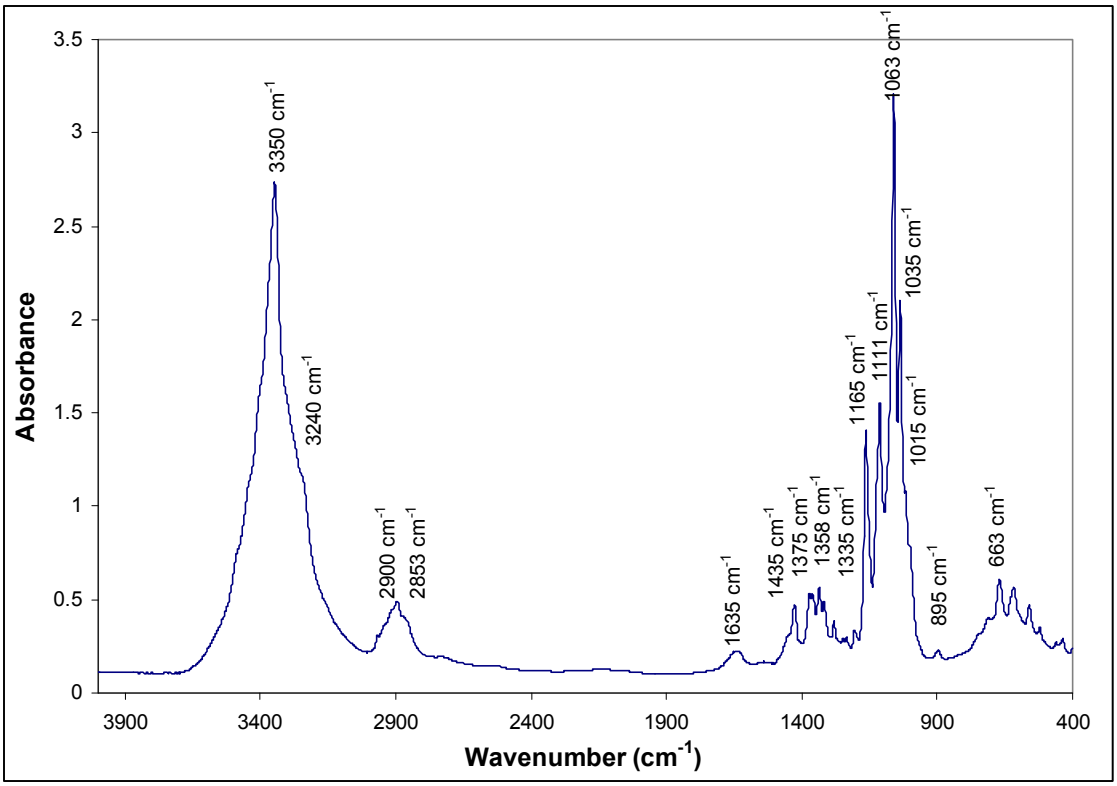

Figure 4.11: IR spectrum of native bacterial cellulose

residues (pyranose rings) connected by glycosidic (C_1-O-C_4) linkages. There is also an abundance of hydroxyl groups in the cellulose polymer (31.5% of its total weight). The characteristic absorption bands of cellulose are given in Table 4.1.

The IR spectrum of the composite BC-90% HAP is given in Figure 4.12. The IR spectrum of stoichiometric HAP from Rehman and Bonfield [108] is given in the inset of Figure 4.12 as a comparison. It is seen that the cellulose backbone is hardly distinguishable indicating that hydroxyapatite is the dominant component in the composite. The characteristic IR absorption bands of hydroxyapatite corresponding to phosphate and hydroxyl vibrational modes are identified in Table 4.2.

Phosphate has four phosphate vibrational modes: ν_1 is the symmetric stretching mode, ν_2 is the symmetric bending mode, ν_3 is the antisymmetric stretching mode, and ν_4 is the out-of-plane bending mode [109]. The unique doublet of the ν_4 phosphate vibrational mode gives

Table 4.1: Characteristic bands of native bacterial cellulose

Frequency	Relative Intensity	Assignment	Ref
3350 cm^{-1}	Strong	OH Stretching (involved in intermolecular hydrogen bonding)	[110]
3240 cm^{-1}	Medium	OH Stretching (characteristic of hydrogen bonding in cellulose Iα structure)	[110]
2900 cm^{-1}	Medium	CH Stretching	[111]
2853 cm^{-1}	Medium	CH_2 Symmetric Stretching	[111]
1653 cm^{-1}		Absorbed H_2O	[111]
1435 cm^{-1}	Medium	CH_2 Symmetric Bending	[111]
1375 cm^{-1}	Medium	CH Bending	[111]
1358 cm^{-1}	Medium	CH Bending	[111]
1335 cm^{-1}	Medium	OH in-plane bending	[111]
1165 cm^{-1}	Strong	Antisymmetric bridge COC stretching	[111]
1111 cm^{-1}	Strong	Antisymmetric in-phase ring stretching	[111]
1063 cm^{-1}	Strong	Skeletal vibrations involving C-O stretching	[111]
1035 cm^{-1}	Strong	Skeletal vibrations involving C-O stretching	[111]
1015 cm^{-1}	Medium	Skeletal vibrations involving C-O stretching	[111]
895 cm^{-1}	Weak	Antisymmetric out-of-phase ring stretching	[111]
663 cm^{-1}	Medium	OH out-of-plane bending	[111]

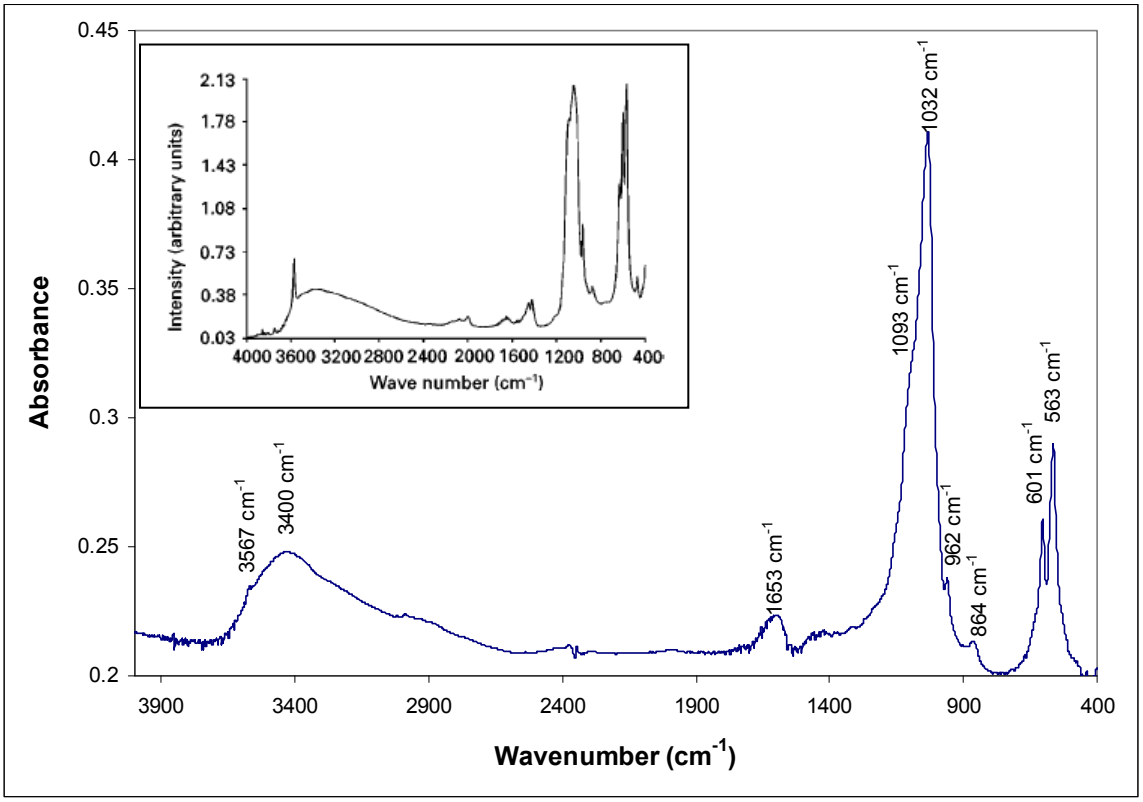

Figure 4.12: IR spectrum of hydroxyapatite cellulose (BC-90% HAP). Inset: IR spectrum of commercial stoichiometric hydroxyapatite powder [image taken from reference 108]

Table 4.2: Characteristic IR bands of calcium-deficient hydroxyapatite

Frequency	Relative Intensity	Assignment	Ref
3567 cm^{-1}	Strong	OH Stretching	[108]
3400 cm^{-1}	Broad	Absorbed H_2O	[108]
1653 cm^{-1}		Absorbed H_2O	[111]
1093 cm^{-1}	Very Strong	Phosphate (PO_4^{-3}) v_3 vibrational mode	[108]
1032 cm^{-1}	Very Strong	Phosphate (PO_4^{-3}) v_3 vibrational mode	[108]
962 cm^{-1}	Medium	Phosphate (PO_4^{-3}) v_1 vibrational mode	[108]
864 cm^{-1}	Weak	Hydrogen Phosphate (HPO_4^{-2}) vibrational mode	[112]
601 cm^{-1}	Very Strong	Phosphate (PO_4^{-3}) v_4 vibrational mode	[108]
563 cm^{-1}	Very Strong	Phosphate (PO_4^{-3}) v_4 vibrational mode	[108]

information about the HAP formation and will be discussed in a later section. The presence of the HPO_4 band at 864 cm^{-1} and the decrease in the hydroxyl band intensity at 864 cm^{-1} (in comparison to the stoichiometric HAP powder in given in the inset of Figure 4.12) indicates that this composite consists of calcium-deficient hydroxyapatite [108,112].

The IR spectra of the BC and BC-HAP composites are given in Figure 4.13. The absorbances of the phosphate peaks were graphed against the weight percent of hydroxyapatite in the composite (Figure 4.14). The absorbances were normalized by dividing the phosphate absorbance by the cellulose CH peak absorbance at 2905 cm^{-1}. This peak was chosen because its absorbance remains constant in all the samples since the amount of cellulose in the composite stays the same. This rise in absorbance correlates to the increased of concentration of hydroxyapatite as dictated by the Beer-Lambert Law. While the intensity of all the phosphate absorption bands increase with the concentration of HAP, the absorbance corresponding to the ν_3 modes exhibit more scatter than those corresponding to the ν_1 and ν_4 vibrational modes. The variation in the ν_3 modes may be attributed to the antisymmetric stretching of the dipole. Variation in band absorbance may also be due to small differences in the amount of material in the KBr pellets.

4.4.1. Deconvolution of the Hydroxyl Absorption Band

Even though the samples were dried in a vacuum oven at 100°C, a broad peak appears at 3400 cm^{-1} in the CdHAP IR spectra which is attributed to water absorption [108]. This

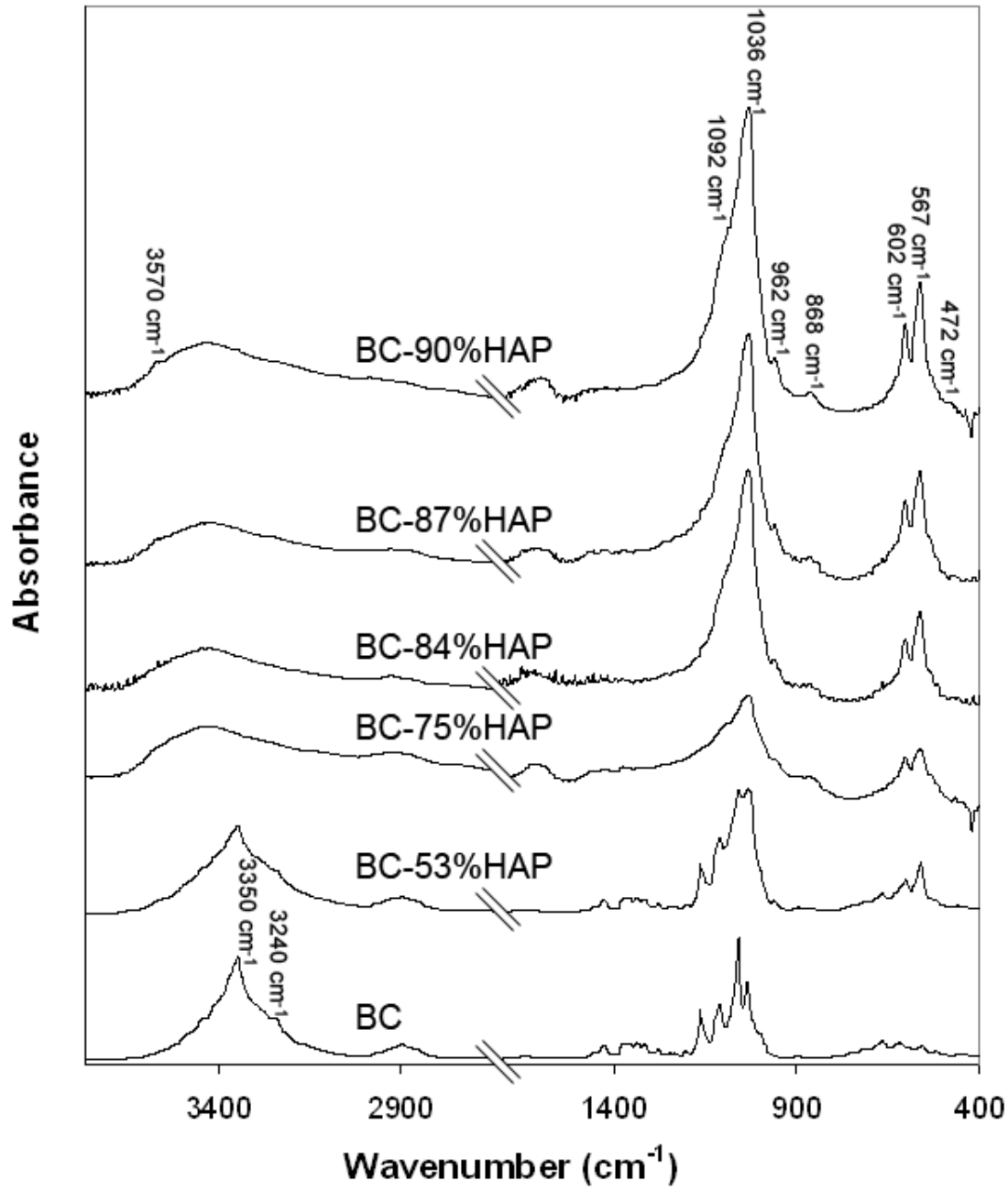

Figure 4.13: IR spectra of bacterial cellulose (BC) and bacterial cellulose-hydroxyapatite composites (BC-HAP) [84]

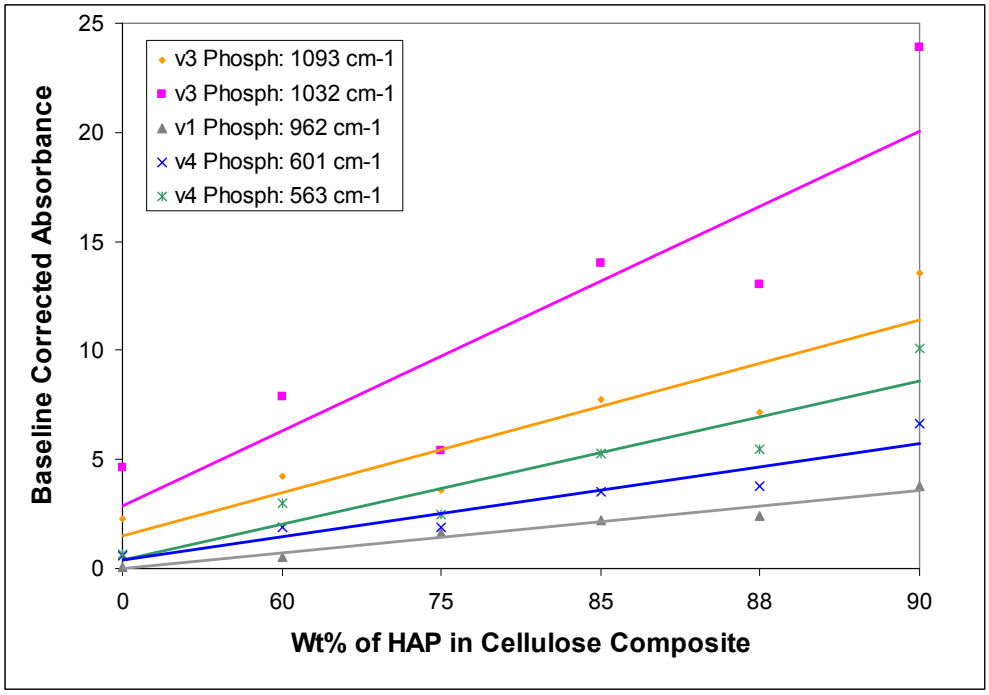

Figure 4.14: Graph of phosphate peak absorbance versus weight percent of hydroxyapatite

suggests that hydroxyapatite binds water. The diffuse peak dominates the spectra from 3600-3100 cm^{-1} hindering the observance of the cellulose hydroxyl stretching bands at 3350 and 3240 cm^{-1}. To observe how the presence of the CdHAP phase affected the cellulose hydroxyl groups, these absorption bands were investigated by spectral deconvolution. The deconvoluted bands of BC and BC-HAP composites are shown in Figure 4.15-4.20. It was observed that the cellulose hydroxyl groups shifted to lower wavenumbers in the presence of hydroxyapatite. The precise wavenumber shifts of the 3350 cm^{-1} and 3240 cm^{-1} hydroxyl IR bands from the original cellulose conformation are shown in Figures 4.15-4.20 as red and blue arrows respectively. For the BC-90%HAP composite, the hydroxyl absorption band at 3350 cm^{-1} shifted downwards 106 cm^{-1} while the OH absorption band at 3240 cm^{-1} shifted downwards 155 cm^{-1}.

Infrared spectroscopy is capable of distinguishing between a free and hydrogen bonded hydroxyl group. As characteristic infrared absorption bands shift to lower wavenumbers, it indicates the possible formation of a new chemical bond with another molecule [95]. In the case

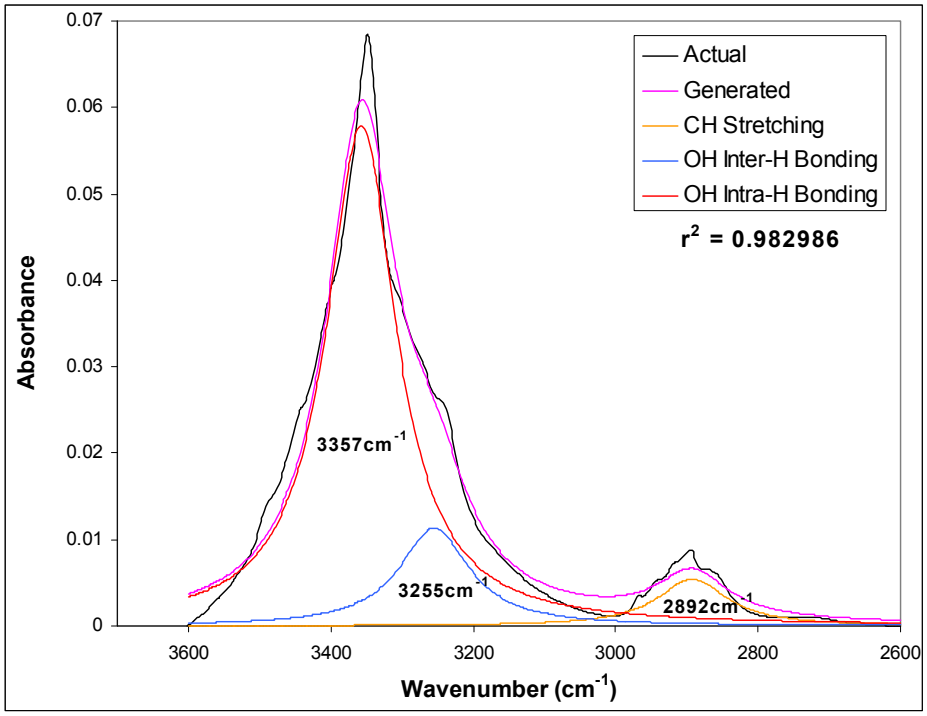

Figure 4.15: Deconvoluted IR spectrum of native cellulose

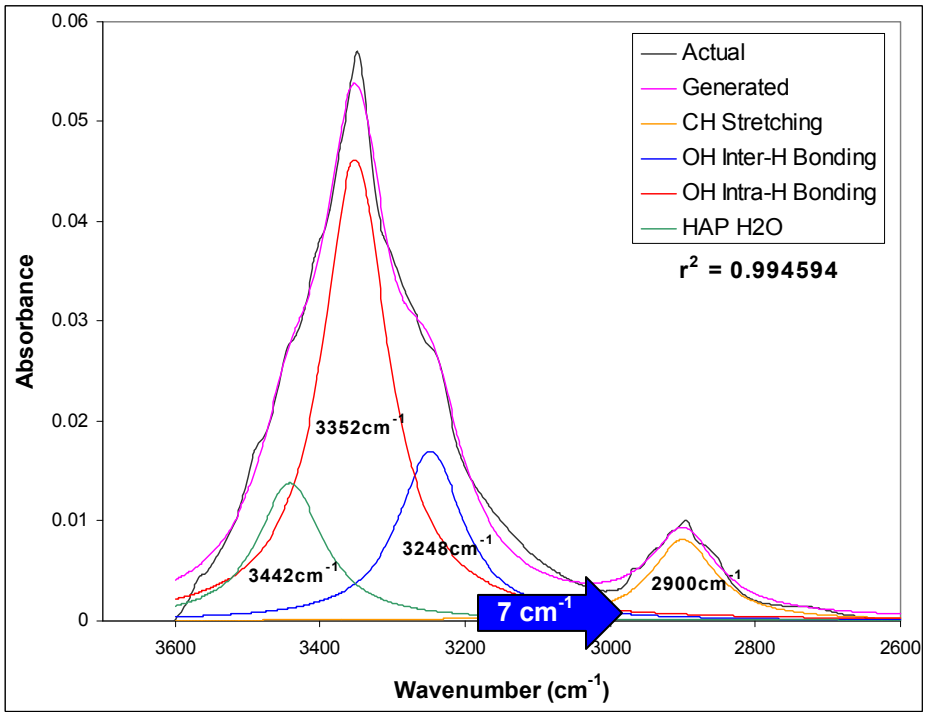

Figure 4.16: Deconvoluted IR spectrum of BC-53% HAP

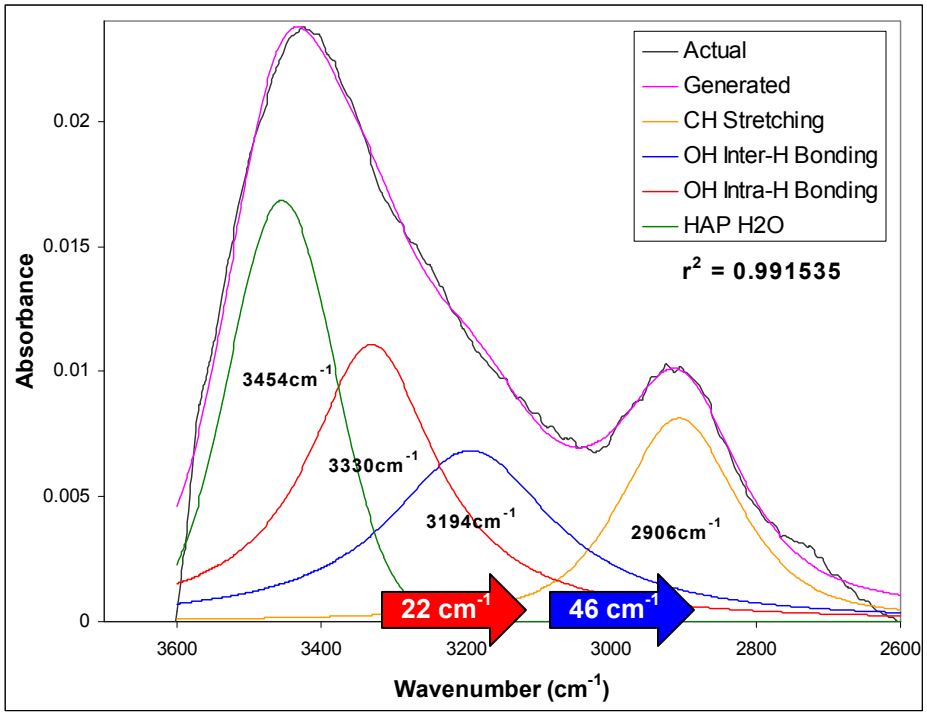

Figure 4.17: Deconvoluted IR spectrum of BC-75% HAP

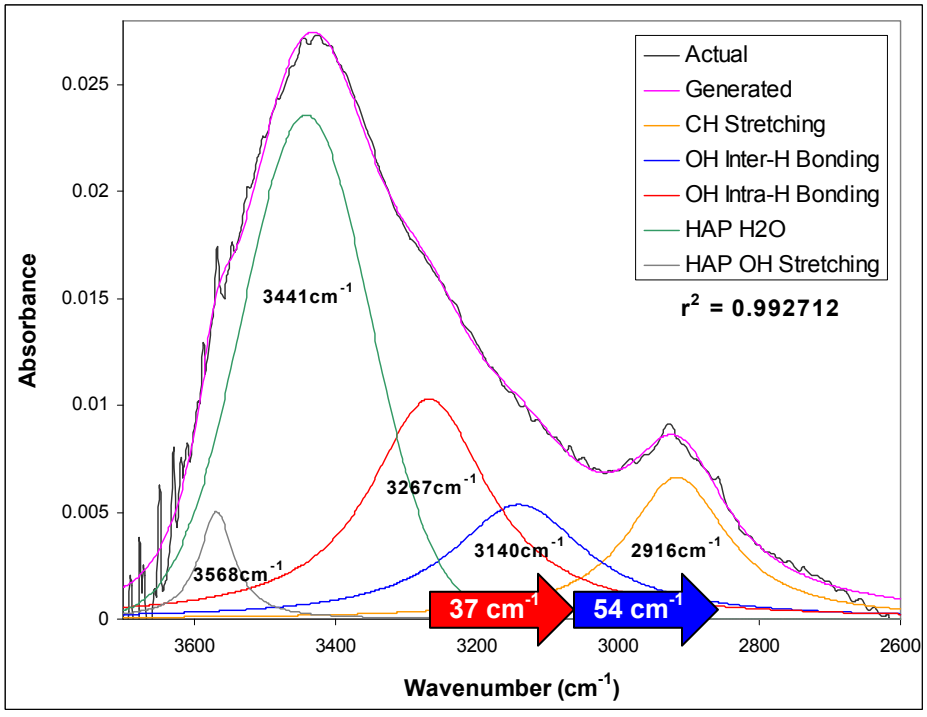

Figure 4.18: Deconvoluted IR spectrum of BC-84% HAP

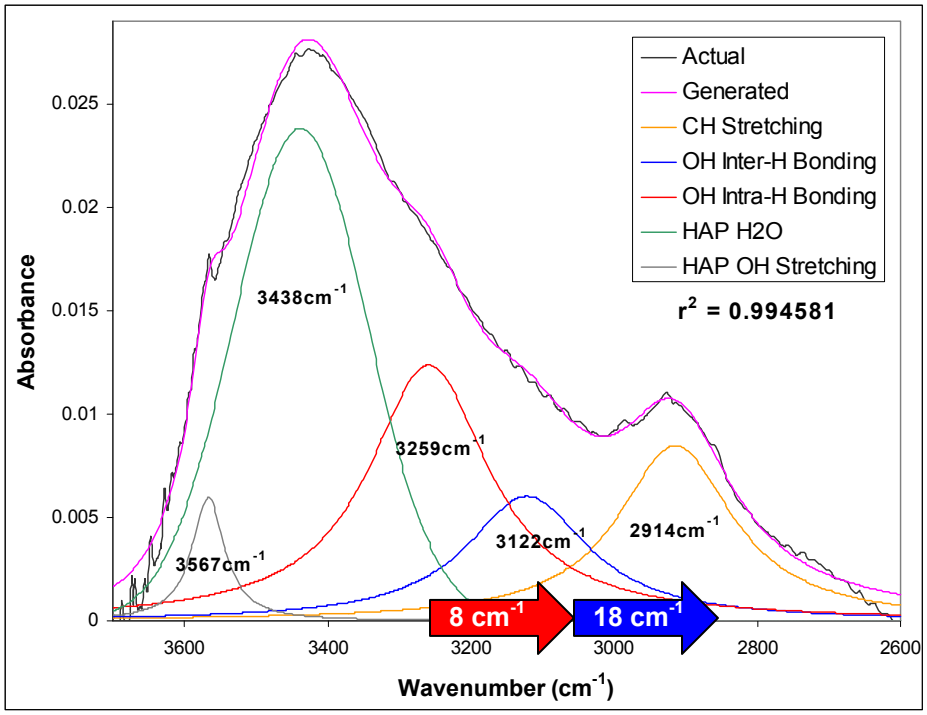

Figure 4.19: Deconvoluted IR spectrum of BC-88% HAP

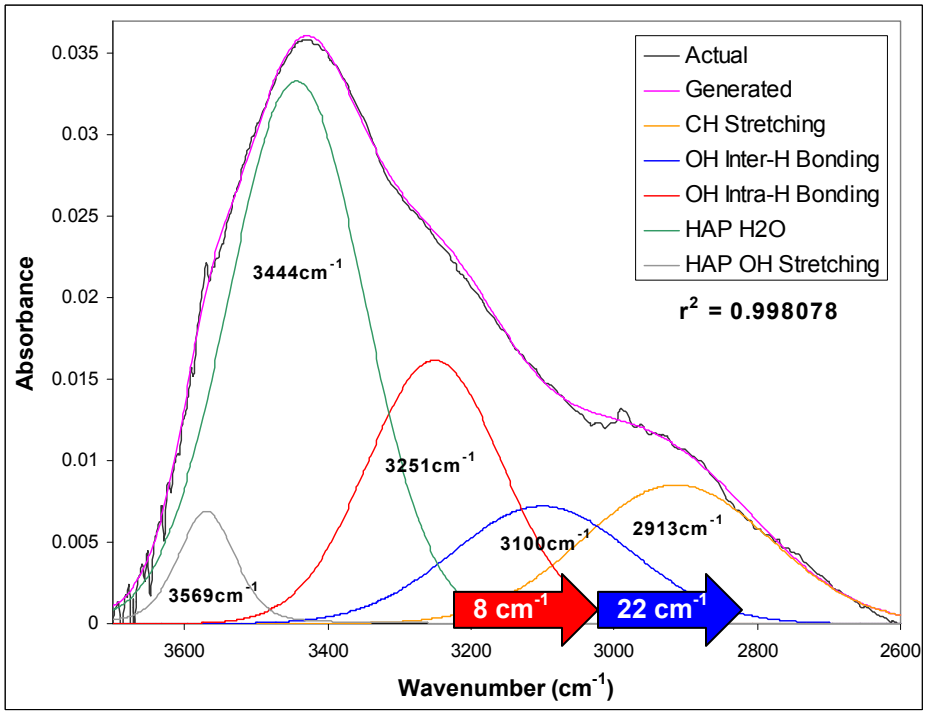

Figure 4.20: Deconvoluted IR spectrum of BC-90% HAP

of the BC-HAP composites, cellulose hydroxyl groups involved with intramolecular hydrogen bonding shifted to lower wavenumbers suggesting that the OH groups are bonding with the apatite. The formation of a chemical bond between the CdHAP and the BC stabilizes the composite so that it can maintain the mechanical integrity necessary for bone substitution. If implanted in the body, chemical bonding would prevent the tiny CdHAP particles from being released to surrounding tissues and initiating dystrophic calcification [113]. By having a distribution of CdHAP bonded throughout the BC, the polymer matrix transfers the stresses to the apatite component in such a way that the particles can bear the load [114].

Previous studies have claimed that functional groups such as hydroxyl and carboxyl groups initiate the nucleation of calcium phosphate [115,116]. Dobbins *et al.* claimed that calcium bonds to cellulose more firmly than water solvent molecules through specific bonding to carboxyl and/or cis-hydroxyl groups [117]. Hartgerink *et al.* stated that materials with repetitive patterns of anionic groups concentrate inorganic cations and proceed to nucleate oriented crystals *in-vivo* [118]. The hydroxyl groups of the cellulose have a strong negative dipole which could chelate free Ca^{2+} cations in the $CaCl_2$ solution and form a coordinated bond. Phosphate ions may then bond with the cellulose-associated calcium to form calcium phosphate.

4.4.2. Octacalcium Precursor of Calcium-Deficient Hydroxyapatite

The IR spectra offer additional information about how the hydroxyapatite was formed in the cellulose matrix. Hydroxyapatite formation from metastable aqueous solutions is usually preceded by a precursor phase, most commonly amorphous calcium phosphate (ACP) ($Ca_2(PO_4)_3$) or octacalcium phosphate (OCP) ($Ca_8H_2(PO_4)_6$). The precursor calcium phosphate then hydrolyzes into the more thermodynamically stable hydroxyapatite. The precursor phase depends on the conditions present in the solution during the precipitation reaction [119]. The presence of the ν_4 PO_4^{3-} doublet at 602 and 567 cm^{-1} in all the composites strongly suggests that the precursor phase of the hydroxyapatite was octacalcium phosphate [119]. During OCP formation, Ca^{2+} first complexes with another species before combining with phosphate. By

organizing the calcium cations onto a matrix prior to mineralization, the OCP precursor ensures a more crystalline and ordered hydroxyapatite phase [119]. If the precursor had been ACP, these PO_4^{3-} bands would be a broad singlet instead of a doublet [120]. ACP precipitation usually requires the rapid interaction between $Ca^{2+}$and PO_4^{3-} at high supersaturation instead of precursor complexation with other species. This precludes the spatial ordering of the ions into a crystal lattice resulting in a poorly crystalline (though not amorphous) mineral [120].

The two main theories of bone mineralization are extracellular nucleation of apatite crystals onto type I collagen fibers or the release of precursor apatite crystals formed within matrix vesicles [121]. In both cases, the calcium first associates with a matrix (a functional group in collagen or the matrix vesicle) before forming the calcium phosphate precursor. OCP has been found to be the precursor calcium phosphate phase in an *in-vitro* study of matrix vesicle formation of apatite [119]. In this study, the calcium ions first may first be complexing with the cellulose. This fact is supported by the other IR results which suggested chemical bonding between the apatite and the cellulose hydroxyl groups. The ordered arrangement and negative dipole of the hydroxyl groups in the crystalline BC matrix provides a structured template for the nucleation and formation of the OCP. The thermodynamically unstable OCP then hydrolyzes into a crystalline hydroxyapatite phase which is confirmed by the low background and sharp peaks of the XRD pattern. By having an OCP precursor, the formation of CdHAP in the cellulose mimics the biomineralization of physiological bone.

4.5. Conclusion

It was demonstrated that bacterial cellulose (BC) provides a template for the ordered formation of calcium-deficient hydroxyapatite (CdHAP). SEM showed that ~1 μm CdHAP spherical clusters composed of nanosized crystallites had formed within the BC network. XRD demonstrated that the CdHAP is comprised of anisotropic 10-50 nm crystallites which are elongated in the c-axis mimicking the size and geometry of bone apatite crystals. FTIR spectroscopy strongly suggests that the CdHAP is bonding with the BC via the cellulose hydroxyl

groups and that it is highly likely the CdHAP had an octacalcium precursor similar to natural bone apatite. The formation of this composite is similar to the physiological biomineralization of bone producing apatite crystals of comparable shape and size. Previous studies suggest that the presence of CdHAP in this composite will induce bone colonization when implanted into hard tissue defects. Since CdHAP implants rapidly incorporate into the bone tissue, the need for a second surgery would be eliminated. The bioactivity of the calcium-deficient hydroxyapatite and the biocompatibility of the bacterial cellulose hydrogel substantiates this composite as a potential orthopedic biomaterial.

Chapter 5

Analysis of Oxidized BC and Oxidized BC-CdHAP

In this section, bacterial cellulose (BC) was chemically modified via periodate oxidation to render the material degradable in mammalian systems. Oxidized BC and oxidized BC mineralized with calcium-deficient hydroxyapatite (CdHAP) were synthesized, characterized, and compared to native BC and native BC-CdHAP. The degradation properties were then analyzed by incubating the samples in HEPES buffer (pH 7.4) at 37°C under static and dynamic conditions. The samples were measured for weight loss while the buffer was analyzed for degradation products. The results of this study will be submitted to the journal *Biomaterials* [122]. A patent application has also been filed for this technology.

5.1 Synthesis of Samples

Two batches of bacterial cellulose were cultured as described in section 2.1.1 and 2.1.2. Six centimeter pellicles which were ~3 mm thick were produced by culturing the bacteria for 30 days. Forty-four pellicles were produced for the first batch. Half of these samples were oxidized using sodium periodate in n-propanol using the protocol in section 2.1.3. Eleven native BC samples and eleven oxidized BC samples were mineralized with CdHAP as given in section 2.1.4. In all, four groups of eleven samples were made: native BC, oxidized BC, native BC-CdHAP, and oxidized BC-CdHAP. The second batch consisted of the same four groups with six samples produced for each to be used for the second in-vitro degradation experiment.

Periodate oxidation is a preferred technique since it can be performed on crystalline bacterial cellulose and reacts in a specific and predictable manner [68]. The most significant side reaction is the production of free radicals during oxidation that can cause non-specific chain breakages. This can be mitigated against by addition of n-propanol as a free-radical scavenger during the reaction. After periodate oxidation with n-propanol, there was no visible change in the morphology of the cellulose pellicles when compared to unaltered native bacterial cellulose. The

absence of this reagent resulted in gross changes to the bacterial cellulose structure and resulted in a three-fold decrease in the volume of the hydrogels (data not shown).

After incubating the oxidized BC in aqueous calcium and phosphate solutions, it turned from clear to a white color indicating mineralization.

The samples were weighed in hydrated and dried states (Figure 5.1). The first indication that oxidation resulted in changes to the structure of the cellulose was that the wet weight of the oxidized BC was significantly less than native BC (Figure 5.1a). In contrast, their dry weights were not significantly different (Figure 5.1b). This data indicates that periodate oxidation did not degrade the cellulose network, but the molecular structure undergoes a change that compromises its ability to retain water. It is likely that alteration in the hydrogen bonding pattern and network structure due to the formation of aldehyde groups is responsible for its lower affinity for water. Both native and oxidized bacterial cellulose pellicles formed hydroxyapatite within their porous structure after sequential incubation in sodium hydrogen phosphate and calcium chloride solutions. Interestingly, after drying and weighing the samples, it was observed that more CdHAP formed in the native BC (62% CdHAP) compared to the oxidized BC (55% CdHAP) (Figure 5.1b). This supports the view that alteration in the network structure of the cellulose due to oxidation imposes some restriction on the access of the calcium and phosphate salts and results in decreased hydroxyapatite formation. It is also possible that the oxidation of hydroxyl to aldehyde

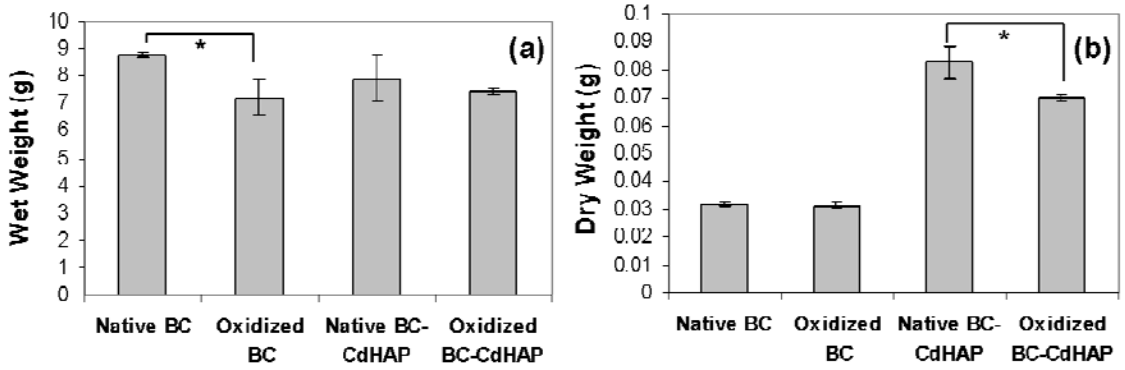

Figure 5.1: Comparison of (a) wet weights and (b) dry weights of native BC, oxidized BC, native BC-CdHAP, and oxidized BC-CdHAP [122]

groups affects apatite nucleation.

5.2. Fourier Transform Infrared Spectroscopy

The FTIR spectra of native and oxidized BC are shown in Figure 5.2. In the oxidized BC spectrum, an absorption band appears at 1740 cm^{-1} that corresponds to the aldehyde carbonyl group introduced during peroidate oxidation (Figure 5.2b). A band at 1652 cm^{-1} that represents carbonyl groups involved in hydrogen bonding is present along with a band at 1530 cm^{-1} which most likely corresponds to conjugated aldehyde groups (Figure 5.2b). The native BC spectrum is devoid of these absorption bands (Figure 5d), confirming that periodate oxidation converts BC into dialdehyde cellulose. After depositing CdHAP into the oxidized BC, the carbonyl absorption bands shift to lower wavenumbers (Figure 5.2a) indicating the formation of a new chemical bond with another molecule [95]. It is likely that the negative dipoles of the cellulose aldehyde groups bond to the calcium cations of the CdHAP mineral. A shift in the hydroxyl groups of the oxidized

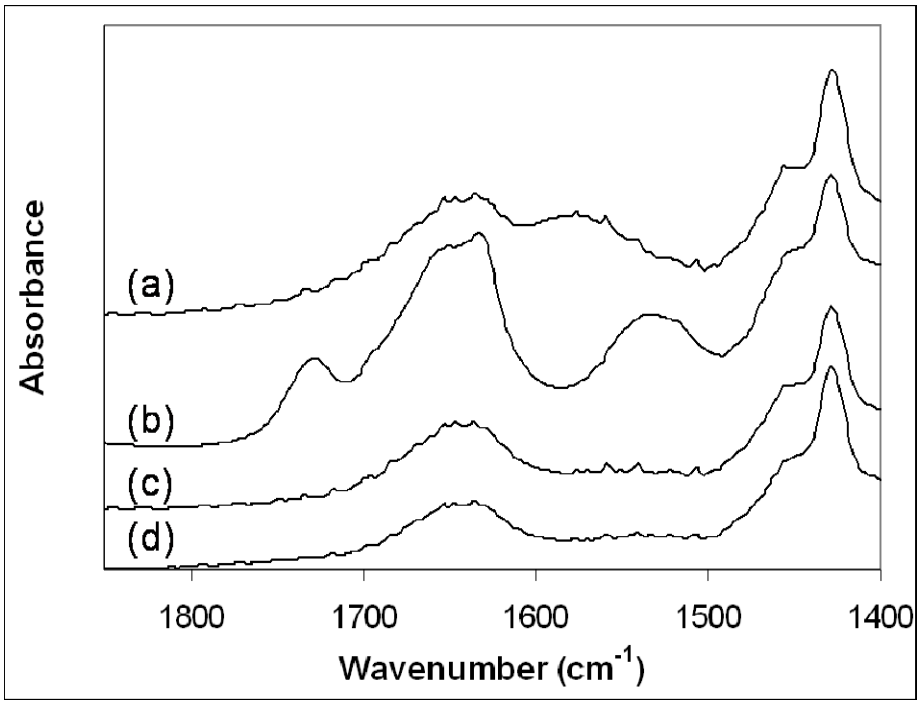

Figure 5.2: FTIR spectra of (a) oxidized BC-CdHAP, (b) oxidized BC, (c) native BC-CdHAP, and (d) native BC [122]

cellulose was not observed indicating the apatite was interacting predominantly with the aldheyde groups. Having the CdHAP particles chemically bound to the oxidized BC ensures that the composite will stay conjunct upon implantation. It also prevents the CdHAP particles from being released which could cause damage to the surrounding tissues and nitiate dystrophic calcification [113].

5.3. X-Ray Diffraction

X-ray diffraction was performed on the dried native and oxidized materials to determine how the oxidation reactions affected the crystallinity of the materials. The x-ray diffraction (XRD) pattern of BC (Figure 5.3a) showed the typical crystalline structure of native cellulose (PDF#03-0289) as defined by sharp defined peaks at 14.7 and 23.1° *2θ*. Treatment of cellulose with 50 mM periodate for 24 hours at 23°C did not appreciably disrupt the crystalline structure of BC

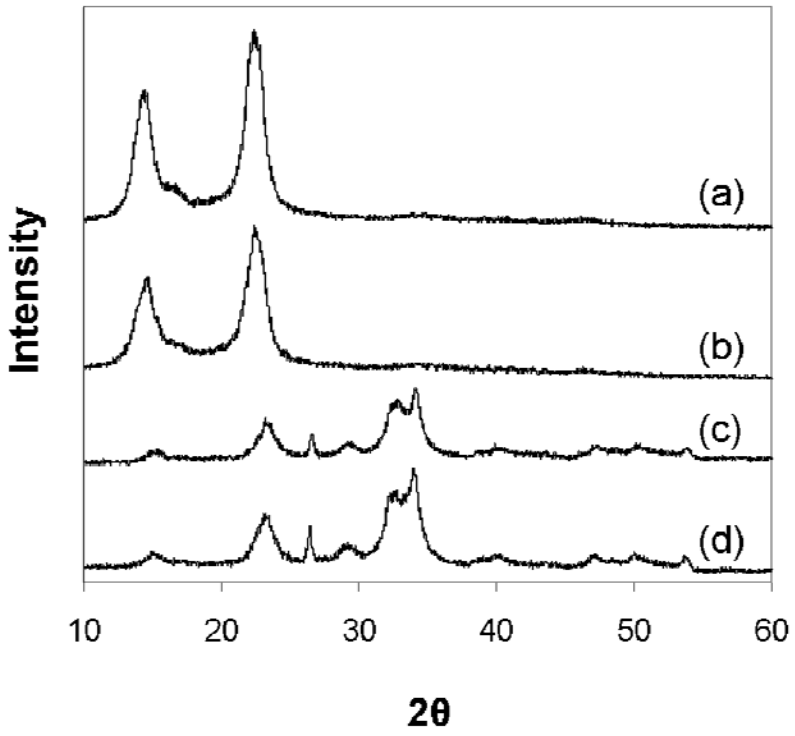

Figure 5.3: X-ray diffraction patterns of (a) native BC, (b) oxidized BC, (c) native BC-CdHAP, and (d) oxidized BC-CdHAP [122]

(Figure 5.3b). In addition XRD confirmed that the oxidized material formed CdHAP after sequential incubation in calcium and phosphate solutions (PDF#46-0905) (Figure 5.3c). Therefore we can conclude that the oxidized cellulose forms CdHAP with a similar pattern to that formed in native cellulose (Figure 5.3d).

5.4. Scanning Electron Microscopy

SEM images of the samples are shown in Figure 5.4. The fine fibrils of native BC are seen in Figure 6a. The oxidized BC had a similar morphology (Figure 5.4b) showing that the oxidation did not disrupt the structure of the polymer. In the native BC-CdHAP sample, it is observed that regular 1 μm hydroxyapatite clusters had formed within the cellulose fibrils composed of discrete needle and plate-like crystallites (Figure 5.4c). The oxidized BC-CdHAP sample also contained spherical 1 μm clusters with a similar morphology (Figure 5.4d). The

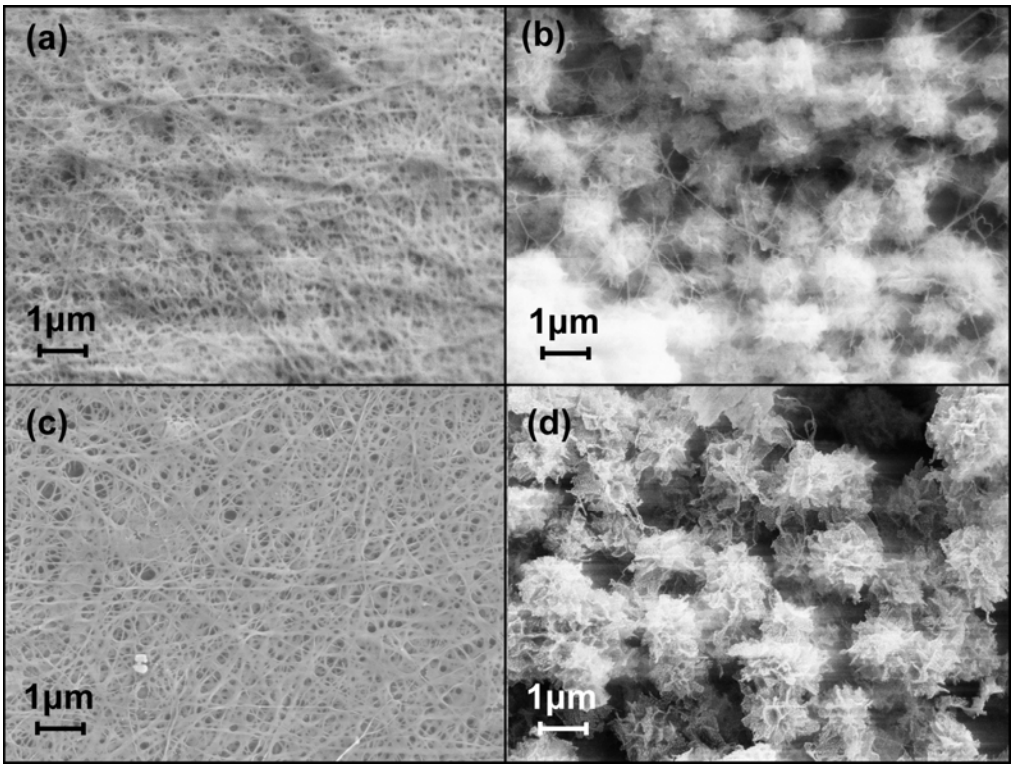

Figure 5.4: SEM images of (a) native BC, (b) native BC-CdHAP, (c) oxidized BC, and (d) oxidized BC-CdHAP [122]

previous chapter confirmed that the CdHAP formed in native BC had similar size, shape, morphology, and chemistry to natural apatite found in bone. As discussed in the previous chapter, “calcospherites” like those seen here have also been observed during natural bone calcification and are favorable for the adhesion and spreading of osteoblasts [107].

5.5. Mechanical Testing

The mechanical tensile properties of the oxidized and native materials, with and without hydroxyapaptite, were determined to establish the relationship between chemical alteration and the resulting physical properties. The engineering stress-strain curves of the hydrated samples are shown in Figure 5.5. The ultimate tensile strength and elastic modulus values were calculated from these curves and are compared in Figure 5.6. The data show that oxidation does not appreciably affect the ultimate tensile strength or elastic modulus of the bacterial cellulose. However, presence of the CdHAP in both the native and oxidized cellulose causes an approximate 50% decrease in ultimate tensile strength. Formation of the CdHAP crystallites

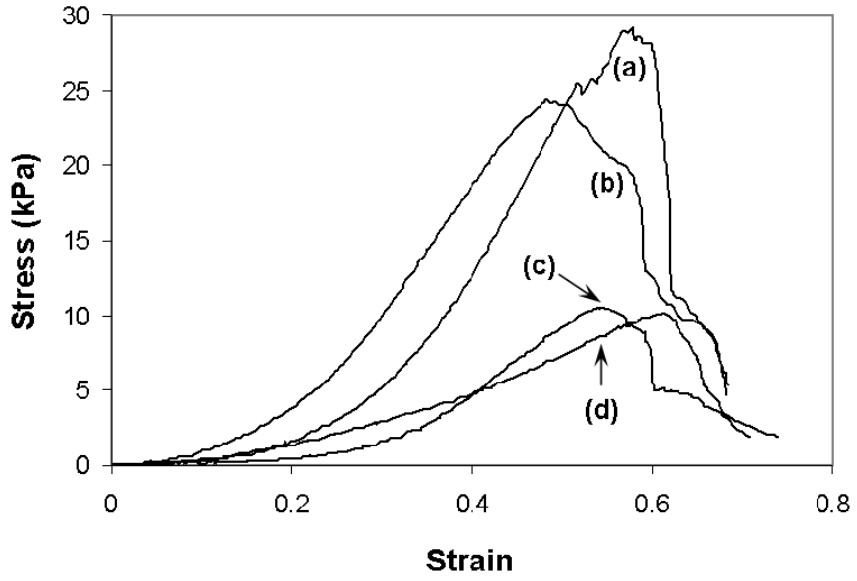

Figure 5.5: Engineering stress-strain curve of (a) native BC, (b) oxidized BC, (c) native BC-CdHAP, and (d) oxidized BC-CdHAP [122]

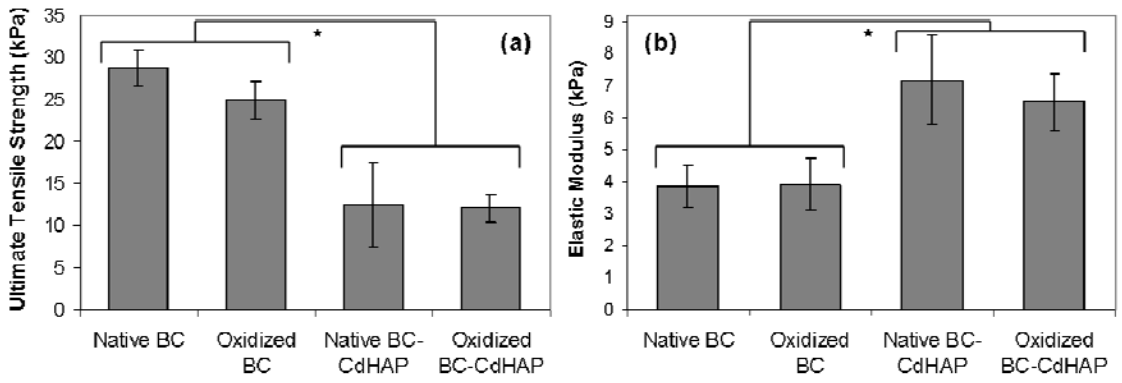

Figure 5.6: Comparison of (a) ultimate tensile strengths and (b) elastic moduli of native BC, oxidized BC, native BC-CdHAP, and oxidized BC-CdHAP [122]

which are bonded to the cellulose hydroxyl and/or aldehyde groups may interrupt the natural hydrogen bonding and weaken the mechanical properties. Presence of CdHAP imparted brittleness in both the native and oxidized BC, causing an approximately 40% increase in elastic modulus.

The mechanical properties of the BC-CdHAP material correspond to particulate composite theory. The elastic modulus of a particule-reinforced composite increases with filler content [42]. Addition of the particulate filler decreases strength in tension and increases strength in compression. As is evident in Figure 5.6, adding the CdHAP nanoparticles increased the elastic modulus and decreased tensile strength in both the native and oxidized BC. Though not carried out, it is expected the compressive strength of the CdHAP composites would be greater than the native or oxidized BC.

5.6. In-Vitro Degradation Testing of the Oxidized Cellulose Samples

The degradation of the samples were monitored as described in section 2.3. The first batch of samples was incubated in HEPES buffer which was analyzed every other day for degradation products using UV-Visible spectroscopy. At the end of the study, the samples were rinsed, dried, and weighed. The second batch of samples remained in the same volume of

HEPES buffer throughout the study. At the end of the study, the buffer was assayed for free carbohydrate and glycolic acid.

5.6.1. Weight Loss of Samples

After placing the samples in a simulated aqueous physiological environment at pH 7.4 and 37°C for 14 days under static and dynamic conditions, the oxidized BC lost significant mass compared to the native material (Figure 5.7). An average, the dry mass of oxidized BC was reduced by 38% and 36% after static and dynamic incubation respectively. In contrast, the native material was decreased by an average of 8% and 20% when incubated under the same conditions, but the loss was not statistically significant. The fact that weight loss was similar in the samples that underwent static and dynamic incubation indicates that the degradation of periodate oxidized cellulose is not due to physical disruption during agitation, but is a result of the action of the simulated physiological buffer on the material.

Oxidized BC-CdHAP only lost significant weight after dynamic incubation in the HEPES buffer at 37°C, losing 23% of its mass on average. Mechanical disruption therefore did affect the mass loss of the oxidized BC-CdHAP composite. The chemical bonding between the oxidized

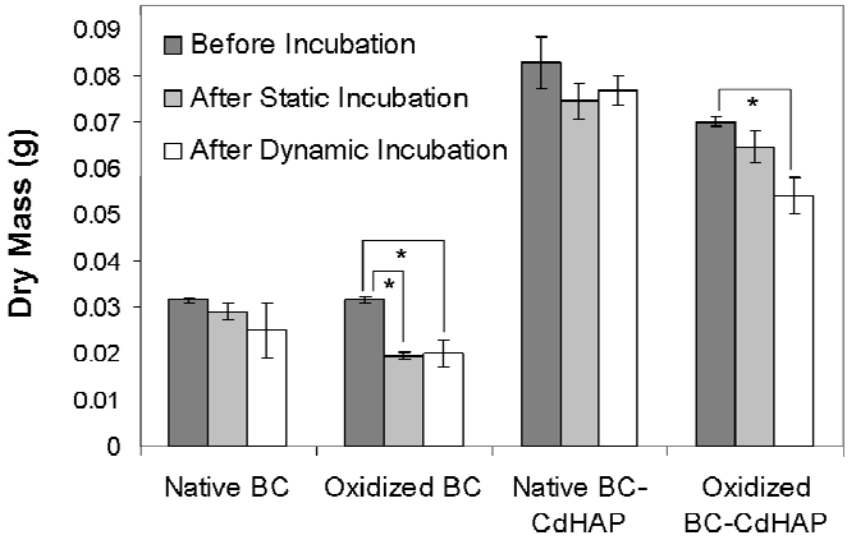

Figure 5.7: Comparison of sample masses before and after incubation in low salt HEPES buffer (pH 7.4) at 37°C in static and dynamic conditions [122]

cellulose and CdHAP may not be as strong as that between the native cellulose and apatite, causing some of the CdHAP particles to detach when it is continuously agitated.

5.6.2. Measuring Degradation by UV-Visible Spectroscopy

It was of interest to identify and quantify the degradation products that are released from the cellulose hydrogels by incubation in simulated physiological buffer. The main components expected were carbohydrate, glycolic acid and 2,4-dihydroxybutyric acid. Direct measurement of cellulose degradation products by UV-visible spectrophotometry was carried out.

A previous investigation demonstrated that an absorption band appeared at 240 nm during degradation of plant cellulose powder. This band was assigned to the n-π^* transition of carbonyl groups [123]. Both glycolic acid and 2,4-dihydroxybutyric acid, as well as intermediate degradation products contain carbonyl groups which absorb in this region [123]. In addition, previous cellulose degradation studies have observed an absorbance peak at 260 nm as a result of ultraviolet photolytic degradation [124], enzymatic hydrolysis [125], and acid hydrolysis [126]. This peak was assigned to a weak chromophore associated with acetal groups, which form the linkages between glucose residues in cellulose [127]. An experiment was conducted to determine if cellulooligosaccharides absorb in this region. A bacterial cellulose sample was homogenized in water using a commercial blender and after centrifugation of the resulting suspension, a peak at 260 nm was observed in the supernatant. This indicates that mechanical disruption releases cellulose fragments which absorb at 260 nm.

Representative spectra of the oxidized and native BC HEPES supernatant after 4 days are shown in Figure 5.8. It can be seen that the native material releases a small amount of material with a peak at 260nm, whereas the oxidized BC has peaks at both 240 and 260nm. This indicates that the oxidized cellulose releases cellulooligosaccharides (260 nm) and carbonyl containing species (240 nm) which are most likely glycolic acid and/or 2,4-dihydroxybutyric acid. Conversely, native cellulose does not break down into carbonyl products and only releases soluble cellulose fragments (260 nm).

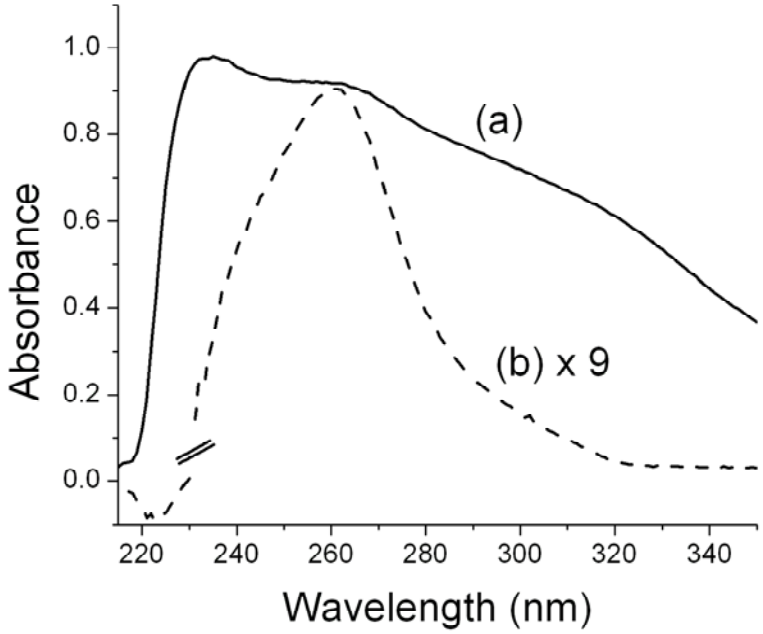

Figure 5.8: UV-Vis spectrum of HEPES supernatant from (a) oxidized BC after 4 day dynamic incubation at 37°C (b) native BC after 4 day dynamic incubation at 37°C

The absorption spectra of the fluid surrounding the oxidized and native cellulose samples under static conditions were recorded at intervals during the degradation study. The absorbance versus time plots are given for the static samples at 240 nm (Figure 5.9), static samples at 260 nm (Figure 5.10), dynamic samples at 240 nm (Figure 5.11), and dynamic samples at 260 nm (Figure 5.12). Oxidized BC released a high concentration of degradation products that absorbed at 240 nm and 260 nm during the early time periods which eventually decayed to an equilibrium value. The degradation products are most likely carbonyl species and cellulooligosaccharides. Oxidized BC-CdHAP also released these products in a similar manner, though not as much as the oxidized BC alone. Native BC and native BC-CdHAP did not release any carbonyl degradation products and only a small amount of soluble carbohydrate was detected. This supports the gravimetric analysis on these samples. The graphs were similar under both static and shaken conditions.

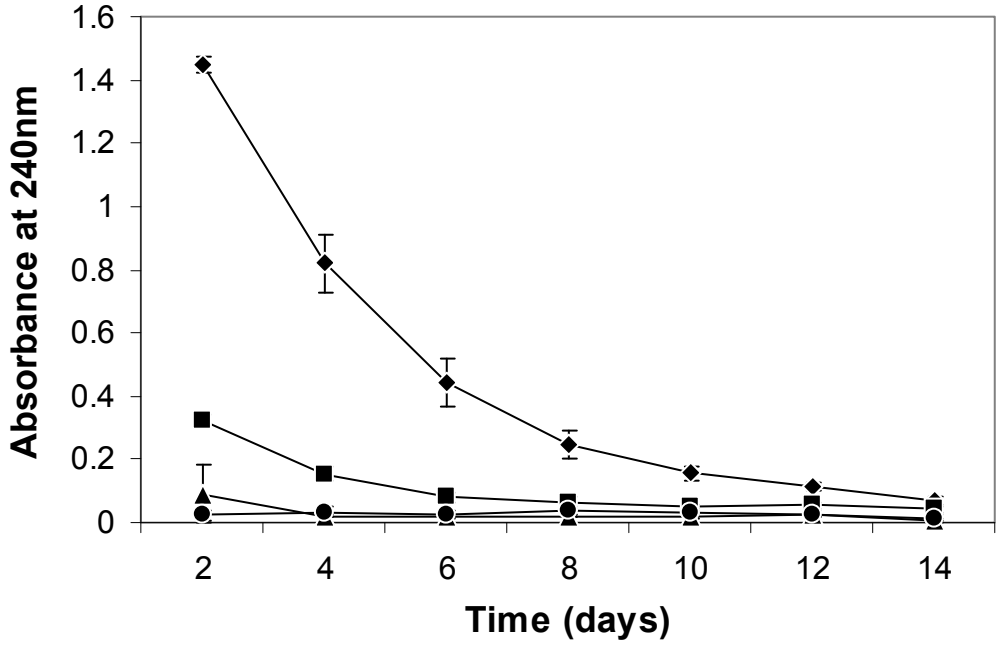

Figure 5.9: Absorbance versus time of HEPES supernatant of static samples at 240 nm. ♦ - oxidized BC, ■ - oxidized BC-CdHAP, ● - native BC-CdHAP, ▲- native BC [122]

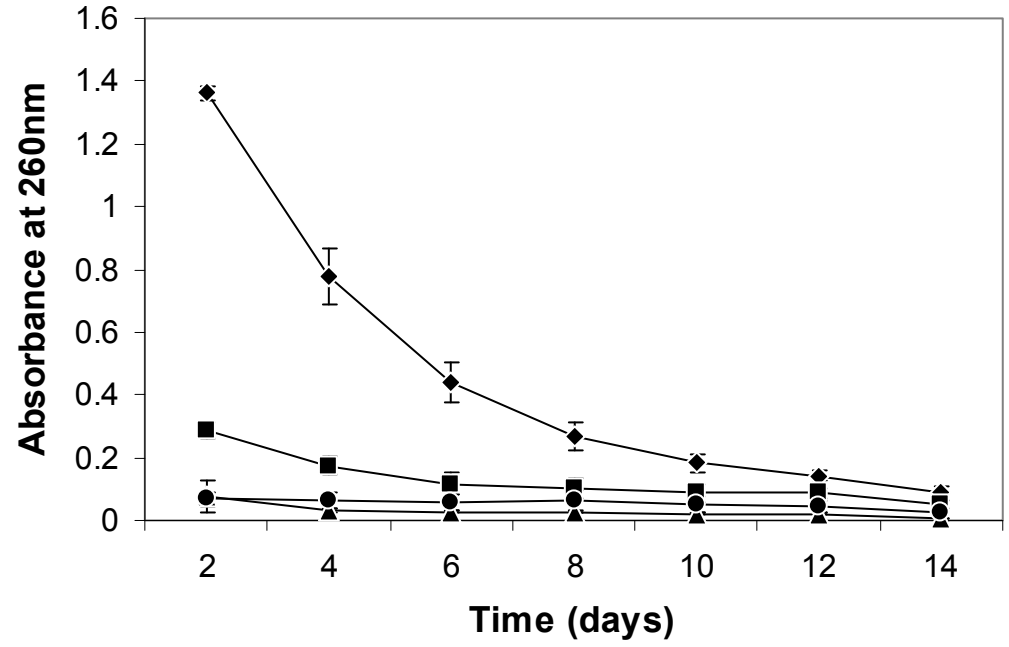

Figure 5.10: Absorbance versus time of HEPES supernatant of static samples at 260 nm. ♦ - oxidized BC, ■ - oxidized BC-CdHAP, ● - native BC-CdHAP, ▲- native BC [122]

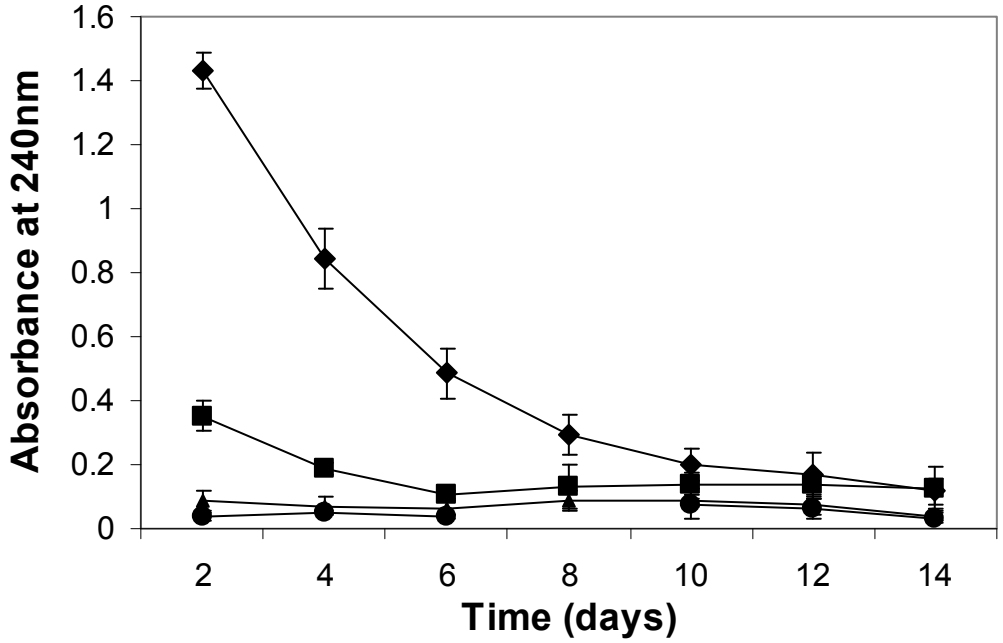

Figure 5.11: Absorbance versus time of HEPES supernatant of dynamic samples at 240 nm. ♦ - oxidized BC, ■ - oxidized BC-CdHAP, ● - native BC-CdHAP, ▲- native BC

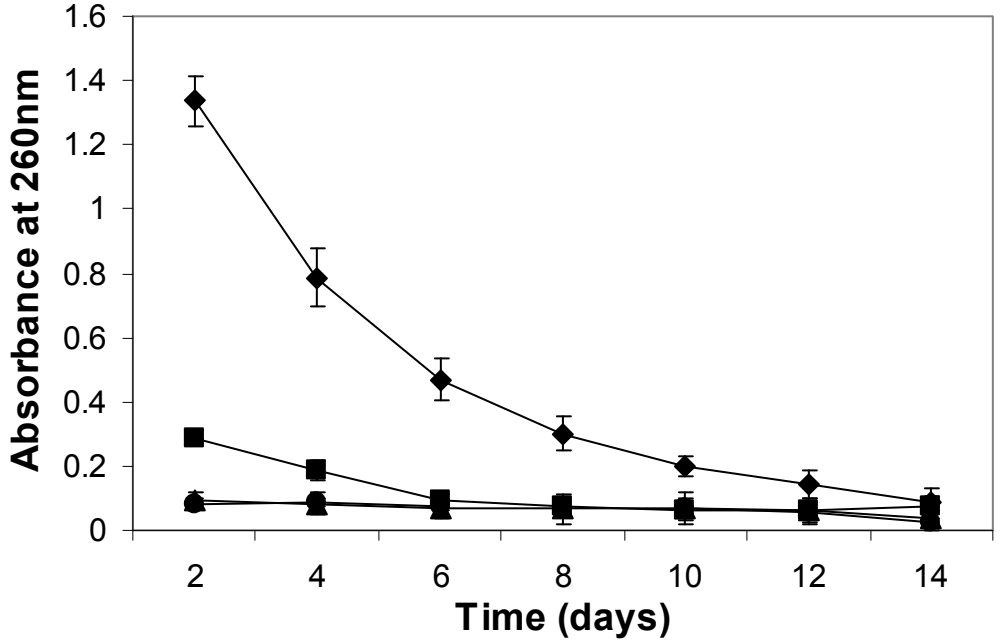

Figure 5.12: Absorbance versus time of HEPES supernatant of dynamic samples at 260 nm. ♦ - oxidized BC, ■ - oxidized BC-CdHAP, ● - native BC-CdHAP, ▲- native BC

5.6.3. Identification of Degradation Products

The HEPES supernatant was assayed for free carbohydrate and glycolic acid as described in section 2.3.1. One assay used anthrone in concentrated sulfuric acid to detect free carbohydrate [77]. Although the results showed that all of the samples released free carbohydrate, the variance between samples was too high to accurately quantify the amount of carbohydrate released (Figure 5.13).

Dihydroxynaphthalene has been reported to preferentially react with glycolic acid [128] and has been used to in previous degradation studies of dialdehyde cellulose [77,78]. As reported in several papers, glycolic acid is an expected byproduct of dialdehyde cellulose hydrolysis [77,78]. The characteristic violet color was observed after reacting 2,7-dihydroxynaphthalene with the supernatants of the oxidized cellulose samples (Figure 5.14). However, a similar color change was also observed in the native cellulose samples (Figure 5.14).

In this reaction, formaldehyde is released from glycolic acid in the presence of concentrated sulfuric acid [128]. The formaldehyde then reacts with the 2,7-dihydroxynaphthalene and produces a violet color [128]. It was determined that this 2,7-

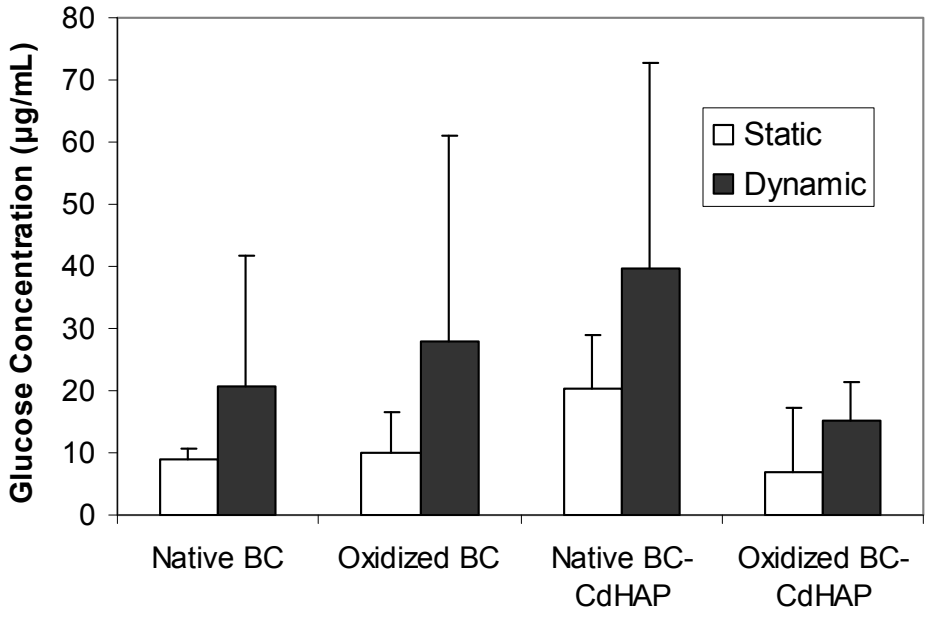

Figure 5.13: Results of free carbohydrate assay using anthrone in concentrated sulfuric acid

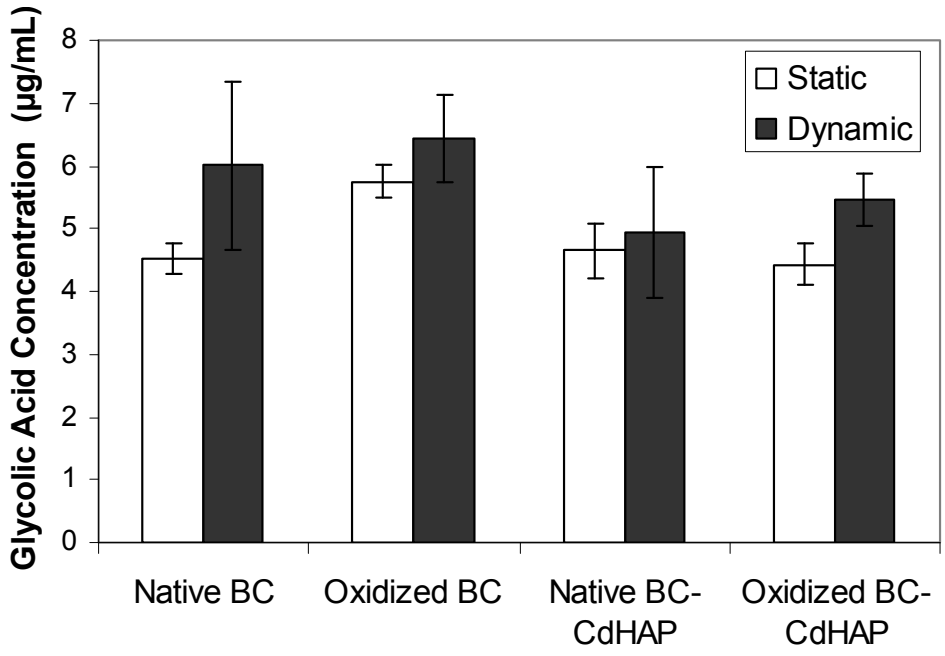

Figure 5.14: Results of glycolic acid assay using 2,7-dihydroxynaphthalene in concentrated sulfuric acid

dihydroxynaphthalene reacts strongly with glucose in the presence of concentrated sulfuric acid in this study (data not shown). Correspondingly, aldehyde groups on the cellulose reducing ends that were hydrolyzed by the concentrated sulfuric acid most probably react in the same manner. Additionally, it has also been published that other aldehydes react similarly with 2,7-dihydroxynaphthalene [128]. In conclusion, this assay is not specific for glycolic acid detection since it reacts positively with free cellulose and glucose in the supernatant. Alternative tests must be carried out to confirm whether glycolic acid was released from the samples.

5.7. Conclusion

The aim of this study was to chemically alter BC so that it would safely resorb when implanted *in-vivo*. The modification had to preserve the structural properties of the BC and retain its ability to biomimetically form CdHAP nanocrystallites when incubated in calcium and phosphate solutions.

Periodate oxidation is a preferred technique since it can be performed on crystalline bacterial cellulose, reacts in a specific and predictable manner, and is devoid of significant side reactions [68]. To ensure that the periodate oxidation would not degrade or disrupt the native structure of BC, a free-radical scavenger (n-propanol) was added. After periodate oxidation with n-propanol, there was no apparent change in the cellulose structure when compared to unaltered native bacterial cellulose. BC oxidized by periodate retains the ability to initiate the mineralization of CdHAP which is chemically bonded to the polymer via its carbonyl functional groups. The CdHAP produced in oxidized BC is similar in morphology and chemistry to that produced in native BC which has been previously shown to be similar to natural bone apatite.

It was shown that periodate oxidized BC and BC-CdHAP degrades in a simulated aqueous physiological environment. *In-vitro* degradation in HEPES buffer (pH 7.4) under static and dynamic conditions at 37°C caused the oxidized BC and oxidized BC-CdHAP to significantly lose mass. Though it was attempted to identify and quantify the degradation products released via colorimetric analysis, it was determined that the assays selected were not sufficient for this system. UV-Vis spectrophotometry was a better method to measure the release of degradation products which are most likely small cellulose fragments, glycolic acid, or 2,4-dihydroxybutyric acid. Bioactive CdHAP has been proven to regenerate bone when implanted into osseous defects and subsequently degrades. By immobilizing nanocrystallites of CdHAP into oxidized cellulose, the entire composite has the capacity to eventually be resorbed and replaced by natural bone.

Chapter 6

Clinical Applications of BC-CdHAP Composite

Bone grafts are used in various areas of medicine in different areas of the human body. It is necessary for the bone graft to have the specific material properties suitable for its particular application. For example, a bone graft used to reconstruct the bone around a hip joint must have the proper mechanical properties to bear the patient's weight, or be used in conjunction with another structural appliance.

It has been shown that the calcium-deficient hydroxyapatite component of the bacterial cellulose composite mimics the composition, chemistry, and size of physiological apatite giving the composite the potential of substituting bone. However, it is necessary to find the specific application and bone site for which the material properties of this composite would be suitable. To accomplish this, the candidate interviewed several surgeons representing the three main areas of medicine that utilize bone grafts to gather their input about possible applications for the BC-CdHAP composite. Physician input is very important in developing medical devices since they ultimately select the products which they believe are scientifically sound and are comfortable using. This chapter summarizes these findings and proposes specific bone graft procedures for which this material could be used.

6.1 Bone Graft Procedures

A breakdown of bone graft procedures performed in 2004 is given in Figure 6.1. As is apparent, bone graft procedures predominantly fall into three main areas of medicine: neurosurgery, orthopaedics, and oral / maxillofacial surgery [129]. Neurosurgeons perform spinal fusions which account for almost half of the bone grafting procedures in the U.S. [129]. Orthopaedic surgeons repair severe long bone fractures and bone damaged by artificial joints during revision surgery. Oral and maxillofacial surgeons also utilize bone grafts though not as frequently as neurosurgeons or orthopaedic surgeons [129]. The specific bone graft procedures associated with these fields are discussed in the following sections.

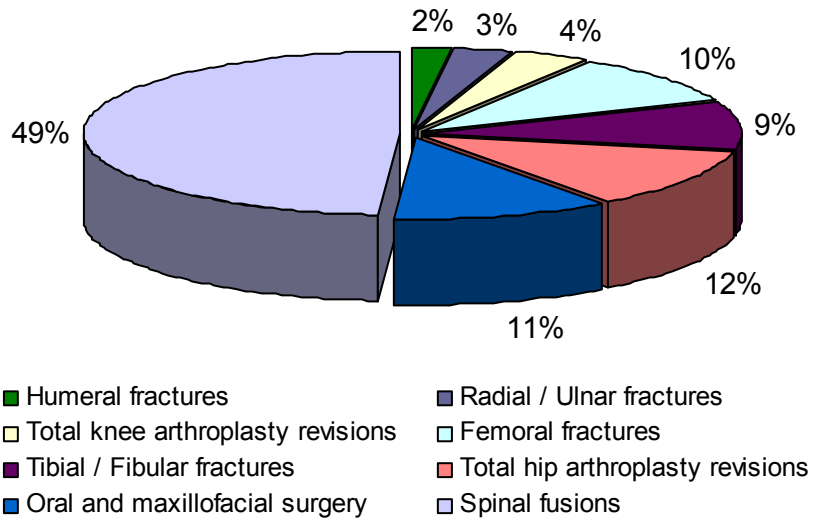

Figure 6.1: Bone graft procedures in the U.S.A., 2004 [129]

6.2. Neurosurgery

Spinal fusion is one of the most common forms of spine surgery. An estimated 380,000 spinal arthrodesis procedures were performed in the U.S. in 2004 [130]. Most spinal fusion is performed in the lumbar (lower back) region of the spine, but can also be used to treat cervical (neck) and thoracic (chest region) problems [131]. Patients who suffer from severe pain or neurological deficits may elect spinal fusion surgery to alleviate their symptoms. The most common conditions requiring spinal fusion are degenerative disc disease, stenosis, scoliosis, spondylolisthesis, and trauma [131].

There are many surgical techniques to accomplish spinal fusion, but the most common is the posterolateral lumbar intertransverse process [132]. In this procedure, the spine is accessed from the back and the muscle is removed from the transverse processes. Bone graft is then placed between the transverse processes of the vertebrae and muscle is replaced to hold the graft in place. A 10-40% non-union rate has been reported in patients with single-level fusions using the posterolateral lumbar intertransverse process. The rate of non-union increases when multiple fusion levels are attempted [132]. To provide greater support and a better chance of fusion, spine surgery instrumentation is implemented. These include pedicle screws, wires, rods, plates, and cages to provide internal fixation between the vertebrae (Figure 6.2) [132].

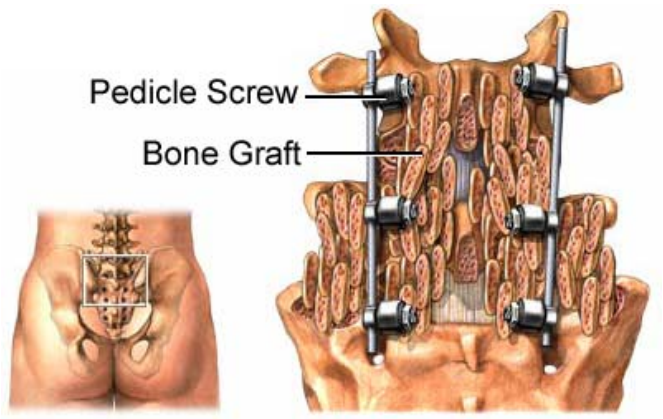

Figure 6.2: Instrumented posterolateral lumbar intertransverse spinal fusion [image modified from http://adam.about.com/encyclopedia/]

However, a 10-15% pseudarthrosis rate (or movement caused by non-union) has been reported in patients who had posterolateral intertransverse lumbar spinal fusion with internal fixation [132].

Another technique to enhance arthrodesis is to perform a posterior lumbar interbody fusion (PLIF). This entails the complete removal of the intervertebral disc, decortication of the vertebral endplates, and insertion of an intervertebral bone graft [133]. Either a bone graft is placed alone, or an interbody spacer (made of metal or polyetheretherketone) filled with bone graft is inserted into the cleared disc space (Figure 6.3). Pedicle screws are then used to provide stability [133].

It is also possible to perform posterior and interbody fusions simultaneously, termed a circumferential or 360° fusion. While this provides a much higher chance of successful fusion, circumferential fusions require a longer operating time, greater blood loss, higher cost, and a longer hospital stay [133].

As with most current bone grafting procedures, autograft bone remains the most common graft type used in spinal fusion procedures. However, the increased postoperative pain and cost that autografts add to spinal procedures creates a demand for bone graft substitutes [133]. Allograft and demineralized bone are also commonly used in spinal fusion, but carry risk of immunogenic response and disease transmission, and have decreased osteogenic potential and strength due to processing [133]. Alloplasts such as hydroxyapatite, tricalcium phosphate, and

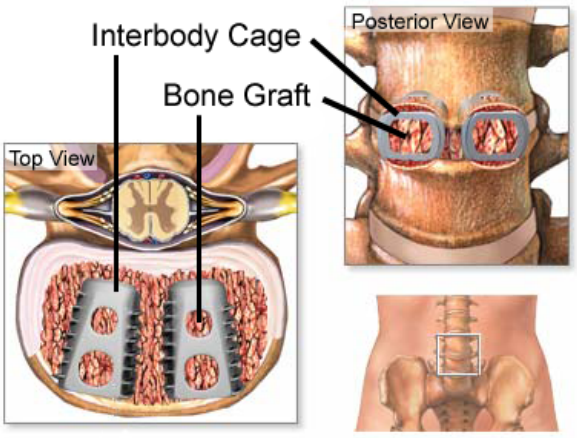

Figure 6.3: Interbody spinal fusion using a titanium cage filled with bone graft [image modified from http://adam.about.com/encyclopedia/]

coral derivatives relieve the hazards of disease transmission and immune response. However, they produce much lower fusion rates when used alone in comparison to autograft and allograft [133].

6.2.1. BC-CdHAP for Spinal Fusion

Neurosurgeons were presented with samples of the BC-CdHAP and subsequently surveyed. The surgeons indicated that they liked the morphology, feel, and handling properties of the BC-CdHAP membrane. They stated that they liked working with flexible membranes which could easily be cut and shaped for specific defect sites. They are much easier to handle than synthetic grafts that come in a powder, morsel, or putty form. An Implant Technician and Planner from a hospital operating room stated that neurosurgeons prefer a flexible sheet form for bone grafts as it gives doctors more options for application. A common practice is to roll the flexible membrane into a “cigar” and insert it into the cavity or gap. The technician also believed that since the BC-CdHAP can be used straight out of the package, it is much more user friendly in comparison with other products which must be mixed or combined right before application. The Infuse® product comes in two components and cannot be implanted until a precise time after mixing. As mentioned, interbody cages are commonly used in spinal fusion procedures which are

filled with the bone graft. Thus, the regenerative properties of the BC-CdHAP could easily be packed into the cages which would provide structural support. It was also commented that if the BC-CdHAP could be cost-effectively produced, a lower price would be a major incentive for many surgeons and hospitals to use this material.

A highly competitive bone graft currently on the market is called Infuse® (Medtronic: Minneapolis, MN, U.S.A.). This product utilizes biologic growth factors to stimulate rapid bone growth. Infuse® features recombinant human bone morphogenetic protein 2 (rhBMP-2) in a bovine Type I collagen sponge carrier.

While this product has found great success in spinal fusion, BMP-2 is very expensive. This discourages many hospitals and physicians from using Infuse® since insurance cannot cover its cost. Other difficulties arise in the preparation and delivery of this product. Infuse® comes in two components, the collagen sponge and a syringe with the rhBMP-2. The rhBMP-2 must injected into the sponge at least one half hour, but no more than 2 hours, prior to implantation.

BC-CdHAP may be an efficient delivery system to BMP-2 since proteins readily bind to hydroxyapatite via electrostatic interactions. If the BC-CdHAP could release BMP-2 in an efficient manner, less protein would be needed and the product would be less expensive. Additionally, if the protein is preloaded onto the BC-CdHAP, there would be no need to mix the components prior to implantation.

6.3. Orthopaedics

Orthopaedic surgeons use bone grafts primarily in two areas: repairing severe fractures and reconstruction during artificial joint revisions. As evident in Figure 6.1, fractures requiring bone grafts primarily occur in the femur, tibia, and fibula; but also occur in the humerus, radius, and ulna. A significant number of bone grafting procedures were performed on total hip arthroplasty revisions, with a smaller number utilized in total knee arthroplasty revisions (Figure 6.1).

6.3.1. Fracture Repair

It has been estimated that 7.9 million fractures occur annually in the United States and between 5-10% of these result in delayed or impaired healing [134]. The three main options for bone fracture treatment are casting, open reduction followed by internal fixation, and open reduction followed by external fixation. The latter two procedures require surgery to repair the fracture via screws, plates, and/or rods under the skin (internal fixation) or placement of an external frame (external fixation) to support the bone and keep it in place. Bone grafts may be used to ensure proper healing or to accelerate fracture healing [134]. In general, bone graft substitutes alone provide no stability to the fracture site and must be used in conjunction with internal or external fixation. They are typically employed early after a fracture if there is a significant loss of bone, a considerable gap between the broken ends (non-union), or to prevent delayed healing.

As previously mentioned, autografting and allografting present severe problems and risks which may be alleviated with the development of efficacious alloplasts. Various alloplasts have been used for bone fracture repair including ceramics (hydroxyapatite, tricalcium phosphate) and polymers (polymethylmethacrylate, polyglycolide, poly-L-lactide). One study found that hydroxyapatite performed equally as well as autograft in the treatment of tibial plateau fractures [136]. Another successful product is an injectable calcium phosphate cement called Norian SRS® (Synthes: West Chester, PA, U.S.A.) which sets into carbonated apatite which can be remodeled into natural bone [135]. Norian SRS® is appropriate for non-weightbearing applications or to augment fixation devices (33, 135). It is strongly believed that synthetic scaffolds may be developed in conjunction with biologics (BMP, TGF- β) to produce an alloplast with superior compressive resistance and comparable osteogenic capacity than that of autograft bone [135].

6.3.2. Joint Revision Reconstruction

The number of revision total hip arthroplasties increased from approximately 24,000 in 1990 to 43,000 in 2002, while the number of revision total knee arthroplasties increased from

approximately 12,000 in 1990 to 35,000 in 2002 [137]. The large number of failed joint replacements has significantly increased the demand for bone grafts [138]. After the failure of a primary joint arthroplasty, less bone is available due to stress shielding, osteolysis, loosening, or infection [139]. More bone may also be removed during implant removal [139]. During revisions, deficient bone stock must be reconstructed to restore proper kinematics and allow component fixation [138].

Bone defects repaired during joint revision surgery are usually quite substantial. Autograft bone is uncommon in most revision procedures due to size limitations, donor site morbidity, and concerns about bone quality in elderly and postmenopausal female patients [140]. Subsequently, allograft is the most common bone graft used in joint revision surgery [139, 141].

During revision knee arthroplasty, bone stock in the femur and tibia is typically reconstituted by bulk allograft or impaction morselized allograft bone grafting which can be supplemented by cement or metal augments (Figure 6.4) [141]. During revision hip arthroplasty, the acetabular component can be reconstructed using cancellous autograft with hemispheric components, grafting of osteolytic defects with cementless cup retention, cancellous allograft with acetabular reconstruction cages, and acetabular impaction grafting with cement [140]. Revision hip reconstruction of the femoral component can be accomplished via impaction cancellous grafting with cementing, grafting around well-fixed components, and grafting of osteolytic lesions

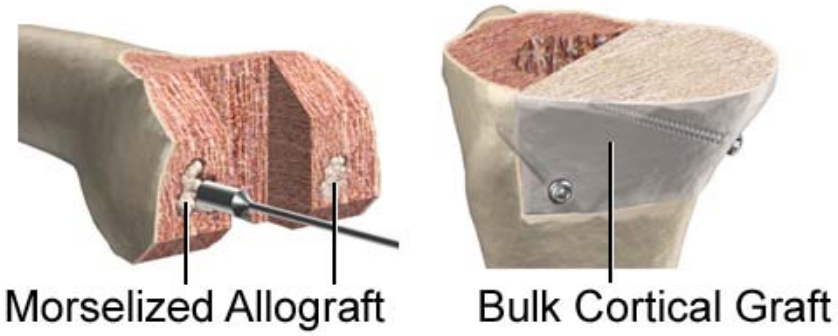

Figure 6.4: Illustration of knee revision arthroplasty reconstruction of femoral component with morselized bone graft (left) and bulk cortical allograft reconstruction of tibial component (right) [image modified from http://www.eorthopod.com]

in the greater trochanter [140].

Impaction grafting using morselized allograft is a prevalent method in both knee and hip revision procedures [142, 143]. An illustration of femoral impaction grafting during hip revision from Nellisen *et al.* is shown in Figure 6.5 [142]. The basic steps of impaction grafting entail the removal of the old implant and cement, restriction of the canal by using a bony pedestal or cement restrictor, reinforcing the bone wall with screening or wires, impacting cancellous bone chips using a tamper, insertion of cement to incorporate with the bone graft, and implantation of the new stem while the cement is setting [142, 143].

Ceramic alloplasts are approved for filling nonweightbearing bone defects in the extremities and pelvis, but the efficacy of their use in revision arthroplasty procedures has not been sufficiently studied [140]. There are also concerns about the possible migration of ceramic grafts into the joint space which could cause third body wear [140].

A significant drawback in the development of efficacious bone grafts for joint revision procedures is insufficient testing and data. One reason is the lack of appropriate animal models to simulate the biologic environment of arthroplasty procedures. The few studies of bone graft incorporation in humans that have been completed were analyzed radiographically. Radiographic results do not necessarily correlate with histologic incorporation. Additionally, there are few randomized or comparative studies to determine whether one bone graft option is clinically superior to another [140].

6.3.3. BC-CdHAP for Orthopaedic Bone Grafting

Orthopaedic surgeons surveyed claim that the BC-CdHAP may be used to treat cavitary or contained defects during revision surgery. Significant bone deficiencies found in segmental defects, uncontained defects, or pelvic discontinuities typically require structural grafts and/or metal augments to ensure proper mechanical stability. However, the surgeons claimed that a variety of grafts perform adequately in contained defects. Thus, cost is a major factor in selection

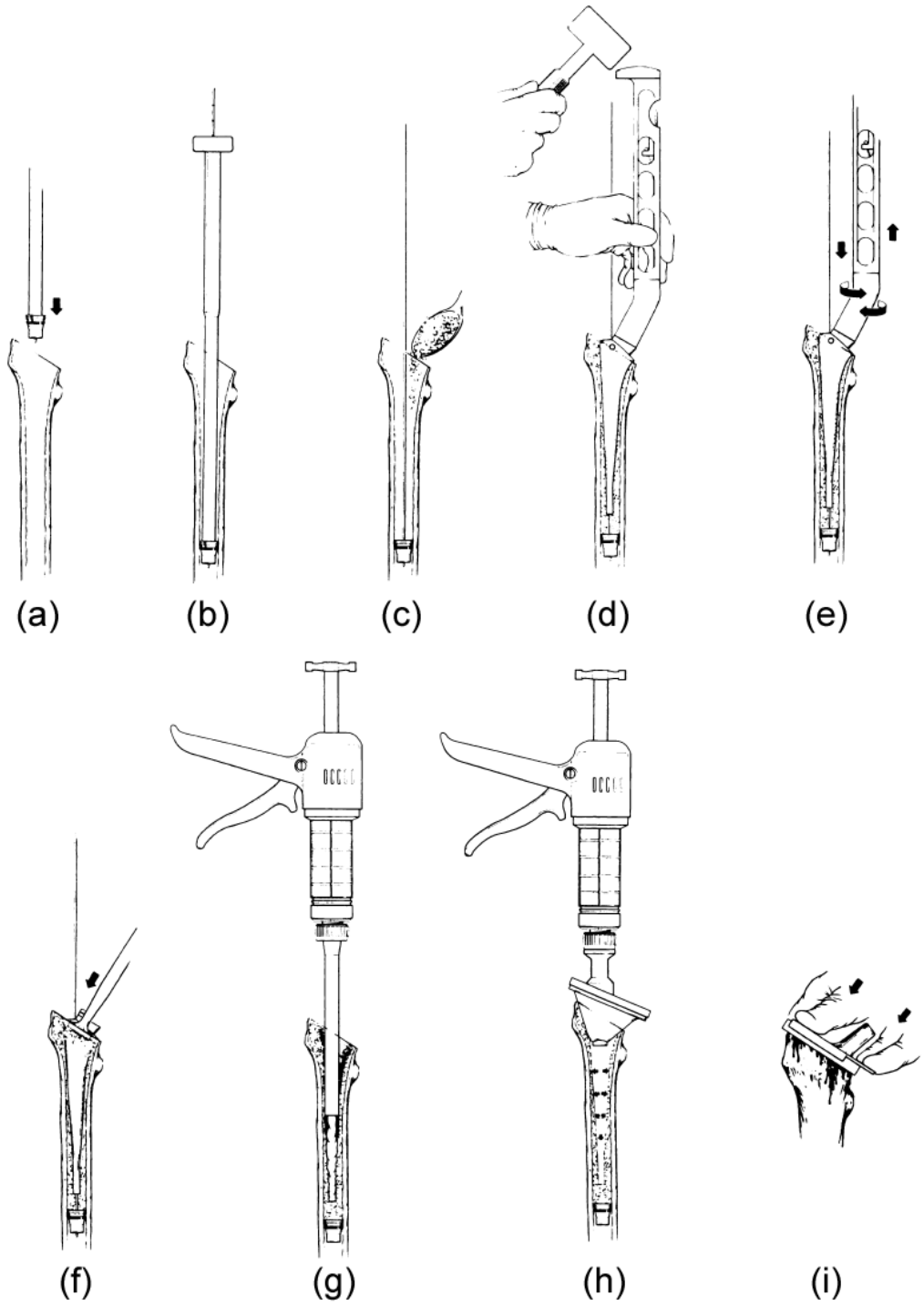

Figure 6.5: Steps involved with impaction grafting of proximal femur: (a) insertion of distal cement plug, (b) plug is driven to distal areas of lytic bone, (c) bone graft is placed into femoral canal, (d) bone graft is packed with cannulated tamp, (e) rotation is applied for adequate tamp seating, (f) additional bone graft is packed near proximal line of resection, (g) cement is introduced into neomedullary canal, (h) cement is pressured with proximal seal, (i) implant stem is introduced and cement is further pressurized with a plate [imaged modified from reference 142]

of grafts for contained defects. If the BC-CdHAP could be made and sold at a competitive price, it would make it an attractive option as an orthopaedic bone graft for contained defects.

6.4. Oral and Maxillofacial Surgery

Bone grafts are used in maxillofacial and oral surgery to repair bone defects caused by trauma, tumors, congenital defects, infection, and jaw resorption due to edentulism. Oral surgeons were interviewed and described the main bone grafting procedures they perform along with the type of graft typically used.

Patients who have significant bone loss due to cancer and removal of tumors undergo bone grafting after disease treatment. The surgeons stated that they almost exclusively used autograft bone for larger defects. They claim the autogeneous bone produces a quicker, safer, and more complete bone restoration than allograft or synthetic grafts. However, the surgeons are more likely to use allografts or alloplasts for smaller defects. Similar comments were made about defects due to trauma: autograft bone for larger defects while allograft and alloplast materials for smaller repair sites.

A common congenital defect that oral/maxillofacial surgeons address is cleft palate. Bone grafting is standard treatment for treating patients with facial clefts. This provides support for teeth, lip, nose, premaxilla, and provides improved symmetry of appearance. Gaps present in the alveolus and palate are filled with bone graft. Autograft is most commonly used, although allograft bone is used on occasion.

The most common bone grafting procedures oral and maxillofacial surgeons entails the restoration and preservation of the jaw and alveolar ridge due to tooth loss or periodontal disease. Many times, these procedures are termed “dental bone grafts” since they are conducted in preparation of dental implants. Dental implants are increasingly accepted as a replacement for missing or extracted teeth and offer improved aesthetics and function compared to dentures. Dental implants are surgically anchored into the jawbone via titanium screws [14]. The success

of the dental implant is dependent on the bone quantity and quality where it is placed. For that reason, grafting is essential to create a strong osseous foundation for dental implantation.

Patients who must have teeth removed as a result of trauma, periodontal disease, or caries are susceptible to bone loss in the jaw. After a tooth is extracted, there is a 25% decrease in the width of alveolar bone during the first year. In the first year following multiple extractions, alveolar bone height decreases an average of 4 mm [14]. A procedure that prevents jaw resorption after tooth removal is site extraction preservation. Oral surgeons will fill the socket with bone graft to stimulate new bone growth (Figure 6.6). Commonly, allograft bone chips or ceramic particles are used. To ensure the graft stays in place, the site is typically covered with a resorbable membrane (Figure 6.6). Surgeons surveyed use a variety of grafts for this procedure including demineralized allograft bone, β-tricalcium phosphate particles, or Bio-Oss® xenograft (Osteohealth: Shirley, NY, U.S.A.).

Patients who have suffered tooth loss without site extraction preservation typically

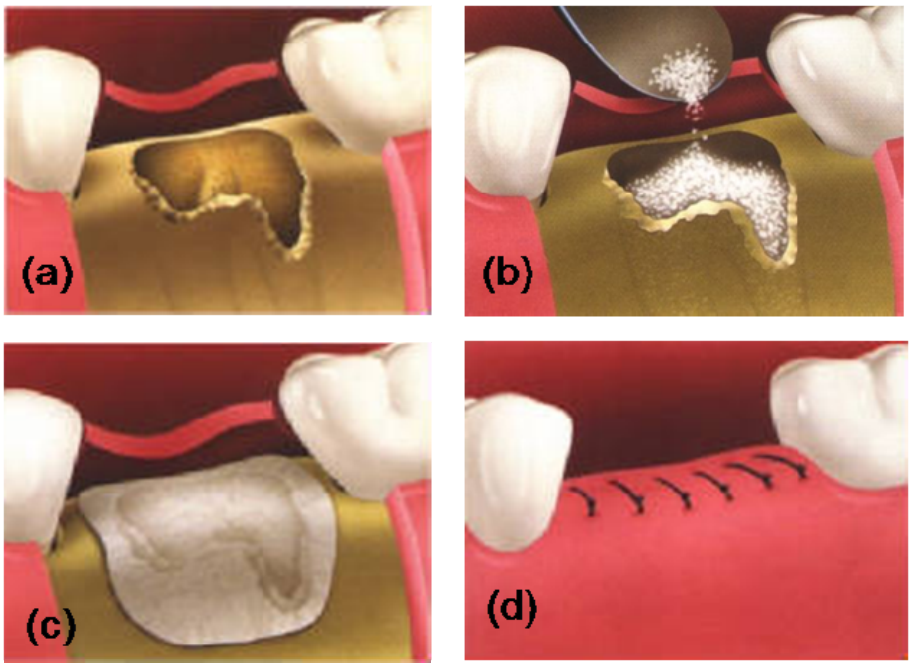

Figure 6.6: Site extraction preservation procedure: (a) tooth is removed, (b) bone graft material is placed into the extraction socket, (c) a membrane is often placed over the grafted material, (d) sutures are placed into the gum tissue [image modified from http://henryschwartz.tripod.com]

develop a defect in the jaw ridge. One method to repair this is ridge augmentation [14]. During this procedure, the bony ridge of the jaw is expanded with metal rods. The inner spongy component of the ridge bone is compressed and the outer cortexed is expanded with tapping expanders to create a socket. Bone graft is placed in the socket to stimulate new bone growth (Figure 6.7). Surgeons surveyed typically use autogenous bone from the back of the mandible (ramus) or chin for ridge augmentation, or demineralized freeze-dried bone.

Alternatively, bone can be regenerated on top of the upper jaw with a sinus lift procedure (Figure 6.7). In this technique, a window is created in the maxillary sinus. The sinus membranes are lifted, and the resulting gap is filled with bone graft. Sinus lifts can also be performed in conjunction with the placement of dental implants (Figure 6.8). Surgeons surveyed use demineralized freeze-dried bone, β-tricalcium phosphate, or Bio-Oss® xenograft for sinus lift procedures. Larger sinus lifts may require autograft bone obtained from the chin or back of the jaw.

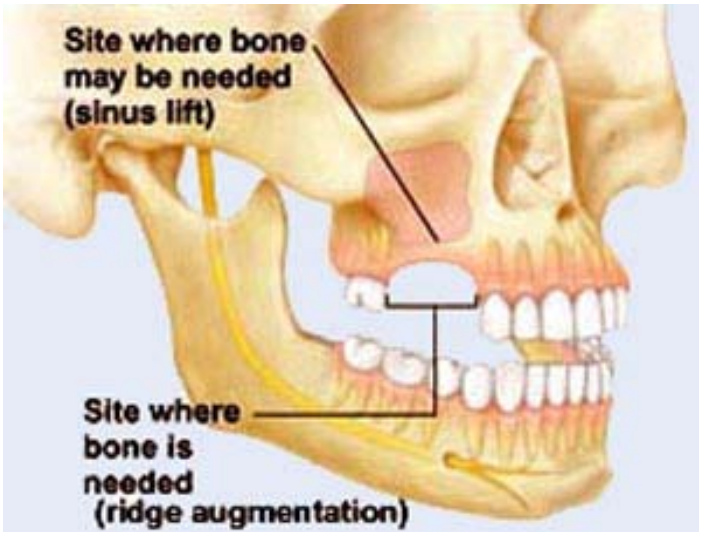

Figure 6.7: Dental bone grafting sites for ridge augmentation and sinus lifts [image taken from http://www.americandental.ru]

6.4.1. BC-CdHAP for Dental Bone Grafting

Direct feedback from oral surgeons indicated that the BC-CdHAP material has ideal material properties for dental bone grafting procedures. Bone in this area is in close proximity to soft tissues including gingiva, nerves, and sinus membranes. Traditional bone grafting materials including allograft bone chips, xenograft hydroxyapatite particles, or β-tricalcium phosphate granules have great potential to damage surrounding soft tissues. Additionally, these loose grafts are prone to leakage and migration.

The BC-CdHAP material features a flexible and supple membrane than can easily be packed into defects of various shapes and sizes. The CdHAP nanocrystallites are evenly dispersed throughout the bacterial cellulose producing a strong flexible sheet with a soft nonabrasive surface. The nanocrystallites also have high surface area which provides active sites for bone cell attachment. Since the particles are chemically bound to the cellulose, this ensures that the bioactive CdHAP is immobilized in the defect site. This provides direct osteoconduction and prevents migration of the CdHAP to surrounding tissues.

In site extraction preservation procedures, the socket is filled with bone chips and

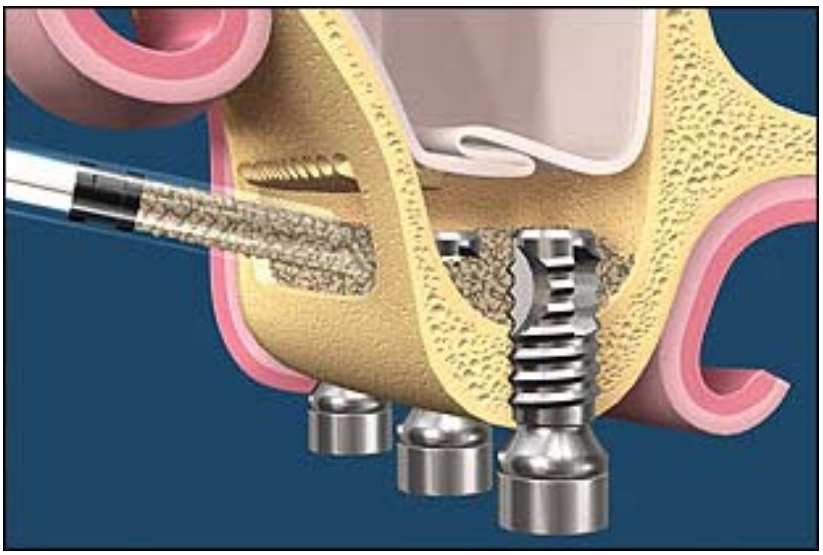

Figure 6.8: Sinus lift procedure performed in conjunction with dental implantation [image taken from http://www.dr4est.com]

ceramic particles. The socket is then covered with a membrane to keep the graft in place. The flexible and supple BC-CdHAP material can easily be packed into extraction sites. The nonabrasive CdHAP nanocrystallites will not damage the surrounding gum tissues. The cellulose carrier also prevents the CdHAP particles from migrating to neighboring areas. An extra membrane to cover the graft is thus unnecessary.

During sinus lifts, the delicate Schneidian membrane of the sinus is prone to damage [145]. Traditional bone chips and brittle ceramic particle bone grafts can puncture this membrane up to 60% of the time [145]. The particles can then migrate into the sinus cavity and cause complications such as graft contamination, bacterial infection, and sinusitis. Being soft, flexible, and nonabrasive; the BC-CdHAP matrix can be packed against the sinus membranes and not cause damage. If perforation does occur during the operation, the CdHAP particles are immobilized in the cellulose and would not migrate into the sinus cavity.

Chapter 7

Future Studies: Preclinical Animal Testing

Additional testing must be carried out before this product can be put to clinical use as a bone substitute. These remaining evaluations are outlined in Table 7.1. A research and development director from a medical products company was consulted to estimate the approximate cost and time to execute these tasks.

Another crucial step before this composite can be used is obtaining FDA approval. BC-CdHAP is classified as a Class II device (FDA Section 872.3930) and would most likely qualify for the less rigorous 510(k) procedure as opposed to the substantial Premarket Approval process. In the 510(k), it must be demonstrated that BC-CdHAP is composed of materials that are substantially equivalent to devices that have already been FDA-approved.

Table 7.1: Remaining steps towards bringing BC-CdHAP to clinical use

	Item	Cost	Duration
	Misc. Development*	$ 10,000	24 mo
	Preclinical Efficacy - Large Mammal	$ 80,000	12 mo
Preclinical Safety	Cytotoxicity	$ 1,500	3 mo
	Irritation	$ 1,000	3 mo
	Sensitization	$ 7,000	3 mo
	Acute Systemic Toxicity	$ 750	6 mo
	Hemolysis	$ 750	3 mo
	Genotoxicity / mutagenicity	$ 23,000	6 mo
	Subchronic Toxicity	$ 21,000	6 mo
	Chronic Toxicity	$ 30,000	9 mo
	Scale-up/Validation*	$ 10,000	6 mo
	FDA Regulatory Fees - 510(k)	$ 3,000	4 mo
	Clinical Evaluation**	$ 300,000	18 mo
	Misc. Consulting	$ 24,000	24 mo
	Capital estimate***	$ 300,000	24 mo
	TOTAL	**$ 812,000**	

* Does not include capital equipment needs
** Assumes 20 patients at $15,000 each
*** Includes growing, cleaining, and processing of raw material; product preparation, formulation, and packaging in controlled environment

Xylos® Corporation (Langhorne, PA, U.S.A.) obtained FDA approval for their bacterial cellulose wound dressing called XCell® as well as bacterial cellulose repair material for the dura mater and rotator cuff. Xylos® was able to receive all their FDA approvals via the 510(k) process.

Since both bacterial cellulose and hydroxyapatite have been used in several FDA-approved medical devices, it can be proved that BC-CdHAP is substantially equivalent to these existing products. It is anticipated that a 510(k) application can be approved without much difficulty.

A logical next step in the development of BC-CdHAP is preclinical animal testing. Though not carried out, a protocol to evaluate the composite using a rabbit calvarial model was designed and will be described in this chapter.

7.1. Necessity of In-Vivo versus In-Vitro Testing

Before a biomaterial can be employed in clinical use, it must undergo rigorous evaluation with a variety of tests to ensure its safety and efficacy. An integral component of this evaluation is biological testing to prove that it is compatible and will function in a biologically appropriate manner in the clinical *in-vivo* environment [146l]. *In-vitro* testing with isolated mammalian cells gives some indication of a material's biocompatibility, but it is important to determine the biological response in a fully integrated system. A material which may show a positive *in-vitro* response may produce completely different results when implanted in a living organism. Ratner offers the example of how most mammalian cells will attach and proliferate on surface-modified tissue culture polystyrene, but none will attach or grow on untreated polystyrene, however both materials react indistinguishably when implanted *in-vivo* and heal with a thin foreign body capsule [146]. *In-vivo* testing with animal models gives a much closer indication of how a material responds to all the chemical/biological species and physical stimuli present in a living organism. Preclinical testing in small mammals is a standard requirement in the development of medical devices and materials for human clinical use. The FDA, ASTM, and USP all provide procedures,

protocols, guidelines, and standards that may be used in the *in-vivo* assessment of the tissue compatibility of medical devices [147].

7.2. Selection of Animal and Bone Defect Model

Pigs, dogs, rabbits, rats, and mice are accepted animal models for the *in-vivo* assessment of bone substitutes [147]. Rabbits are selected for this study since there is a large presence of previous work in the literature that validates the use of rats in bone substitute testing, and they can be easily and economically obtained through reputable vendors. Based on the surgeon interviews reported in the last chapter, it was concluded that this particular bone graft would ideally be used in oral and maxillofacial applications. Direct feedback from the surgeons indicated that this material would find great success for site extraction preservation and sinus lift procedures.

The rabbit calvarial model is ideal for the assessment of bone grafts for the regeneration of craniofacial defects [148]. The calvarium has a low incidence of morbidity, has close proximity to the operative site, has a decreased amount of resorption as a result of its membranous nature, and does not require fixation due to the support provided by the dura and overlying skin. The critical size defect in rabbit calvaria has well studied and extensively used in the evaluation of potential bone grafts [149,150,151]. The results of these studies have shown the value of this model to evaluate the bioactivity and biocompatibility of bone graft materials. The steps of this procedure, the necessary animal care, and the size of the defects required are well established.

7.3. Alternatives Search

The Institute for Animal Care and Use Committee (IACUC) and USDA mandate that alternative procedures must be considered for procedures involving all live vertebrate animals, which obviously cause more than momentary pain, distress, or discomfort. The USDA (Policy 11 & 12) states that any procedure, which requires the use of an anesthetic or analgesic to prevent pain or discomfort, is by definition a painful procedure. A literature must be performed to find

alternatives that can either replace animal methods with non-animal methods, reduce the number of animals needed, or refine research procedures to minimize pain and discomfort.

A literature search was conducted using Medline / Pubmed, Web of Science, and Agricola. Keywords used were “Calcium-deficient hydroxyapatite and bone substitute,” “Calcium-deficient hydroxyapatite and in-vivo”, “Bacterial Cellulose,” “Bone substitute and rabbit and calvarium,” “Rabbit and calvarium and critical size defect.”

This literature search confirmed that there has been no biological testing done on this proposed bone graft consisting of calcium-deficient hydroxyapatite and bacterial cellulose (BC-CdHAP). A study by Bourgeois *et al.* performed in-vivo testing on calcium-deficient hydroxyaptite (CdHAP) particles suspended in hydroxypropylmethylcellulose (plant derived) in a rabbit femur [37]. However, the CdHAP used in this study was a 40-80 µg powder made via a completely different synthesis route. The CdHAP in the bacterial cellulose (BC) matrix has a similar size (10-50 nm) and geometry to bone apatite and is chemically bonded to the BC matrix. BC also has a similar nanofibril structure to natural collagen found in bone. However, Bourgeois *et al.* did confirm that CdHAP was a biocompatible and bioactive substance that elicited new bone ingrowth [37].

As there has not been a preclinical animal study performed on this specific material, there is not a sufficient replacement method for this important work. As previously stated, *in-vitro* testing gives some indication of a material’s biocompatibility; but an integrated biological system (e.g. animal model) is necessary to thoroughly assess the safety and efficacy of a clinical biomaterial. For this reason, an animal study must be conducted to validate use of this potential bone graft. If successful, this bone graft could be used to treat animals and humans alike.

7.4. Statistical Determination of Replicates

It is necessary to precisely calculate how many replicates will be required so that enough statistical data can be obtained while minimizing the number of animals that must be used. The services of the University of Tennessee Statistical Consulting Center were used to determine the

sample size necessary for a statistically strong study. The results of a similar study was used to determine an approximate standard deviation. JMP statistical software (SAS: Cary, NC, U.S.A.) was used to determine the sample size necessary for detect a given difference in means with a given statistical power (Table 7.2). The number of replicates vary depending on the amount of statistical power desired and the degree of sensitivity required to detect significant difference between means.

This would be a new study, which makes it difficult to anticipate the ranges of means and standard deviations. Previous studies were surveyed to determine what number of replicates had previously been used for similar testing [149,150,151]. The number of replicates varied significantly from study to study, ranging from as many as twenty to as little as three [149,150]. However, most studies used average of 4-6 replicates. Other biostatistics references have cited that four to six animals per study group is the minimum necessary for adequate statistical power to gain useful information using analysis of variance for repeated measures to assess any statistical differences within and between groups and times [152]. Based on these results, it was determined that six replicates would be sufficient for this study.

7.5. Testing Protocols

To thoroughly analyze the bone regeneration potential of the proposed material, two separate studies will be carried out. Since different synthesis parameters of the material may

Table 7.2: Statistical determination of replicates using JMP Software (SAS: Cary, NC, U.S.A.)

	Number of Replicates for 80% Statistical Power	Number of Replicates for 90% Statistical Power
To detect a 5% difference in bone ingrowth between groups	10	20
To detect a 10% difference in bone ingrowth between groups	5	6
To detect a 15% difference in bone ingrowth between groups	3	4
To detect a 20% difference in bone ingrowth between groups	3	3

affect bone growth, the first test will be a screening study to determine what specific material formulation elicits the most bone growth. The optimal material determined in the screening study will then undergo a second study where it will be implanted in a critical size defect.

7.5.1. Screening Study

The two main factors that will be tested are the use of native versus oxidized cellulose and varying the weight percentage of the calcium-deficient hydroxyapatite (CdHAP). Native and oxidized cellulose will be tested with three 3 different weight percentages of CdHAP (15, 30, and 50 wt%). In all, nine conditions will be analyzed as described in Table 7.3.

Since this will be a brief evaluative study, a smaller defect size (6 mm) and short test duration will be used (one month). A New Zealand rabbit calvarium can accommodate four 6 mm defects (Figure 7.1). Fourteen rabbits will be used in all for the screening study providing 56

Table 7.3: Sample conditions and abbreviations for first screening study

Testing Condition	Condition Abbreviation
Empty defect	Emp
Native bacterial cellulose	Nat
Native bacterial cellulose with 15wt% CdHAP	Nat15
Native bacterial cellulose with 30wt% CdHAP	Nat30
Native bacterial cellulose with 50wt% CdHAP	Nat50
Oxidized bacterial cellulose	Ox
Oxidized bacterial cellulose with 15wt% CdHAP	Ox15
Oxidized bacterial cellulose with 30wt% CdHAP	Ox30
Oxidized bacterial cellulose with 50wt% CdHAP	Ox50

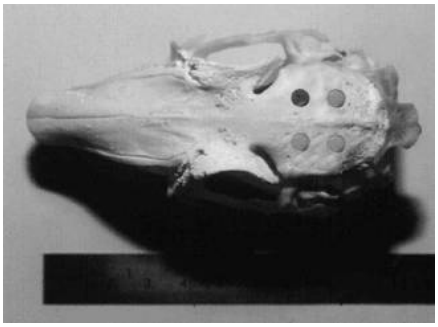

Figure 7.1: Rabbit calvarium with four six millimeter defects [modified from reference IV]

defects. To produce a statistically sufficient study, each of the 9 conditions will be expressed at least six times with two conditions will be expressed seven times. Each rabbit defect will been randomly allocated a sample to reduce statistical error as shown in Figure 7.2.

After implantation, the implant site will be evaluated to determine the capacity of the composite to regenerate bone. The total bone volume in the defect will be determined using histological staining with calcein green. Additionally, bone ingrowth will be assessed using histomorphometry with tetracycline double labeling. This technique calculates kinetic data on bone turnover. Tetracycline binds to newly formed bone at the bone/osteoid (unmineralized bone) interface where it produces a linear fluorescence. Doses of tetracycline are administered to the active site ten and three days prior to sacrifice. The amount of bone formed between tetracycline injections can be calculated by measuring the distance between the two fluorescent labels.

7.5.2. Full Critical Size Defect Study

A well-established model for testing potential bone repair materials (BRM) is the critical size defect as developed by Schmitz and Hollinger [153]. A successful BRM will heal more quickly than a control (empty) defect [154]. An ideal testing model would demonstrate defect healing only in the presence of a BRM [154]. A critical size defect (CSD) is the smallest intraosseous wound that will not heal by bone formation during the lifetime of the animal, and is specific to the species and location of the bone [153]. Testing potential BRMs in a CSD model provides affirmative and scientifically sound conclusions as to whether a material possesses bone regeneration properties [153].

Based on the results of the screening study, the most successful composite formulation will be used in a full critical size defect study in rabbit calvaria. Schmitz and Hollinger determined that the critical size defect for rabbit calvaria is 15mm [153]. A rabbit calvarium can accommodate two full 15 mm critical size defects (Figure 7.3). For this study, one defect will be

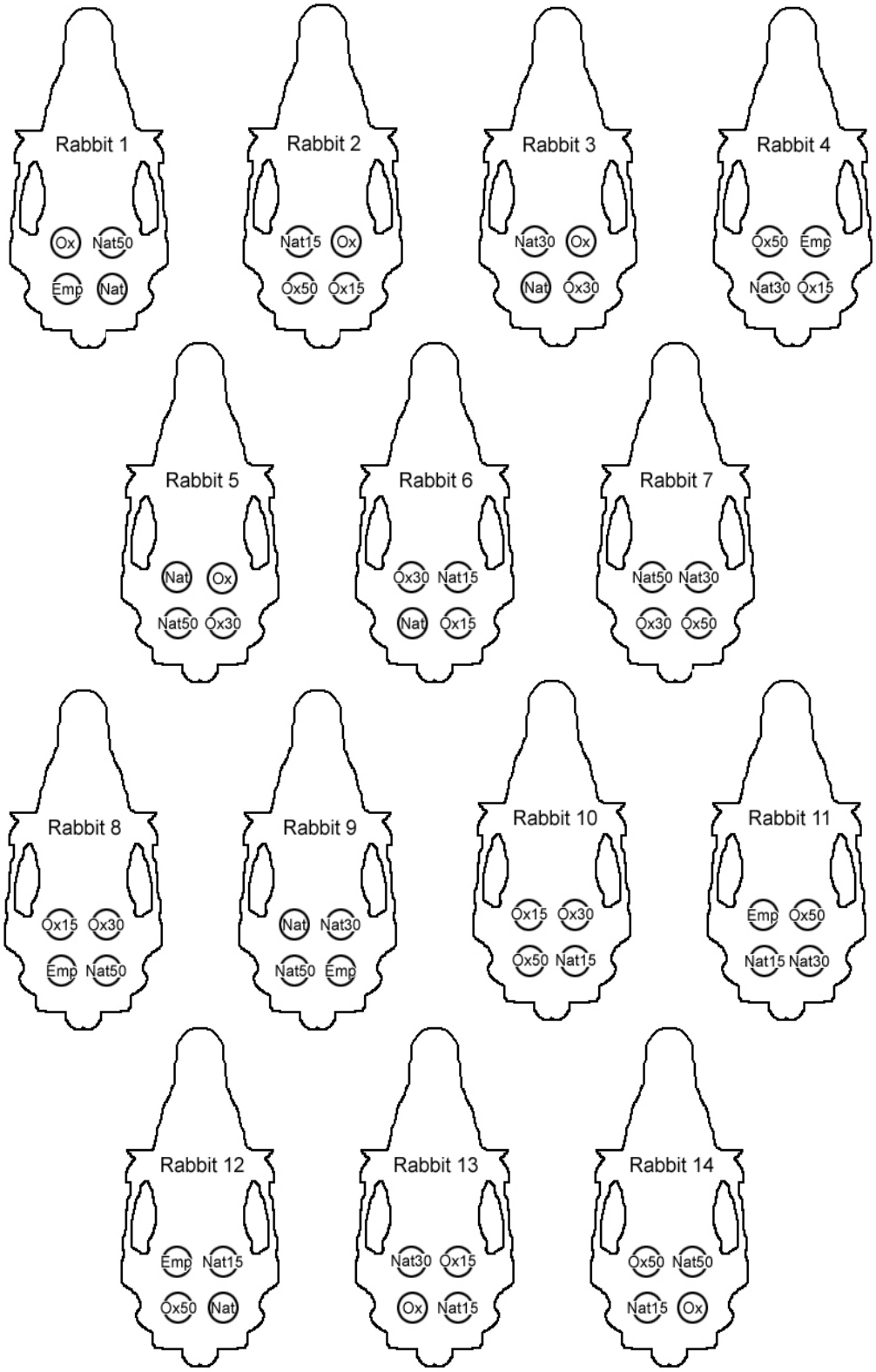

Figure 7.2: Random assignment of samples to rabbit calvarial defects for screening study

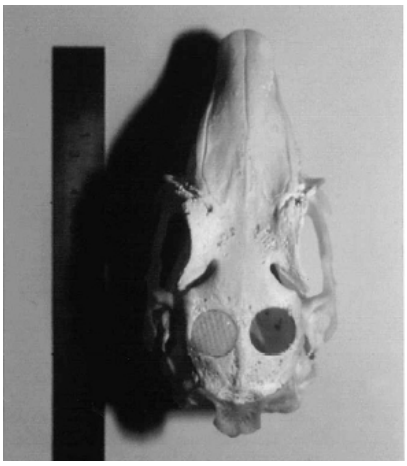

Figure 7.3: Rabbit calvarium with two 15 millimeter full critical size defects [IV]

filled with the composite material while the other defect will be left empty for comparison. Eighteen rabbits will be used in all over three months, with three one month timepoints taken. After each month, six rabbits will be sacrificed and evaluated for bone ingrowth using histology and histomorphometry as described in the screening study.

7.5.3. Description of Animal Procedures

Specific Pathogen Free New Zealand White Rabbits will be purchased from Myrtle's Rabbitry (Thompson Station, TN, U.S.A.). Fourteen rabbits (6-7 lbs, male and female) will be acquired for the screening study and eighteen will be used for the critical size defect study. Rabbits will be tattooed for identification at the rabbitry prior to shipping. The animals will be placed in appropriate shipping crates and a gel pack will be provided for each rabbit. They will be flown into Tyson McGhee Airport where a courier service will pick them up and deliver them to animal facility.

At the animal facility, rabbits will be housed in separate stainless steel cages where they will be provided with food and water by the animal facility staff. The animals will have a one week acclimation period to recover from stress and environment change.

Food and water intake will be restricted twelve hours prior to surgery. Surgery will be carried out under aseptic conditions in a dedicated surgical suite. Half an hour before surgery,

Buprenorphine (0.02 mg/kg IM), Atropine (0.1 mg/kg IM), and Ancef (3.5 mg/kg IM) will be administered to each animal.

The animals will be anesthetized with Ketamine (3.5 mg/kg IM) and Xylazine (5 mg/kg IM). Level of anesthesia will be constantly monitored by observing respiration rate, heart rate, corneal reflex, color of mucus membranes, and muscular relaxation. The surgical site (calvarium) will be prepared by shaving and sterilization with betadine. A 3-4 cm vertical incision will be made along the midline of the calvarium with blunt dissection down to the bone followed by elevation of the periosteum. Four 6 mm diameter defects will be made using a standard bone trephine: two on either side of the midline. Sterile samples of the composite bone graft material will be placed into certain defects while other defects will remain empty for comparison.

The periosteum will then be replaced over incision and sutured (3-0 Vicryl). Fascia, subdermal, and skin layers will then also be closed by suturing (3-0 PDS and 3-0 Vicryl). Buprenorphine (0.02 mg/kg IM) will be administered immediately post-surgery, and then again as needed for pain. Rabbits will be monitored post-operatively for anesthesia and surgical recovery by measuring heart and respiration rate and observing color of mucus membranes, corneal reflex, muscle coordination, and return to normal eating habits and activity levels.

Post-surgery, rabbits will be monitored at least twice daily by observation of respiration, eating habits, fecal output, and activity levels. Animals will be weighed at the beginning of the study and once a week subsequently.

On the tenth and third day prior to sacrifice, each animal will be administered an injection of tetracycline (10 mg/kg IM). Animals will be euthanized by a lethal dose of Beuthanasia (1 mg/kg IV). After histological and histomorphometric analysis, carcasses will be disposed by incineration.

References

[1] Van de Graff KM, Rhees RW. *Human anatomy and physiology*. New York, NY: McGraw-Hill (2001)

[2] Hench LL, Best S. "Ceramics, glasses, and glass-ceramics." In *Biomaterials Science.* Ratner BD, Hoffman AS, Schoen FJ, Lemons JE (eds.) San Diego, CA: Elsevier Academic Press (2004) 153-170

[3] Bilezikian JP, Raisz LG, Rodan GA. *Principles of Bone Biology.* San Diego, CA: Academic Press (1996)

[4] Marks SC, Popoff SN. "Bone Cell Biology: The Regulation of Development, Structure, and Function in the Skeleton." *Am J Ana.* 183 (1988) 1-44

[5] Mundy GR, Martin TJ. *Physiology and Pharmacology of Bone.* New York, NY: Springer-Verlag (1993)

[6] Bruder SP, Caplan AI. "Bone regeneration through cellular engineering." In *Principles of Tissue Engineering.* Lanza RP, Langer R, Vacanti J (eds.) San Diego, CA: Academic Press (2000) 683-696

[7] Bukka P, McKee MD, Karaplis AC. "Molecular regulation of osteoblast differentiation." In *Bone Formation*. Bronner F, Farach-Carson MC (eds.) London, UK: Springer-Verlag (2004) 1-17

[8] Urist MR. "Bone: formation by autoinduction." *Science* 150 (1965) 893-899

[9] Urist MR, Mikulski A, Lietze A. "Solubilized and insolubilized bone morphogenetic protein." *Proc Natl Acad Sci USA* 76 (1979) 1828-1832

[10] Bensen CV, An YH, Friedman RJ. "Preclinical evaluation of bone graft substitutes," In *Biomaterials and Bioengineering Handbook.* Wise DL (ed.) New York, NY: Marcel Dekker, Inc. (2000) 675-697

[11] Gresser JD, Trantolo DJ, Wise DL, Lewandrowski K-W. "Engineering of resorbable grafts for craniofacial reconstruction." In *Biomaterials and Bioengineering Handbook.* Wise DL (ed.) New York, NY: Marcel Dekker, Inc. (2000) 675-697

[12] Ashman A, Gross JS. "Synthetic osseous grafting." In *Biomaterials Engineering and Devices Human Applications, Volume 2: Orthopedic, Dental, and Bone Graft Applications.* Wise DL, Trantolo DJ, Lewandrowski K-W, Gresser JD, Cattaneo MV, Yaszemski MJ (eds.) Totowa, NJ: Humana Press (2000) 133-154

[13] Lewandrowski K-U, Gresser JD, Wise DL, Trantolo DJ. "Bioresorbable bone graft substitutes of different osteoconductivities: a histologic evaluation of osteointegration of poly(propylene glycol-co-fumaric acid)-based cement implants in rats." *Biomaterials* (2000) 757-764

[14] Implant-Based Dental Reconstruction: The Worldwide Dental Implant and Bone Graft Market, 2nd Edition. Pub ID KLI1399457, April 2007. Kalorama Information (Rockville, MD, U.S.A.)

[15] European Markets for Current and Emerging Orthopedic Biomaterials. Report #A325, September 2006. Medtech Insight (Newport Beach, CA, U.S.A.)

[16] Leupold JA, Barfield WR, An YH, Harsock LA. "A comparison of ProOsteon, DBX, and Collagraft in a rabbit model." *J Biomed Mater Res Part B: Appl Biomater* 79B (2006) 292-297

[17] Ley JP, Cranin AN, Katzap M. "Biomaterials used in implant dentistry." In *Biomaterials Engineering and Devices Human Applications, Volume 2: Orthopedic, Dental, and Bone Graft Applications.* Wise DL, Trantolo DJ, Lewandrowski K-W, Gresser JD, Cattaneo MV, Yaszemski MJ (eds.) Totowa, NJ: Humana Press (2000) 3-24

[18] Gazdag AR, Lane JM, Glaser D, Forster RA. "Alternatives to autogenous bone graft: efficacy and indications." *J Am Acad Orthop Surg* 3 (1995) 1-8

[19] Ahlmann E, Patzakis M, Roidis N, Shepherd L, Holtom P. "Comparison of anterior and posterior iliac crest bone grafts in terms of harvest-site morbidity and functional outcomes." *J Bone Joint Surg Am* 84A (2002) 716-720

[20] Alt V, Meeder P-J, Seligson D, Schad A, Atienza C. "The proximal tibia metaphysic: a reliable donor site for bone grafting?" *Clin Orthop Relat Res* 414 (2003) 315-321

[21] Shamsaldin M, Mouchaty H, Desogus N, Costagliola C, Di Lorenzo N. "Evaluation of donor site pain after anterior iliac crest harvesting for cervical fusion: a prospective stud on 50 patients." *Acta Neurochir* 148 (2006) 1071-1074

[22] Joshi A, Kostakis GC. "An investigation of post-operative morbidity following iliac crest graft harvesting." *Br Dent J* 196 (2004) 167-71

[23] Patka P, Haarman HJThM, van der Elst M, Bakker FC. "Artificial bone,2" In *Biomaterials Engineering and Devices Human Applications, Volume 2: Orthopedic, Dental, and Bone Graft Applications.* Wise DL, Trantolo DJ, Lewandrowski K-W, Gresser JD, Cattaneo MV, Yaszemski MJ (eds.) Totowa, NJ: Humana Press (2000) 95-109

[24] Lewandrowski K-U, Schollmeier G, Ekkernkamp A, Mankin KJ, Uthoff K, Tomford WW. "Enhancing cortical allograft incorporation processing by partial demineralization and laser perforation." In *Biomaterials and Bioengineering Handbook*. Wise DL (ed.) New York, NY: Marcel Dekker, Inc. (2000) 111-132

[25] De Boever AL, De Boever JA. "A one-stage approach for nonsubmerged implants using a xenograft in narrow ridges: Report on seven cases." *Int J Periodontics Restorative Dent* 232 (2003) 169-175

[26] Hammerle CHF, Chiantella GC, Karring T, Lang NP. "The effect of a deproteinized bovine bone mineral on bone regeneration around titanium dental implants." *Clin Oral Implants Res* 9 (1998) 151-162

[27] Schultheiss M, Sarkar M, Arand M, Kramer M, Wilke HJ, Kinzl L, Hartwig E. "Solvent-preserved, bovine cancellous bone blocks used for reconstruction of thoracolumbar fractures in minimally invasive spinal surgery - first clinical results." *Eur Spine J* 14 (2005) 192-196

[28] Xie Y, Chopin D, Hardouin P, Li J. "Clinical, radiological and histological study of the failure of cervical interbody fusions with bone substitutes." *Eur Spine J* 15 (2006) 1196-1203

[29] Charalambides C, Beer M, Cobb AG. "Poor results after augmenting autograft with xenograft (Surgibone) in hip revision surgery - A report of 27 cases." *Acta Orthopaedica* 76 (2006) 544-549

[30] Levai JP, Bringer O, Descamps S, Boisgard S. "Xenograft-related complications after filling valgus open wedge tibial osteotomy defects." *Revue de Chirurgie Orthopédique et Réparatrice de l'Appareil Moteur* 89 (2003) 707-711

[31] Anderson LA, Mucalo MR, Johnson GS, Lorier MA. "The processing and characterization of animal-derived bone to yield materials with biomedical applications. Part III: material and mechanical properties of fresh and processed bovine cancellous bone." *J Mat Sci: Mat in Med* 11 (2000) 743-749

[32] Brånemark R, Brånemark P-I, Rydevik B, Myers RR. "Osseointegration in skeletal reconstruction and rehabilitation: a review." *J Rehabil Res Dev* 38 (2001) 175-181

[33] Parikh SN. "Bone graft substitutes: past, present, future." *J Postgrad Med* 48 (2002) 142-148

[34] Gresser JD, Lewandrowski K-U, Trantolo DJ, Wise DL, Hsu Y-Y. "Soluble calcium salts in resorbable bone grafts." In *Biomaterials Engineering and Devices Human Applications, Volume 2: Orthopedic, Dental, and Bone Graft Applications.* Wise DL, Trantolo DJ, Lewandrowski K-W, Gresser JD, Cattaneo MV, Yaszemski MJ (eds.) Totowa, NJ: Humana Press (2000) 171-188

[35] Vallet-Regi M, Rodriguez-Lorenzo LM, Salinas AJ, "Synthesis and characterization of calcium deficient apatite." *Solid State Ionics* 101-103 (1997) 1279-1285

[36] Mavrapoulos E, Rossi AM, da Rocha CC, Soares GA, Moreira JC, Moure GT. "Dissolution of calcium-deficient hydroxyapatite synthesized at different conditions." *Materials Characterization* 50 (2003) 203-207

[37] Bourgeois B, Laboux O, Obadia L, Gauthier O, Betti E, Aguado E, Daculsi G, Bouler J-M. "Calcium-deficient apatite: a first in vivo study concerning bone ingrowth." *J Biomed Mat Res* 65A (2003) 402-408

[38] Chern Lin JH, Kuo KH, Ding SJ, Ju CP. "Surface reaction of stoichiometric and calcium-deficient hydroxyapatite in simulated body fluid." *J of Mat Sci: Mat in Med* 12 (2001) 731-741

[39] Ducheyne P, Qiu Q. "Bioactive ceramics: the effect of surface reactivity on bone formation and bone cell function." *Biomaterials* 20 (1999) 2287-2303

[40] Miyamoto Y, Taketomo T, Ishikawa K, Yuasa T, Nagayama M, Suzuki K. "Effect of added $NaHCO_3$ on the basic properties of apatite cement." *J Biomed Mat Res* 54 (2001) 311-319

[41] Leamy P, Brown PW, TenHuisen K, Randall C. "Fluoride uptake by hydroxyapatite formed by the hydrolysis of α-tricalcium phosphate." *J Biomed Mat Res* 42 (1998) 458-464

[42] Migliaresi C, Alexander H. "Composites." In *Biomaterials Science.* Ratner BD, Hoffman AS, Schoen FJ, Lemons JE (eds.) San Diego, CA: Elsevier Academic Press (2004) 181-197

[43] Bonfield W. "Composite biomaterials: present and future." In *Bioceramics Volume 11.* New York: World Scientific Publishing Company (1998) 37-40

[44] Heller J, Hoffman AS. "Drug delivery systems." In *Biomaterials Science.* Ratner BD, Hoffman AS, Schoen FJ, Lemons JE (eds.) San Diego, CA: Elsevier Academic Press (2004) 628-648

[45] Walton AG, Blackwell J. *Biopolymers.* New York, NY: Academic Press (1973)

[46] Bielecki ES, Krystoynowicz, Turkiewicz M, Kalinowska H. "Bacterial Cellulose" In Vandamme E.J., De Baets S., Steinbüchel A., (eds.) *Biopolymers, Volume 5, Polysaccharides I: Polysaccharides from Prokaryotes*. Weinham: Wiley (2001) 37-90

[47] Xylos® Corporation: https://xyloscorp.com

[48] Nishiyama Y, Sugiyama J, Chanzy H, Langan P. "Crystal structure and hydrogen bonding system in cellulose I_α from synchrotron x-ray and neutron fiber diffraction." *J Am Chem Soc* 125 (2003) 14300-14306

[49] Nishi Y, Uryu M, Yamanaka S, Watanabe K, Kitamura N, Iguchi M, Mitsuhashi S. "The structure and mechanical properties of sheets prepared form bacterial cellulose. Part 2: Improvement of the mechanical properties of sheets and their applicability of electroacoustic transducers." *J Mat Sci* 25 (1990) 2997-3001

[50] White DG, Brown Jr. RM. "Prospects for the commercialization of the biosynthesis of microbial cellulose." In: Schuerch C, (ed). *Cellulose and Wood – Chemistry and Technology*. New York: Wiley (1989) 573-90

[51] Evans BR, O'Neill HM, Malyvanh VP, Lee I, Woodward J. "Palladium-bacterial cellulose membranes for fuel cells." *Biosens Bioelectron* 18 (2003) 917-923

[52] Shah J, Brown MB. "Towards electronic paper displays made from microbial cellulose." *Appl Microbiol Biotechnol* 66 (2005) 352-355

[53] Yoon SH, Jin H-J, Kook M-C, Pyun YR. "Electrically conductive bacterial cellulose by incorporation of carbon nanotubes." *Biomacromolecules* 7 (2006) 1280-1284

[54] Miyamoto T, Takahashi S, Ito H, Inagaki H. "Tissue biocompatibility of cellulose and its derivatives." *J Biomat Res* 23 (1989) 125-133

[55] Park KE, Jung SY, Lee SJ, Min B-M, Park WH. "Biomimetic nanofibrous scaffolds: preparation and characterization of chitin/silk fibroin blend nanofibers." *Int J Biol Macromol* 38 (2006) 165-173

[56] Thomas V, Dean DR, Vohra YK. "Nanostructured biomaterials for regenerative medicine." *Current Nanoscience* 2 (2006) 155-177

[57] Bäckdahl H, Helenius G, Bodin A, Nannmark U, Johansson BR, Risberg B, Gatenholm P. "Mechanical properties of bacterial cellulose and interactions with smooth muscle cells." *Biomaterials* 27 (2006) 2141-2149

[58] Dumitru S, Vidal PF, Chronet E. "Hydrogels based on polysaccharides." In: Dumitru S (ed.) *Polysaccharides in Medicinal Applications*. New York: Marcel Dekker (1996) 87-105

[59] Watanabe K, Eto Y, Takano S, Nakamori S, Shibai H, Yamanaka S. "A new bacterial cellulose substrate for mammalian cell culture." *Cytotechnology* 13 (1993) 107-114

[60] Svensson A, Nicklasson E, Harrah T, Panilaitis B, Kaplan DL, Brittberg M, Gatenholm P. "Bacterial cellulose as a potential scaffold for tissue engineering of cartilage." *Biomaterials* 26 (2005) 419-431

[61] Hutchens SA, "Synthesis and Initial Characterization of a Calcium-Deficient Hydroxyapatite-Bacterial Cellulose Composite" Masters Thesis: University of Tennessee (2004)

[62] Helenius G, Bäckdahl H, Bodin A, Nannmark U, Gatenholm P, Risberg B. "In vivo biocompatibility of bacterial cellulose." *J Biomed Mater Res* 76A (2006) 431-438

[63] Klemm D, Schumann D, Udhardt U, Marsch S. “Bacterial synthesized cellulose – artificial blood vessels for microsurgery.” *Prog Polym Sci* 26 (2001) 1561-1603

[64] Novaes AB Jr., Novaes AB, Grisi FM, Soares UN, Gabarra F. “Gengiflex, an alkali-cellulose membrane for GTR: histologic observations.” *Braz Dent J* 4 (1991) 65-71

[65] Mello LR, Feltrin LT, Neto PTF, Ferraz FAP. “Duraplasty with biosynthetic cellulose: an experimental study.” *J Neurosurg* 86 (1997) 143-150

[66] Azuma C, Yasuda K, Tanabe Y, Taniguro H, Kanaya F, Nakayama A, Chen YM, Gong JP, Osada Y. “Biodegradation of high-toughness double network hydrogels as potential materials for artificial cartilage.” *J Biomed Mater Res* 81A (2007) 373-380

[67] Czaja W, Krystnowicz A, Bielecki S, Brown RM. “Microbial cellulose-the natural power to heal wounds.” *Biomaterials* 27 (2006) 145-151

[68] Nevell TP. “Oxidation.” In Histler RL (ed.) *Methods in Carbohydrate Chemistry.* New York: Academic Press (1963) 164-189

[69] Surgicel™ Product Labeling (Ethicon, Inc.: Somerville, NJ, U.S.A.).

[70] U.S. Food and Drug Administration Medical Devices Advisory Committee: General and Plastic Surgery Devices Panel Meeting (Transcript) July 24, 2003

[71] Uysal AC, Alagoz, MS, Orbay H, Sensoz O. “An alternative dressing material for the split-thickness skin graft donor site – oxidized regenerated cellulose.” *Ann Plast Surg* 57 (2006) 60-64

[72] Erol OO. “The Turkish delight: a pliable graft for rhinoplasty.” *Plast Reconstr Surg* 105 (2000) 2229-2241

[73] Gago LA, Saed G, Elhammady E, Diamond MP. “Effect of oxidized regenerated cellulose (Interceed®) on the expression of tissue plasminogen activator and plasminogen activator inhibitor-1 in human peritoneal fibroblasts and mesothelial cells.” *Fertil Steril* 86 (2006) 1223-1227

[74] Seal-On™ Product Information (Alltracel Pharma Ltd: Dublin, Ireland)

[75] Dias GJ, Pelow PV. “Osseous regeneration in the presence of oxidized cellulose and collagen.” *J Mat Sci: Mat in Med* 14 (2003) 739-745

[76] Kim U-J, Kuga S, Wada M, Okano T, Kondo T. “Periodate oxidation of crystalline cellulose.” *Biomacromolecules* 1 (2000) 488-492

[77] Laurence S, Bareille R, Baquey C, Fricain JC. “Development of a resorbable macroporous cellulosic material used as hemostatic in an osseous environment.” *J Biomed Mater Res* 73A (2005) 422–429

[78] RoyChowdhury P, Kumar V. “Fabrication and evaluation of porous 2,3-dialdehydecellulose membrane as a potential biodegradable tissue-engineering scaffold.” *J Biomed Mater Res* 76A (2006) 300–309

[79] Kim U-J, Wada M, Kuga S. “Solubilization of dialdehyde cellulose by hot water.” *Carbohydr Polym* 56 (2004) 7–10

[80] Maekawa E, Koshijima T. “Properties of 2,3-dicarboxy cellulose combined with various metallic ions.” *J Appl Polym Sci* 29 (1984) 2289-2297

[81] Calvini P, Conio G, Lorenzoni M, Pedemonte E. “Viscometric determination of dialdehyde content in periodate oxycellulose. Part I. Methodology.” *Cellulose* 11 (2004) 99–107

[82] Schoen FJ, Levy RJ. “Pathological calcification of biomaterials.” In *Biomaterials Science.* Ratner BD, Hoffman AS, Schoen FJ, Lemons JE (eds.) San Diego, CA: Elsevier Academic Press (2004) 439-453

[83] Hutchens SA, Woodward J, Evans BR, O’Neill HM. Composite Material. U.S. Patent Application No. 20040096509

[84] Hutchens SA, Benson RS, Evans BR, O’Neill HM, Rawn CJ. “Biomimetic synthesis of calcium-deficient hydroxyapatite in a natural hydrogel.” *Biomaterials* 27 (2006) 4661-4670

[85] Bodin A, Gustafsson L, Gatenholm P. “Surface-engineered bacterial cellulose template for crystallization of calcium phosphate.” *J Biomed Sci Polymer Edn* 17 (2006) 435-447

[86] Hong L, Wang YL, Jia SR, Huang Y, Gao C, Wan YZ. “Hydroxyapatite/bacterial cellulose composites synthesized via a biomimetic route.” *Materials Letters* 60 (2006) 1710-1713

[87] Wan YZ, Hong L, Jia SR, Huang Y, Zhu Y, Wang YL, Jiang HJ. “Synthesis and characterization of hydroxyapatite-bacterial cellulose nanocomposites.” *Composites Science and Technology* 66 (2006) 1825-1832

[88] Nge TT, Sugiyama J. “Surface functional group dependent apatite formation on bacterial cellulose microfibrils network in a simulated body fluid.” *J Biomed Mater Res* 81A (2007) 124-134

[89] Schramm M, Hestrin S. “Factors affecting production of cellulose at the air-liquid interface of a culture of *Acetobacter xylinum.*” *J Gen Microbiol* 11 (1954) 123-129

[90] Hutchens SA, León RV, O’Neill HM, Evans BR. “Statistical analysis of optimal culture conditions for *Gluconacetobacter hansenii* cellulose production.” *Lett Appl Microbiol* 44 (2007) 175-180

[91] Painter TJ. “Control of depolymerization during the preparation of reduced dialdehyde cellulose.” *Carbohydr Res* 179 (1988) 259-268

[92] Cullity BD. *Elements of X-Ray Diffraction,* 3rd Edition. Prentice Hall: Upper Saddle River, NJ (2001)

[93] Ratner BD. "Surface properties of materials." In *Biomaterials Science.* Ratner BD, Hoffman AS, Schoen FJ, Lemons JE (eds.) San Diego, CA: Elsevier Academic Press (2004) 40-59

[94] Christy AA, Ozaki Y, Greggorioli VG. *Comprehensive Analytical Chemistry: Volume 35, Modern Fourier Transform Infrared Spectroscopy.* Amsterdam, The Netherlands: Elsevier Science (2001)

[95] Bellamy LJ. *The Infrared Spectra of Complex Molecules.* New York, NY: Chapman & Hall (1974)

[96] Peakfit® v4.6 Information Manual. SeaSolve Software Incorporated (Framingham, MA, U.S.A.)

[97] Richards, GN. “Alkaline Degradation,” In Histler RL (ed.) *Methods in Carbohydrate Chemistry.* New York: Academic Press (1963) 154-164

[98] De Faveri D, Torre P, Molinari F, Perego P, Converti A. “Carbon material balances and bioenergetics of 2,3-butanediol bio-oxidation by *Acetobacter hansenii*.” *Enzyme Microb Technol* 33 (2003) 708-719

[99] Park JK, Jung JY, Park YH. “Cellulose production by *Gluconacetobacter hansenii* in a medium containing ethanol.” *Biotechnol Lett* 25 (2003) 2055-2059

[100] Hirai A, Tsujii Y, Tsuji M, Horii F. “AFM observation of band-like cellulose assemblies produced by *Acetobacter xylnium*.” *Biomacromolecules* 5 (2004) 2079-2081

[101] Brown A. “On an acetic ferment which forms cellulose.” *J Chem Soc* 49 (1886) 432-439

[102] Krystynowicz A, Czaja W, Wiktoroskowa-Jezierska A, Gonçalvez-Miśkiewicz M, Turkiewicz M, Bielecki S. “Factors affecting yield and properties of bacterial cellulose.” *J Ind Microbiol Biotechnol* 29 (2002) 189-195

[103] Matsushita K, Fujii Y, Ano Y, Toyama H, Shinjoh M, Tomiyama M, Miyazaki T, Sugisawa T, Hoshino T, Odachi O. “5-Keto-2-gluconate production is catalyzed by a quinoprotein glycerol dehydrogenase, major polyol dehydrogenase, in Gluconobacter spp.” *Appl Environ Microbiol* 69 (2003) 1959-1966

[104] Mowshovitz S, Avigad G, Englard S. “5-Keto-D-fructose: Formation and utilization in the course of D-fructose assimilation by *Gluconobacter cerinus*.” *J Bacteriol* 118 (1973) 1051-1058

[105] Danilchenko SN, Moseke C, Sukhodub LF, Sulkio-Cleff B. “X-ray diffraction studies of bone apatite under acid demineralization.” *Cryst Res Technol* 39 (2004) 71-77

[106] Park JB. *Biomaterials Science and Engineering*. New York: Plenum Publishing (1984)

[107] Filmon R, Baslé MF, Barbier A. Chappard D. “Adherence of osteoblast-like cells on calcospherites developed on a biomaterial combining poly(2-hydroxyethyl) methacrylate and alkaline phosphatase.” *Bone* 20 (2002) 152-158

[108] Rehman I, Bonfield W. “Characterization of hydroxyapatite and carbonated apatite by photo acoustic FTIR spectroscopy.” *J Mat Sci: Mat in Med* 8 (1997) 1-4

[109] Martens W, Frost RL. “An infrared spectroscopic study of the basic copper phosphate minerals: cornetite, libethenite, and pseudomalachite.” *American Mineralogist* 88 (2003) 37-46

[110] Sugiyama J, Persson J, Chanzy H. “Combined infrared and electron diffraction study of the polymorphism of native celluloses.” *Macromolecules* 24 (1991) 2461-2466

[111] Marchessault RH, Sundarajan PR. “Cellulose.” In: *The Polysaccharides Volume 2*. Aspinall GO (ed.) New York, NY: Academic Press (1983) 11-95

[112] Wilson RM, Elliott JC, Dowker SEP, Rodriguez-Lorenzo LM. “Rietveld refinements and spectroscopic studies of the structure of Ca-deficient apatite.” *Biomaterials* 26 (2005) 1317-1327

[113] Murugan R, Ramakrishna S. “Bioresorbable composite bone paste using polysaccharide based nano hydroxyapatite.” *Biomaterials* 25 (2004) 3829-3835

[114] Alexander H. “Composites.” In: Ratner BD, Hoffman AS, Shoen FJ, Lemons JE, (eds.) *Biomaterials Science*. San Diego: Academic Press (1996) 94-105

[115] Kokubo T, Kim H-M, Kawashita M. “Novel bioactive materials with different mechanical properties.” *Biomaterials* 24 (2003) 2161-2175

[116] Dupraz A, Nguyen TP, Richard M, Daculsi G, Passuti N. “Influence of a cellulosic ether carrier on the structure of biphasic calcium phosphate ceramic particles in an injectable composite material.” *Biomaterials* 20 (1999) 663-673

[117] Dobbins RJ. “Solute-solvent interactions in polysaccharide systems.” In: Whistler RL, BeMiller JN, (eds.) *Industrial gums, polysaccharides and their derivatives, 2nd ed.* New York: Academic Press (1973)

[118] Hartgerink JD, Beniash E, Stupp SI. “Self-assembly and mineralization of peptide-amphiphile nanofibers.” *Science* 294 (2001) 1684-1688

[119] Sauer GR, Wuthier RE. “Fourier transform infrared characterization of mineral phases formed during induction of mineralization by collagenase-released matrix vesicles in vitro.” *J Biol Chem* 27 (1988) 13718-13724

[120] Granja PL, Barbosa MA. “Cellulose phosphates as biomaterials. Mineralization of chemically modified regenerated cellulose hydrogels.” *J Mat Sci* 36 (2001) 2163-2172

[121] Anderson HC, Morris DC. “Mineralization.” In: Mundy GR, Martin TJ, (eds.) *Physiology and Pharmacology of Bone*. Berlin Heidelberg: Springer-Verlag (1993)

[122] Hutchens SA, Benson RS, Evans BR, O’Neill HM, Rawn CJ. “A Resorbable Calcium-Deficient Hydroxyapatite Hydrogel Composite for Osseous Regeneration.” *Biomaterials* (In Preparation)

[123] Singh M, Ray AR, Vasudevan P. “Biodegradation studies on periodate oxidized cellulose.” *Biomaterials* 3 (1982) 16-20

[124] Yatagai M, Zeronian SH. “Effect of ultraviolet light and heat on the properties of cotton cellulose.” *Cellulose* 1 (1994) 205-214

[125] Patel RN, Grabski AC, Jeffries TW. “Chromophore release from kraft pulp by purified *streptomyces roseiscleroticus* xylanases.” *Appl Microbiol Biotechnol* 39 (1993) 405-412

[126] Kalinina IG, Gumargalieva KZ, Zaikov GE, Semenov SA. “Breakdown of Flax and Cotton Pulp in Acid Medium.” *Fibre Chemistry* 33 (2001) 228-231

[127] Hon N-S. “Formation of free radicals in photoirradiated cellulose. I. Effect of wavelength.” *J Polym Sci: Polym Chem Ed* 13 (1975) 1347-1361

[128] Feigl F. *Spot tests in organic analysis.* New York: American Elsevier Publishing Company, Inc. (1966)

[129] U.S. and Western Markets for Bone Graft Substitutes. Report M525, June 2005. MedMarket Diligence (Foothill Ranch, CA, U.S.A.)

[130] U.S. Markets for Spinal Fusion Products. Report A303, August 2005. Medtech Insight (Newport Beach, CA, U.S.A.)

[131] Cowan JA, Dimick JB, Wainess R, Upchurch GR, Chandler WF, La Marca F. “Changes in the utilization of spinal fusion in the United States.” *Neurosurgery* 59 (2006) 15-20

[132] Lee KJH, Roper JG, Wang JC. “Demineralized bone matrix and spinal arthrodesis.” *Spine J* 5 (2005) 217S-223S

[133] Lau S, Lam KS. “Lumbar stabilization techniques.” *Current Orthopaedics* 21 (2007) 25-39

[134] Barnes GL, Einhorn TA. “Enhancement of fracture healing with parathyroid hormone.” *Clinical Reviews in Bone and Mineral Metabolism* 4 (2006) 269-275

[135] Carson JS, Bostrom MPG. “Synthetic bone scaffolds and fracture repair.” *Injury, Int J Care Injured* 38S1 (2007) S33-S37

[136] Bucholz RW, Carlton A, Holmes R. “Interporous hydroxyapatite as a bone graft substitute in tibial plateau fractures.” *Clin.Orthop.* 240 (1989) 53-62

[137] Kurtz S, Mowat F, Ong K, Chan N, Lau E, Halpern M. “Prevalence of primary and revision total hip and knee arthroplasty in the United States from 1990 through 2002.” *J Bone Joint Surg Am* 87 (2005) 1487-1497

[138] Goldberg VM, “Selection of bone grafts for revision total hip arthroplasty.” *Clin Orthop Relat Res* 381 (2000) 68-76

[139] Barker R, Takahashi T, Toms A, Gregson P, Kuiper JH. “Reconstruction of femoral defects in revision hip surgery, risk of fracture and stem migration after impaction bone grafting.” *J Bone Joint Surg (Br)* 88-B (2006) 832-836

[140] Gamradt SC, Lieberman JR, “Bone graft for revision hip arthroplasty.” *Clin Orthop Relat Res* 417 (2003) 183-194

[141] Lotke PA, Carolan GF, Puri N. “Impaction grafting for bone defects in revision total knee arthroplasty.” *Clin Orthop Relat Res* 446 (2006) 99-103

[142] Nelissen RGHH, Bauer TW, Weidenhielm LRA, LeGolvan DP, Mikhail WEM. “Revision hip arthroplasty with the use of cement and impaction grafting.” *J Bone Joint Surg* 77-A (1995) 412-422

[143] Heyligers IC, van Haaren EH, Wuisman PIJM. “Revision knee arthroplasty using impaction grafting and primary implants.” *J Arthroplasty* 16 (2001) 533-537

[144] U.S. Markets for Dental Implants and Dental Bone Substitutes. Report A335, December 2003. Medtech Insight (Newport Beach, CA, U.S.A.)

[145] Ardekian L, Mactel EE. “The clinical significance of sinus membrane perforation during augmentation of the maxillary sinus.” *J Oral Maxillofac Surg* 64 (2006) 277-282

[146] Ratner BD. “Introduction to testing biomaterials.” In: Ratner BD, Hoffman AS, Schoen FJ, Lemons JE (eds.) *Biomaterials Science*. San Diego, CA: Elsevier, 2004. p. 355

[147] Anderson JM, Schoen FJ. “In vivo assessment of tissue compatibility.” In: Ratner BD, Hoffman AS, Schoen FJ, Lemons JE (eds.) *Biomaterials Science*. San Diego, CA: Elsevier, 2004. p. 360-367

[148] Salgado AJ, Coutinho OP, Reis RL. “Bone tissue engineering: state of the art and future trends.” *Macromol Biosci* 4 (2004) 743-765

[149] Schantz J-T, Hutmacher DW, Lam CXF, Brinkmann M, Wong KM, Lim TC, Chou N, Guldberg RE, Teoh SH. “Customised tissue-engineered bone grafts II. Evaluation of cellulose efficiency and efficacy in *vivo*.” *Tissue Engineering* 9 (2003)

[150] Yao C-H, Liu B-S, Hsu S-H, Chen Y-S. “Calvarial bone response to a tricalcium phosphate-genipin crosslinked gelatin composite.” *Biomaterials* 26 (2005) 3065-3074

[151] Miyamoto I, Tsuboi Y, Takahashi K, Hyon S-H, Iizuka T. “Enhancement of bone volume in guided bone augmentation by cell transplants derived from periosteum: an experimental study in rabbit calvarium bone.” *Clin Oral Impl Res* 15 (2004) 308-314

[152] Woodbury LA. *Biostatistics* 1971

[153] Schmitz JP, Hollinger JO. “The critical size defect as an experimental model for craniomandibulofacial nonunions.” *Clin Orthop Relat Res* 205 (1986) 299-308

[154] Hollinger JO, Kleinshmidt JC. “The critical size defect as an experimental model to test bone repair materials.” *Journal of Craniofacial Surgery* 1 (1990) 60-68

Appendix

Appendix A. List of Symbols and Abbreviations

ATCC	American Type Culture Collection
BC	Bacterial Cellulose
BC-CdHAP	Bacterial Cellulose-Calcium Deficient Hydroxyapatite
BCP	Biphasic Calcium Phosphate
BMP-2	Bone Morphogenetic Protein - 2
β-TCP	Beta Tricalcium Phosphate
$CaCl_2$	Calcium Chloride
$Ca(OH)_2$	Calcium Hydroxide
Ca_2SO_4	Calcium Sulfate
CdHAP	Calcium Deficient Hydroxyapatite
DAC	Dialdehyde Cellulose
DBM	Demineralized Bone Matrix
DFDB	Demineralized Freeze-Dried Bone
EDS	Energy Dispersive Spectroscopy
FDA	Food and Drug Administration
FTIR	Fourier Transform Infrared Spectroscopy
FWHM	Full Width at Half Maximum
G. hansenii	*Gluconacetobacter hansenii*
HAP	Hydroxyapatite
HEPES	4-(2-Hydroxyethyl)-1-Piperazineethanesulfonic Acid
H_2SO_4	Sulfuric Acid
IGF	Insulin-like Growth Factor
IR	Infrared
K_2HPO_4	Potassium Phosphate Dibasic
KBr	Potassium Bromide
MSC	Mesenchymal Stem Cell
NaOH	Sodium Hydroxide
Na_2HPO_4	Sodium Phosphate Dibasic
$Na_5P_3O_{10}$	Sodium Tripolyphosphate
OCP	Octacalcium Phosphate
PDGF	Platelet Derived Growth Factor
PDF	Powder Diffraction File
PLIF	Posterior Lumbar Interbody Fusion
PLA	Polylactic Acid
PMMA	Polymethylmethacrylate
PHEMA	Polyhydroxyethylmethacrylate
rhBMP-2	Recombinant Human Bone Morphogenetic Protein - 2
SEM	Scanning Electron Microscopy
sHAP	Stoichiometric Hydroxyapatite
TEM	Transmission Electron Microscopy
TGF-β	Transforming Growth Factor Beta
UV	Ultraviolet
UV-Vis	Ultraviolet-Visible
XRD	X-Ray Diffraction

Vita

Stacy Hutchens was born in Vallejo, CA on February 9, 1979. She moved to Suffield, Connecticut at the age of 3; and then to Saratoga Springs, New York at the age of 4. She went to grammar school at Dorothy Nolan Elementary in Saratoga Springs NY, and then attendance of Saratoga Springs Junior High School. She graduated from Saratoga Springs Senior High School in June of 1997.

Stacy then went to The Cooper Union for the Advancement of Science and Art in New York City on a full tuition scholarship. There she received a Bachelor's of Science degree in Engineering with a focus in Biomedical Engineering.

After graduating from The Cooper Union in May 2001, Stacy moved to Knoxville Tennessee in January 2002. There she worked as a research assistant at Oak Ridge National Laboratory under the Oak Ridge Institute of Science and Engineering Higher Educational Experiences program. She worked in the Chemical Sciences Division of Dr. Elias Greenbaum's Molecular Bioscience and Biotechnology Group under the tutelage Dr. Barbara Evans and Dr. Hugh O'Neill.

In August of 2002, she enrolled in The University of Tennessee's Graduate Program in the Department of Mechanical, Aerospace, and Biomedical Engineering. She was awarded the National Science Foundation Graduate Research Fellowship in the summer of 2003. Stacy received her Master of Science Degree in Engineering Science in May 2004. She is currently pursuing her Doctorate Degree in Biomedical Engineering under the guidance of Dr. Roberto Benson at the University of Tennessee.